
Doctoral Dissertations


Student Theses and Dissertations

Fall 2019

The mechanics of precision presplitting

Anthony Joseph Konya

Follow this and additional works at: https://scholarsmine.mst.edu/doctoral_dissertations

 Part of the [Civil Engineering Commons](#), and the [Explosives Engineering Commons](#)

Department: Mining and Nuclear Engineering

Recommended Citation

Konya, Anthony Joseph, "The mechanics of precision presplitting" (2019). *Doctoral Dissertations*. 2836.
https://scholarsmine.mst.edu/doctoral_dissertations/2836

This thesis is brought to you by Scholars' Mine, a service of the Missouri S&T Library and Learning Resources. This work is protected by U. S. Copyright Law. Unauthorized use including reproduction for redistribution requires the permission of the copyright holder. For more information, please contact scholarsmine@mst.edu.

THE MECHANICS OF PRECISION PRESPLITTING

by

ANTHONY JOSEPH KONYA

A DISSERTATION

Presented to the Faculty of the Graduate School of the
MISSOURI UNIVERSITY OF SCIENCE AND TECHNOLOGY

In Partial Fulfillment of the Requirements for the Degree

DOCTOR OF PHILOSOPHY

in

EXPLOSIVE ENGINEERING

2019

Approved by:

Dr. Paul Worsey, Advisor

Dr. Kyle Perry

Dr. Gillian Worsey

Dr. Cesar Mendoza

Dr. Braden Lusk

© 2019

Anthony Joseph Konya

All Rights Reserved

ABSTRACT

Precision Presplitting is a widely used method of presplit blasting for the mining and construction industries. In recent years considerable effort has gone into the development of empirical equations based on field data to be able to better design the Precision Presplit for various rock types and structural environments. However, the most widely discussed theory about the mechanics of the presplit formation, that of shockwave collisions, does not appear to be applicable for this method of presplitting.

This research has disproven this theory based on insufficient magnitude of the shockwave from modeling with basic wave mechanics. Other authors have suggested alternative theories based on the gas pressurization of the borehole. Recently the concept of hoop stresses as a result of the gas pressurization of the borehole was suggested. No method to analyze the gas pressurization of the borehole and magnitude of the hoop stresses existed. This research seeks to develop the basic theory to determine the hoop stress field for a Precision Presplit blast, using basic laws from thermodynamics and mechanics of materials to present a mathematical proof to determine the borehole pressure from a decoupled charge and the magnitude of the hoop stress developed in the rock.

This modelling approach analyzes the stress from both the shockwave and gas pressure, which are quantified and compared to the tensile strength of the rock. This research shows that the shockwave magnitude is much too low to cause presplit formation while the hoop stress has sufficient magnitude to cause the split.

ACKNOWLEDGMENTS

The author wishes to express his gratitude to his advisor, Dr. Paul Worsey, for his advice, assistance, and encouragement throughout the author's schooling and this project; to Dr. Gillian Worsey for her ongoing support and encouragement through the authors schooling and this project; to Dr. Kyle Perry for his assistance and valued ideas in preparation on this project; to Dr. Cesar Mendoza for his support and encouragement on this project; and to Dr. Braden Lusk for his support and encouragement on this project.

The author also wishes to express gratitude to the Missouri University of Science and Technology and the Mining Engineering and Explosive Engineering programs for ongoing education without which this project would not have been possible. The author also wishes to thank the Missouri S&T Curtis Laws Wilson Library, Interlibrary Loan Services.

The author also wishes to express sincere gratitude to Precision Blasting Services for allowing the author to utilize equipment and unpublished research which were vital to the completion of this project.

The author wishes to express his gratitude to Dr. Calvin J. Konya, without whom none of this would have been possible. The mentorship and knowledge imparted has been the basis for the author's current and ongoing work.

TABLE OF CONTENTS

	Page
ABSTRACT	iii
ACKNOWLEDGMENTS	iv
LIST OF ILLUSTRATIONS	ix
LIST OF TABLES	xi
NOMENCLATURE	xiii
 SECTION	
1. INTRODUCTION	1
2. REVIEW OF LITERATURE	6
2.1. INTRODUCTION OF BLASTING TECHNIQUES	6
2.2. HISTORIC MECHANICS OF BREAKAGE.....	8
2.3. SHOCK BREAKAGE IN COMMERCIAL BLASTING	17
2.3.1. The Discovery of Shockwaves.	17
2.3.2. Shockwave Research in Commercial Blasting.....	20
2.3.2.1. Livingston Cratering Theory.	22
2.3.2.2. U.S. Bureau of Mines Cratering Theory.....	26
2.3.2.3. Shockwave Spallation Theory.	27
2.3.2.4. Strain Wave Theory.....	32
2.3.2.5. Refutation of the application of shockwaves in blasting.	33
2.3.3. Shockwave Theory and Mathematical Concepts.	37
2.4. GAS PRESSURIZATION BREAKAGE IN COMMERCIAL BLASTING ...	40

2.4.1. Becker-Kistiakowsky-Wilson (BKW) Equation of State.....	45
2.4.2. Cook's Equation of State.....	48
2.4.3. Taylor's Equation of State.....	49
2.4.4. Outoayne-Skidmore-Konya (OSK) Equation of State.....	49
2.4.5. Theoretical Borehole Pressure Calculations.	51
2.5. PRESPLITTING.....	52
2.5.1. Traditional Presplitting.....	58
2.5.2. Precision Presplitting.	59
2.5.3. Propellant Presplitting.....	69
3. EMPIRICAL ANALYSIS OF BOREHOLE PRESSURES.....	71
3.1. DEVELOPMENT OF AN EMPIRICAL BOREHOLE PRESSURE MODEL.....	71
3.2. MODIFICATION OF THE EMPIRICAL MODEL	76
3.3. EMPIRICAL MODEL FOR TYPICAL PRECISION PRESPLIT	81
4. THEORETICAL ANALYSIS OF BOREHOLE PRESSURES.....	82
4.1. INTRODUCTION TO THEORETICAL MODELS.....	82
4.1.1. Temperature of Detonation.	83
4.1.2. Specific Heats for Explosive Products.	84
4.1.2.1. Dulong-Petit Limit.....	85
4.1.2.2. PETN detonation products.....	86
4.1.2.3. Specific heat for nitrogen, N ₂	87
4.1.2.4. Specific heat of water vapor, H ₂ O.	87
4.1.2.5. Specific heat for carbon dioxide, CO ₂	88
4.1.2.6. Specific heat for carbon monoxide, CO.....	88

4.1.3. Calculation of the Temperature of the Explosion.	93
4.2. DETONATION PRESSURE MODEL	98
4.2.1. Validation of Equations of State from Experimental Data.....	98
4.2.2. Development of Detonation Pressure Model from Taylor EOS.	102
4.3. DEVELOPMENT OF THERMODYNAMIC MODEL	106
4.4. COMPARISON OF PRESSURE MODELS.....	123
4.5. BOTTOM CHARGE EFFECTS	127
4.6. PRESSURE OF A TYPICAL PRECISION PRESPLIT	131
5. HOOP STRESS MODEL FOR BLASTING.....	132
5.1. DEVELOPMENT OF HOOP STRESS MODEL	132
5.2. SIMPLIFICATION OF HOOP STRESS MODEL	140
5.3. HOOP STRESS OF A PRECISION PRESPLIT BLAST	141
6. MAGNITUDE OF THE SHOCKWAVE FROM PRESPLITTING	147
6.1. SHOCKWAVE MECHANICS	147
6.2. SHOCKWAVE MAGNITUDE FOR A PRECISION PRESPLIT	148
7. RESULTS AND DISCUSSION	151
8. CONCLUSIONS.....	155
APPENDICES	
A. CALCULATIONS OF BOREHOLE PRESSURE FOR PETN	156
B. PRECISION PRESPLIT BOREHOLE PRESSURE	166
C. VALIDATION OF ISOTHERMAL ASSUMPTION	188

D. CIRCUMFERENTIAL STRESSES AROUND A BOREHOLE.....	193
BIBLIOGRAPHY.....	196
VITA.....	207

LIST OF ILLUSTRATIONS

	Page
Figure 2.1 – 90° conical crater from an explosive charge placed at point L	11
Figure 2.2 – Dual-Cratering Theory	13
Figure 2.3 – Shearing Theory from a plan view looking downward on the bench with point ‘b’ as the blasthole	14
Figure 2.4 – Crater after Livingston (erroneously) showing shock breakage.....	25
Figure 2.5 – Hino research on unconfined charges.....	28
Figure 2.6 – Initial conditions of shockwave breakage model	35
Figure 2.7 – Detonation for shockwave breakage model	35
Figure 2.8 – Shockwave can be seen in plexiglass as darkened ring.....	36
Figure 2.9 – Shockwave spallation occurring at 15% of typical burden	36
Figure 2.10 – Final frame of test series showing magnitude of gas breakage (internal) versus shock breakage (external)	37
Figure 2.11 – Pressure in the bore of a cannon from various propellants after Nobel.....	43
Figure 2.12 – Borehole pressure from high explosives after Otuonye	44
Figure 2.13 – First test of a Precision Presplit completed in 1980	61
Figure 2.14 – Decoupling ratio to borehole pressure.....	66
Figure 2.15 – Precision Presplit blast completed in 4 different rock types in Grundy, Virginia	67
Figure 2.16 – Precision Presplit load variations based on typical values for specific rock type.....	68
Figure 3.1 – Explosive load to borehole pressure for large decoupling in a two-inch diameter hole.....	75
Figure 3.2 – Borehole pressure variations of explosive load with constant borehole diameter	79

Figure 3.3 – Borehole pressure variations based on borehole diameter at constant explosive loads.....	80
Figure 4.1 – Specific heat at constant volume for nitrogen with variations in temperature using three data sets.....	89
Figure 4.2 – Specific heat at constant volume for water vapor with variations to temperature using three data sets	90
Figure 4.3 – Specific heat at constant volume for carbon dioxide with variations to temperature using three data sets	91
Figure 4.4 – Specific heat at constant volume for carbon monoxide with variations to temperature using one data set	92
Figure 4.5 – Comparison of Equation 28 and Equation 48 to the measured borehole pressures	111
Figure 4.6 – Comparison of Equation 29 and Equation 49 for borehole pressures from a typical Precision Presplit	112
Figure 4.7 – The basic effects of decoupling ratio on the borehole pressure	113
Figure 4.8 – Thermodynamics pressure model to the measured borehole pressure data from Otuonye	121
Figure 4.9 – Linear regression analysis for the compressibility as a function of explosive load for PETN explosive.....	122
Figure 4.10 – Comparison of borehole pressure models at typical Precision Presplit explosive loads.....	125
Figure 4.11 – Comparison of borehole pressure models for large explosive loads.....	126
Figure 4.12 – Borehole pressure as a function of borehole length showing the effects of the bottom load with a column load of 500 grains per foot	130
Figure 5.1 – Hoop stress field as a function of the distance constant (A)	137
Figure 5.2 – The effect of spacing between boreholes on the hoop stress field magnitude	138
Figure 5.3 – Variations of hoop stress magnitude to borehole diameter halfway between the boreholes	139
Figure 5.4 – Magnitude of hoop stress field near the borehole	145
Figure 5.5 – Magnitude of the hoop stress field farther from the borehole	146

LIST OF TABLES

	Page
Table 2.1 – Measured peak pressure for PETN in borehole simulation device after Otuonye.....	46
Table 2.2 – Pressures from propellants pressure edited to psi.....	47
Table 2.3 – Konya Presplit Factor for various rocks	63
Table 2.4 – Properties of black powder compared to Pyrodex	70
Table 2.5 – Tests completed with propellant presplit v. dynamite	70
Table 3.1 – Borehole pressures compared to charge weight per foot.....	72
Table 3.2 – Decoupling ratio for Otuonye work.....	73
Table 3.3 – Boreholes pressures for Precision Presplitting based on explosive load.....	81
Table 4.1 – Heat of combustion for PETN	86
Table 4.2 – Calculation of specific heat for first run of explosive temperature	93
Table 4.3 – Calculation for temperature of explosion for the first run.....	94
Table 4.4 – Calculation of specific heat for second run of explosive temperature.....	95
Table 4.5 – Calculation for temperature of explosion second run.....	96
Table 4.6 – Calculation of specific heat for second run of explosive temperature.....	96
Table 4.7 – Calculation for temperature of explosion third run	97
Table 4.8 – Explosive gas detonation pressure calculations for various EOS.....	100
Table 4.9 – Charge volume calculations.....	100
Table 4.10 – Pressure calculations for decoupled charge from base equations of state.....	101
Table 4.11 – Mole fractions for gases produced from PETN.....	114
Table 4.12 – Calculation of reduced temperature of PETN gas mixture.....	115

Table 4.13 – Calculation of the reduced pressure, iteration 1	116
Table 4.14 – Calculation of reduced pressure, iteration 2	117
Table 4.15 – Calculation of reduced pressure, iteration 3	118
Table 4.16 – Typical explosive column load for various rock types	127
Table 5.1 – Typical explosive loads for various rock types	142
Table 5.2 – Equivalent explosive loads for various rock types.....	142
Table 5.3 – Comparison of hoop stress at maximum split distance to rock tensile strength.....	143
Table 7.1 – Stresses from Precision Presplitting at one borehole diameter from charge.....	152
Table 7.2 – Stresses from Precision Presplitting at maximum split distance	153

NOMENCLATURE

Symbol	Description
W	Weight of Charge
B	Burden
s	Periphery of the Chamber
G	Shear Modulus
P_g	Gas Pressure in Borehole
I_r	Reflected Intensity Constant
I_t	Transmitted Intensity Constant
D	Detonation Velocity
P_{CJ}	Detonation Pressure
v_s	Sonic Velocity
ρ	Density
b	Co-Volume
T_e	Temperature of Explosion
R	Gas Constant
n	Inverse Average Molecular Weight
P_e	Explosive Pressure
n_i	Moles of Product Divided by Kg of Explosive
Q_e	Heat of Explosion
V_e	Specific Volume of Explosive Gases
N_g	Total Moles of Gaseous Product per Kilogram

Z_c	Compressibility
P_c	Critical Pressure
T_c	Critical Temperature
P_r	Reduced Pressure
T_r	Reduced Temperature
r	Radius
r_o	External Radius
r_i	Internal Radius
p_o	External Pressure
p_i	Internal Pressure
σ_c	Hoop Stress in Circumferential Direction
E	Young's Modulus
K	Konya Presplit Factor
S	Spacing
n_i	Moles of Product Divided by Kg of Explosive

1. INTRODUCTION

Explosives are utilized in both the mining and construction industries for effective and cost-efficient rock excavation. The majority of the explosives used in both of these industries is for production blasting, which is defined as the fragmentation of rock and for mass rock excavation. This type of blasting typically leads to breakage behind the final row of blastholes, termed overbreak or backbreak, which is acceptable in the main body of the excavation but is of major concern when blasting near final excavation limits.

In the construction industry the final excavation limit, often called the 'neat line', is specifically designed to produce a stable slope, which minimizes risk of rockfall to the public or nearby infrastructure. These are typically long-term slopes and any additional overbreak can result in accelerated weathering of the material, increasing the risk of rockfall and requiring rework of the area to stabilize the slope.

In addition to stability of slopes, many projects require pouring of concrete next to the rock wall to build infrastructure such as locks and dams. In these situations, when blasting does not reach the neat line, mechanical excavation and scaling would be required to achieve the final wall. These methods are extremely expensive and time consuming. However, blasting beyond this neat line would result in additional concrete to fill any areas of overbreak, which also results in large increases in cost and time.

In the mining industry, engineers design pits with an overall pit slope to minimize the risk of large-scale slope failures. These slopes are designed primarily based on the natural rock for where the slope is excavated. However, if poor blasting methods are utilized and the rock behind the slope is fractured, then the designers will often 'lay the

slope back' or use a shallower slope to protect against a slope failure. This typically requires the mining of additional waste material, which significantly increases the total cost of the mine and reduces profitability. In today's mining industry, mines are looking to mine deeper, and as a result need to have steeper and more stable slopes, with minimal backbreak to reduce the risk of a slope failure, significantly improving the safety of workers and equipment in the pit and increasing the profitability of the mine.

The mining industry also designs bench angles, which is the angle of an individual bench, to minimize the risk of rockfalls to workers in the mine. Currently numerous methods exist to protect workers including (1) the design of the bench angle to minimize the risk of rockfalls, (2) the use of catch benches to stop material from falling further into the pit, (3) the use of berms to keep rock from reaching work areas and to keep workers out of areas where rock may fall, (4) the use of mechanical scaling of walls to reduce the risk of rockfalls, and (5) the use of overbreak control measures in the blasting process.

The measures used to protect workers all have advantages and disadvantages, which includes the effectiveness of the particular measure, cost to perform, and reliability of the measure. The first three methods are effective to reduce the risk in the design of the mine but are extremely expensive as all lead to mining much larger amounts of waste or missing ore reserves. Method four cannot be viewed as a legitimate method which is relied upon, as it does not ensure that the risk of rockfalls are mitigated. This is due to the inability to reliably scale several benches in a surface mining operation. Instead it would be viewed as a preventative maintenance method, which should be performed to mitigate the risk of major rockfalls. Method five increases the operational costs of a site but

eliminates the need for mining additional waste and/or missing ore. The use of overbreak control to generate smooth walls and minimize rockfalls is also a highly reliable method of mitigating these risks for both short-term and long-term stability. Larger mining operations have traditionally utilized a combination of all these methods to optimize the economics for the life of mine.

The ability for a mining or construction project to generate smooth walls using explosives is paramount to the operation being economically effective and safe for employees. The use of proper presplitting can reduce the amount of scaling required to 1/10 of that required when traditional blasting is utilized (Paine, Holmes, & Clark, 1961). This has large economic savings in reduction of manpower and equipment required and increased excavation capacity. This also leads to a safer project, as less rockfalls occur during the scaling process when men and equipment are near the highwall. The minimization of backbreak is not only seen on the face of the excavation, but the reduction in blast damage is meters thick where proper presplits show no degradation of the rock beyond the presplit line (Matheson & Swindells, 1981).

While traditional presplit methods can be utilized in hard rock types, they do not perform properly when they are applied to weaker rocks. This has led to a false concept that weaker sandstones, shales, mudstones, and siltstones cannot be presplit. However, the method of Precision Presplitting has been applied to all of these rock types effectively and shown presplits with near perfect walls in full-scale construction projects (Spagna, Konya, & Smith, 2005). Traditional presplit methods often caused problems with weaker types of rock, as the explosive load is too great and crushing or cratering around the borehole causes overbreak.

Oftentimes, the structural properties of the geology being blasted also causes backbreak beyond the presplit lines (Worsey, Farmer, & Matheson, 1981; Worsey & Qu, 1987). The solution to minimize the effects of these geologic conditions is to bring the borehole spacing closer together. Traditional presplit design would use a 'split-factor' to adjust the explosive load based on a linear relationship with spacing. However, the explosive load to spacing relationship is not linear (Konya & Konya, 2017b) and this leads to overloading of the charge in the area. With this being completed in poor geologic conditions, oftentimes with heavy jointing and bedding, the presplit will generate overbreak for the entire region and cause joints and bedding planes to open up from gas penetration.

The mechanisms behind a presplit formation are not well understood and false theories are still introduced and propagated by groups and individuals that are not well read in previous literature and tests. The shock breakage theory is still widely taught and studied (International Society of Explosive Engineers, 2016; Salmi & Hosseinzadch, 2014) even though this theory has numerous studies showing how it is not applicable and is a false concept (Konya C. , 1973; Worsey P. , 1981). In fact, under this theory methods such as Precision Presplitting could not work to produce a presplit.

A new theory is that the explosive generated gases in a borehole causes a hoop stress field, which causes the presplit fracture to occur (Konya & Konya, 2017a). This indicates that very small explosive loads could be used, depending on the rock type and structural environment, to generate a fracture without causing any overbreak to the surrounding structure. It is proposed that this hoop stress field is a function of the gas pressure, and the research in this dissertation focuses on defining this gas pressure in a

borehole from both detonating and deflagrating explosives to determine if borehole pressures are possible to generate these hoop stress fields. This dissertation will also focus on the development of a hoop stress model to determine the magnitude of the stress field generated from the borehole pressure.

This thesis analyzes both the shockwave breakage and hoop stress theories to determine the magnitudes of these stresses. This is then compared to various rock properties such as the Brazilian Tensile Strength. The design of the explosive load for a Precision Presplit round based on the tensile strength of the rock is also developed. The models developed and applied are tested against measured borehole pressures. These models are then applied to actual field conditions to confirm applicability of the models and to prove that these theoretical models properly explain why the field conditions occur.

2. REVIEW OF LITERATURE

2.1. INTRODUCTION OF BLASTING TECHNIQUES

The use of explosives in rock blasting began on February 8, 1627 in the Oberbiberstollen of Schemnitz in Hungary which was designed and fired by Caspar Weindl (Guttman, 1892) utilizing black powder. With the success of this first blast, the Hungarian Mine Tribunal quickly disseminated this information throughout Hungary and the utilization of explosives in underground mining spread so that by 1673 the technology had spread throughout the Hungarian underground mining industry (Brown E. M., 1673). Blasting then spread throughout the world where it was introduced in Germany in 1700 and Sweden in 1724 for blasting in the mining industry. With the massive improvements in rock fragmentation, especially in hard rock, which could not be mined previously except with fires, the construction industry soon began employing the use of black powder blasting. The first underground construction tunnel developed with the use of blasting is documented to have occurred in 1679 to develop the Malpas Tunnel in Languedoc, France and by 1696 blasting had begun to be used for surface blasting in the construction industry for the development of roadways on the Abula Pass in Switzerland (Guttman, 1892).

Since explosives first began being used in mining and construction, engineers and scientists have been developing theories to better understand how these explosives work to break rock, in an attempt to improve the efficiency of blasting (Guttman, 1892). These efficiency improvements have been in ways to improve explosives through chemical formulations and manufacturing processes (Quinan, 1912), develop ways to

better design blasts to increase fragmentation and heaving of the muckpile, and to reduce the environmental factors of blasting; such as ground vibration and overbreak of blasts (Brown E. M., 1673). The overbreak of a blast, or breakage beyond the design line, has been of concern since these early construction projects, as overbreak often leads to raveling of rock and incompetent walls. This overbreak can also cause increases in the speed of weathering and water penetration behind the slope which can lead to slope failures. In projects where concrete is used this overbreak requires the additional use of concrete, which can increase project costs by millions. This is also of concern in underground workings where poor blasting along the perimeter of the blast will lead to large pieces of rock hanging on the back and ribs of the excavation, which become immediately dangerous to workers in the area and add significant cost to remove or bolt.

In an effort to prevent overbreak a technique known as presplitting was introduced and worked by breaking a smooth line between holes in the rock (Paine, Holmes, & Clark, 1961). The use of this technique began before explosives were ever introduced into construction; in places such as Egypt wooden wedges were soaked with water and placed in boreholes, heated with fire which caused expansion, which formed a split between boreholes. In northern climates rock was broken in a similar manner; where boreholes could be filled with water, the water was then frozen, and cracks occurred between the holes in the winter. This would create large, smooth blocks that could be used in construction and leave a smooth back wall. Both of these ancient techniques involved drilling close boreholes and applying a pressure inside of the borehole to cause fractures between holes. In ancient times this pressure was often slow building, and in some cases would takes months to fully split the rock (Konya C. , 2015).

It was not until the 1950s, that the first explosive presplitting was utilized on the Lewiston Power Plant (Langefors & Kihlstrom, 1973) as part of the Niagara Powder Project. In order to accomplish this, boreholes would be drilled from 12' to 52', depending on the bench height, and loaded with detonating cord and partial cartridges of dynamite. These boreholes were 3 inches in diameter and fired before the main blast, with all presplit holes being fired at the same time utilizing instantaneous delays. This produced excellent results and essentially eliminated all overbreak on the project. This technique has since had widespread use in the mining and explosive industry to minimize overbreak from explosive blasting. However, while practical rules of thumb exist for designing blasts in a few specific situations, a deep understanding of the mechanics of presplitting is lacking and widely debated.

If an explosive applies a pressure to fragment rock in production blasting, the same pressure must also be responsible for providing the work to break the presplit. Presplitting uses similar explosives to production blasting which exert similar pressures, just to a lesser extent, compared to production blasting. Therefore, the background and understanding of the application of pressure from commercial explosives and the mechanics of breakage in production blasting are critical to understanding the pressures applied in presplit blasting.

2.2. HISTORIC MECHANICS OF BREAKAGE

Black powder was the first explosive applied to the breakage of rock in mining and construction. Black powder is now known as a low explosive, meaning that it fires slower than the speed of sound in the material. This is often called deflagration and can

be considered a slower burning process, which does not result in a shockwave being generated in the explosive. The pressure profile of black powder is considered one of a slow build, where the gas pressure in the borehole slowly increases until the powder is fully consumed, then the pressure is released through either breakage of the rock and flow through the newly generated cracks or the stemming releases and the gas pressure vents through the top of the borehole. Various mixtures of black powder would burn at different rates, which would change the application of this gas pressure; today it is understood that this would change both the peak pressure generated in the borehole and the impulse in the borehole. At this time, the gas pressure was the only pressure that was developed in the borehole and as such was the only work mechanism. This led explosive engineers of the day to focus on ensuring that the maximum gas pressure was utilized and contained in the borehole. This introduced tamping, or the filling of the end of a borehole with inert materials to contain the gas pressure, in 1685 (Guttman, 1892). Similar methods to tamping or as we call it today, stemming, are still employed today in mining and construction operations around the world.

The rate of deflagration in propellants was large and controversy existed on the quality of black powder for commercial use (Hutton, 1778). At the time it was believed that the military used better black powder, which burned at a faster rate and applied greater gas pressures. There was also a major cost difference between black powder which was made for military use and black powder which was made for commercial blasting use. This inferior black powder would generate less heave than the higher quality black powder. From this we can ascertain that the speed at which the gas pressure would build up would have very real, practical effects on the blasting (Burgoyne, 1874).

The world utilized only black powder explosives for over 227 years until 1854, when gun-cotton was first manufactured in Austria. The gun-cotton plant was quickly closed however due to numerous explosions during manufacturing. Around a similar time, Sobrero invented nitroglycerin in 1846 for use as a medicine for angina pectoris. In 1867, Alfred Nobel then invented dynamite with a combination of nitroglycerin and kieselguhr; inventing the first commercial high explosive. Later Nobel would combine nitroglycerin and gun-cotton to make gelatin dynamite and give miners the ability to use these explosives in almost all situations where rock breakage was required. Both explosives are today considered high explosives, as they detonate faster than the speed of sound in the material. This produces a high-pressure shockwave, which is then followed by a rapid increase in gas pressure. This gas pressure build-up is much faster than black powder and at a much higher temperature due to the increased speed of application and larger volume of gas generated.

Before the invention of high explosives, numerous rules governed the use of black powder in the explosives industry. Some of these rules focused on the charge length where the length of black powder used should be greater than six times the diameter, yet less than twelve times the diameter. Due to the mechanical aspects of drilling a borehole, short holes were also used. If a hole was placed vertically into the rock, with only the surface as relief, the borehole would eject a 90° conical crater (Burgoyne, 1874).

With the reduced amount of black powder which could effectively be used in a blast and limitations on drilling, this cratering was likely prevalent and does indeed occur and is seen in work completed nearly a century later (Ash R. , 1974; Livingston C. , 1961). While this cratering mechanism is still used today, it is not an ideal breakage

mechanism from either a performance or an economic standpoint. This theory on breakage had widespread impacts on how blasting was performed from 1627 to the late 1800s where bench corners were shot under the dual-crater theory.

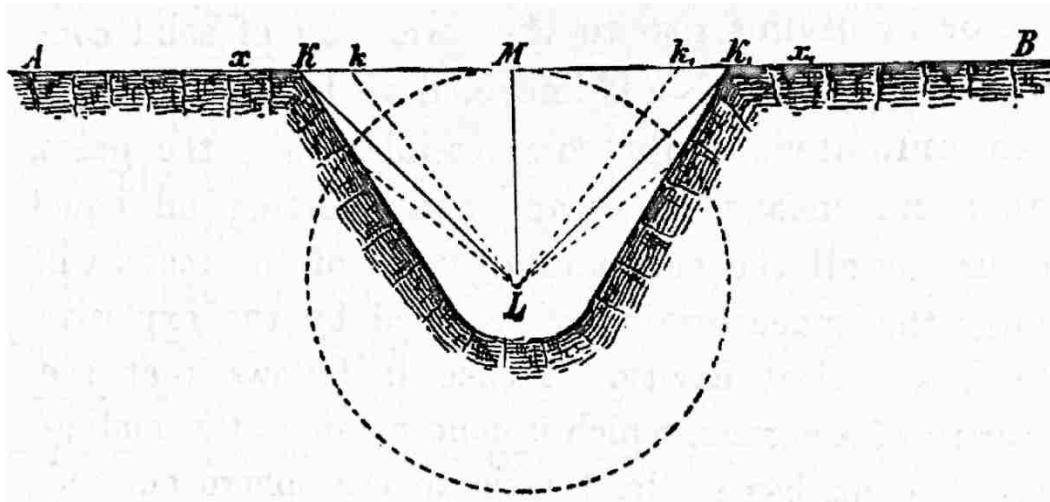


Figure 2.1 - 90° conical crater from an explosive charge placed at point L (Guttman, 1892)

The dual-crater theory was the idea that the distance from L to M (Figure 2.1) was the least resistance in the shot, which is described as the shortest distance from the charge to a free face. The goal was to then place the charge on the edge of a bench to where the vertical burden, horizontal burden, and spacing between holes was equal in distance. This can be seen in Figure 2.2, where the lines AB, BC, and DB are all equidistant. Under this condition the theory states that two distinct craters will be blasted, one above the hole cratering vertically and one on the face cratering outward (Cosgrove, 1913).

With the slow burning of black powder, the pressure in the borehole slowly built up to levels enough to break rock and with the advent of high explosives, particularly

dynamites, this pressure was applied much more rapidly to the borehole walls. Shortly after the advent of dynamite researchers began noticing that all of the rules associated with black powder, such as charge length, did not hold up for dynamite. The prevalent belief was that this may be due to a different breakage mechanism that was causing dynamite to break better than black powder. It was then found that when boreholes were loaded with a high explosive, decoupled, and had full confinement that the borehole would increase in size, in some cases to double the size of the originally drilled hole, around the charge.

This led to the theory of borehole springing, which stated that when a high explosive was utilized, the rapid pressure on the borehole walls would cause compression in the surrounding rock mass, creating a larger borehole. When the borehole was fully loaded this large borehole springing effect would cause the borehole to open large enough that it would move and displace all the rock in-front of it due to crushing actions and momentum of movement (Guttman, 1892).

This springing was also utilized then to compensate for the lack of advance in drilling technology. The boreholes were loaded with small explosive charges and fired, opening larger diameter boreholes in the rock mass. These would then be fully loaded and fired again, as a workaround to small drillholes. This greatly increased drilling efficiency back in the early 1900s. This borehole springing is exhibited still today and the use of springing was used even in the 1970s to develop larger boreholes in hard rocks such as those found in Sweden (Langefors & Kihlstrom, 1973).

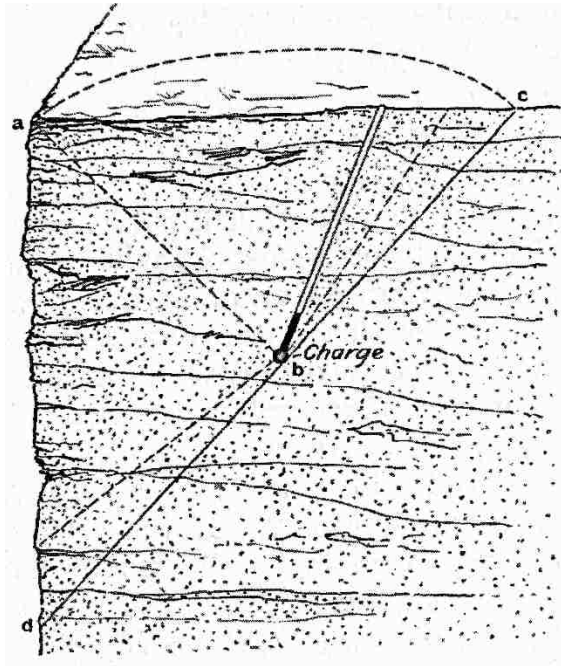


Figure 2.2 - Dual-Cratering Theory (Cosgrove, 1913)

Research later discovered that while this borehole springing was a popular theoretical concept it did not seem to work in the practical world, as it did not properly account for the cohesive strength of the rock, it did not properly calculate the force in the borehole, and it did not account for the relationship between the explosive charge and the free face. Additionally, drilling technology advanced and then longer and larger diameter boreholes could be used in the blast. Longer holes resulted in a large increase in borehole utilization. This was the major downfall of the springing theory, it relied on many of the similar principles of the cratering theory, particularly in using medium length holes, short charges, and large amounts of tamping (stemming). With the explosive engineer now able to use longer holes and fill a larger percentage of the borehole with explosive, it was evident that springing was not causing breakage. Additionally, it was seen that on these longer, highly utilized holes which were loaded with high explosives, the breakage was

not occurring through conical cratering but was instead breaking through the face, with no observation of cratering in the vertical direction of the blast. This was the first realization of the directionality of long charges when aligned with a free face, which was achieved through a long, slender charge instead of a concentrated 'spherical' charge (Daw & Daw, 1898).

This led to the advent of the shearing theory, which stated that when a charge was detonated the rock around borehole would shear away from the borehole in a direction of least resistance, opening up an 80° to 110° crater. This theory stated that "the rock is most economically and conveniently mined in benches with a straight and vertical wall, and that the height of such steps depends on the depth and diameter adopted for the boreholes" (Daw & Daw, 1898).

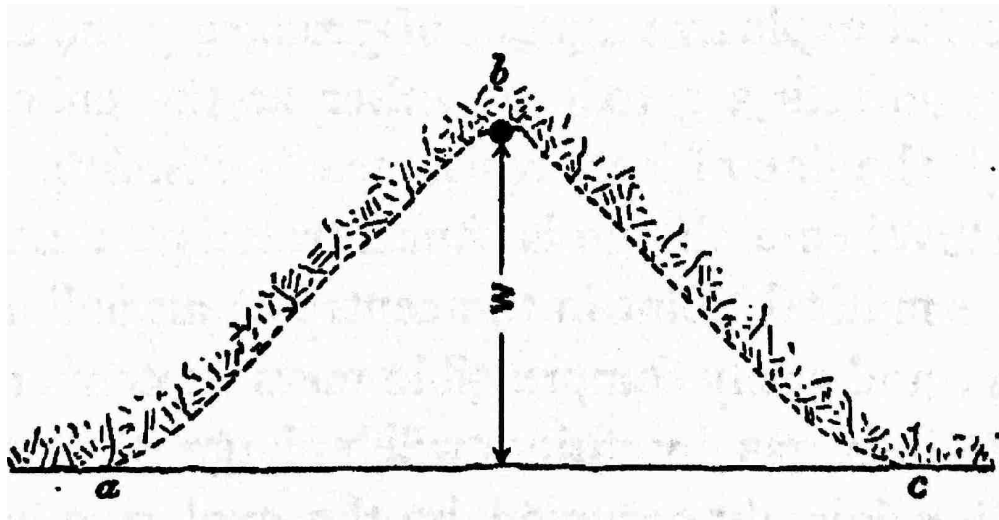


Figure 2.3 - Shearing Theory from a plan view looking downward on the bench with point 'b' as the blasthole (Daw & Daw, 1898)

The belief behind the shearing theory was that if a charge was placed at point b, with the closest distance to relief being W, the lines ab and bc would shear and the rock wedge would be pushed out due to the gas pressure (Figure 2.3). This was due to the large gas pressure generated by the charge and then as the rock was thrown forward it would bend and break into smaller fragments. This was one of the first real developments of an equation to determine the various dimensions in blasting, which was the determination of W called the “Line of Resistance,” now known as Burden (B).

Previously the only method to determine the line of resistance was the use of Hauser’s Law (modified to current blasting terminology), which was an empirical equation developed regardless of the breakage theory. This equation was extremely poor in dealing with changes in explosive power. The constant “C” was an empirical coefficient which can range from 0.02 to 0.50, depending on the strength of a rock.

$$W = CB^3 \quad (1)$$

where W is the weight of the charge in kilograms, C is a constant, and B is the burden in meters.

Daw and Daw then developed an equation using static loading of ice and the shearing theory to provide a new equation for determination of Burden.

$$P_g = sBG \quad (2)$$

where P_g was the borehole pressure in psi, s was the shear strength of the rock in psi, B was the burden in feet, and G was the volume of the chamber in cubic inches. The units in Equation 1 and 2 are the original units as reported by the respective authors.

At this time, all breakage theories relied solely on the gas pressure causing the breakage in rock. The gas pressure was a well-established principle which was

understood easily. Additionally, engineers and scientists did not understand the mechanisms of shockwave and had minimal instrumentation to accurately quantify this occurring from the explosive. However, they did understand that there was a difference and attributed it to the rapid development of gas pressure from dynamite when compared to black powder. At the time, gas pressure was the only pressure that was understood to occur from an explosion, and as such the majority of testing of explosives occurred through the use of mortar testing. It has been easy to calculate the volumes of gas that is formed from a gas mixture based on STP, for centuries, however the difficulty in the development of pressure models was to determine what the temperature of the explosion was, which had dramatic impacts on the results of the pressure. Additionally, with long slender charges the velocity of detonation was another difficulty.

It was mathematically determined that gunpowder would produce a pressure of approximately 85,000 psi. This was then used as a baseline to determine total pressure developed by the various dynamites using a weight-equivalent testing procedure. When using bulk explosives, gun powder was then considered the baseline and had an energy factor of 1.00; therefore, dynamite had a total energy factor of 4.23 meaning that the dynamite was considered over four times stronger than gunpowder (Andre, 1878). This increase in power was theorized to be both from the increase in speed of reaction resulting in a faster force application over a long charge, and in a higher heat of detonation.

The theory of gas pressurization continued well into the beginning of the 20th century and was rapidly expanding as explosive engineers of the time attempted to design explosives to increase the maximum pressure in a blasthole (Quinan, 1912). With the

beginning of the World Wars, many explosive engineers and researchers changed their course of research from application of explosives in rock blasting to military applications. However, those still working in rock blasting from 1910 to 1950 progressively advanced the practical application of the gas pressurization theory, focusing efforts on maximizing the borehole pressure (Roscoe, 1924; Taylor J. , 1945). With the advent of nuclear weaponry and significant research into increasing the power of weapons systems, a new method of damage from explosives began being explored in the early 1940s, i.e. shock breakage.

2.3. SHOCK BREAKAGE IN COMMERCIAL BLASTING

Shockwaves began in the industries as a solely theoretical concept which was not applied to rock blasting. However, as new research was completed shockwaves quickly became a major research area in commercial blasting.

2.3.1. The Discovery of Shockwaves. Black powder was one of many rapidly burning chemicals that existed in the ancient world, yet it was the most popular because its application as a propellant for firearms was quickly recognized (Bacon, 1733) and by 1314 it was recorded being utilized in multiple battles. While black powder combusts very rapidly it does not detonate, instead it deflagrates producing no shockwave. It was not until 1608 that the first high-explosive (Croll, 1609), one that combusts faster than the speed of sound in the material, was invented. The combustion of this high-explosive produces a strong shockwave. In 1659 the first ammonium nitrate compound was produced (Kirk & Othmer, 1947), which today is recognized as a high explosive and is the dominant ingredient in commercial explosives. Fulminating Silver was then

introduced in 1786 (Berthollet, 1786) and Potassium Chlorate followed shortly after (Kapoor, 1970). These compounds were all considered ‘primary explosives’ or those which were too sensitive or powerful for practical use. At the time, the inventors of these compounds had no method to measure the rate at which they combusted, nor did they understand the difference between a deflagration and detonation.

The shockwave which is produced by high explosives and high velocity impacts is unique in terms of wave mechanics, magnitude, and velocity. The origins of the shockwave are developed from acoustical wave theory which was introduced in the mid-1700s (Le Rond D’Alembert, 1747; De Lagrange, 1781). As mathematical theory of acoustic (sound) waves progressed, mathematicians attempted to discover the “size of disturbances” of sound waves, or the intensity of the sound. At this time, it was noted that “the following disturbances could accelerate the propagation of the preceding ones, in such a way that the higher the sound the greater is its speed...” (Euler, 1759). This would help to develop the theory that the speed of a wave depends on its intensity, which is one of the foundational principles of today’s understanding of shockwaves. The initial mathematical theory of acoustic waves was fully developed by 1802 (Biot, 1802).

This acoustical wave theory was then expanded to mathematically incorporate waves of much greater pressures and much faster speeds than typical acoustic waves (Poisson, 1808). This was the first mathematical proof of the existence of shockwaves. Work continued following this in the theory of these waves through the 1800s, but these waves could not be created easily without detonation (Weber & Weber, 1825). The shock wave was observed with sharp boundaries in air and termed the shock wave, using sparks in air (Toepler, 1864), which eventually led to the application of the laws of conservation

of mass, conservation of momentum, and conservation of energy to the shockwave. Then the mathematical proof of a planar shock wave (Christoffel, 1877b) and the propagation of shock waves through an elastic solid medium (Christoffel, 1877a) was developed.

The first real laboratory tests utilized linear percussion techniques to observe the formation of a shockwave (Mach & Somner, 1877). A theoretical treatise addressing the linear relationship between pressure and specific volume of a gas was developed and termed the “Rayleigh Line” (Rayleigh L. J., 1877). In 1881 gaseous explosive mixtures were utilized to prove that a shockwave was produced as a result of a detonation (Berthelot, 1892; Berthelot, 1881). This research first discussed this wave as an ‘explosive wave’ but was later determined to be the shock wave seen in other applications. This explosive wave was observed to have effects comparable to a sound wave, except with high active energy and large pressure.

This led to the development of a general theory of discontinuous one-dimensional flow using Lagrangian coordinates (Hugoniot, 1887), which led to the development of the Rankine-Hugoniot equations. This along with the Rayleigh line gave researchers a mathematical method to determine the pressure and velocity of the shockwave.

The first theory of detonation based on shockwaves was completed to mathematically prove how explosives produce these shockwaves (Mikhel'son, 1893). This was then investigated and further developed to show that during the detonation of the explosive, a shockwave first propagates through the medium, which is followed by a combustion wave (Jouguet, 1904; Jouget E. , 1906). This would go on to be known as the Chapmen-Jouguet theory and is still applied in the study of detonations today. The theory was then further developed to determine shockwave thickness (Prandtl, 1906), the

application of the theory to reactive fluids (Crussard, 1907), determination of entropy and its first three derivatives on either side of the shockwave front (Duhem, 1909), theory of planar waves (Rayleigh L. J., 1910), and the thermodynamics of shockwaves (Taylor G. I., 1910). These were then incorporated and developed into the basis of the shockwave theory which is still utilized today (Jouget E. , 1917; Becker, 1929; Taylor G. I., 1939).

2.3.2. Shockwave Research in Commercial Blasting. The original theory of shockwaves did not initially have any applicability in commercial blasting due to the fact that high explosives, those in which combustion occurs faster than the speed of sound in the material, were not used in the industry. This began to change when Sobrero discovered nitroglycerin, which at the time was used as a medicine for heart disease but could also be easily detonated (Sobrero, 1847). Immanuel Nobel began full scale production of nitroglycerin and Alfred Nobel began investigating the application of nitroglycerin for commercial blasting in the 1850s (Johnson N. , 1974).

During the early days of nitroglycerin use in mining, the liquid explosive was packaged in glass bottles and these bottles were lowered into boreholes. The manufacturing and production of nitroglycerin were both extremely dangerous and numerous accidents and deaths occurred, including that of Alfred Nobel's youngest brother, Emil Oskar, and his explosive chemist, Carl Hertzmann (Krehl, 2009). This led to Alfred Nobel working with analogous substances in an attempt to desensitize the nitroglycerin. Eventually, Alfred Nobel discovered that mixing nitroglycerin with diatomaceous earth would create a substance that was not flame sensitive but was still shock sensitive. This substance would go on to revolutionize the explosive industry,

providing the first safe high explosive to be used in blasting called dynamite (British Patent No. 102, 1867).

High explosives were now being utilized in commercial rock blasting on a regular basis and it was evident that the dynamite performed better than the black powder. However, the theory of shockwaves never progressed from air and water into the concept that they contributed to the rock breakage process. When explosive engineers of the day attempted to explain the difference in the breakage of rock from low or slow explosives, such as black powder, and high or quick explosives, such as dynamite, they believed that slow explosives could not assert as much pressure on a borehole wall before the wall yielded, whereas quick explosives were able to instantaneously apply a much larger degree of pressure before the borehole wall yielded (Daw & Daw, 1898). As time went on the researchers began looking at the optimization of explosive formulations, oftentimes mixtures, to develop oxygen balance and products which had large gas volumes (Quinan, 1912). In the mining world, these new high explosives were thought to have more intimate mixtures of oxygen and fuel along with higher brisance, or the velocity to which it detonated, with higher brisance leading to greater shattering effects (Munroe & Hall, 1915). The application of the shock wave theory to chemical explosives came about in the late 1940s (Brode, 1947). This was then expanded to develop shockwave theory in air (Brinkley & Kirkwood, 1947a; Brinkley & Kirkwood, 1947b) and then came the development of the shockwave theory in water (Cole, 1948). This research then showed the application of shockwaves in multiple mediums and was soon advanced to shockwaves in a rock mass.

2.3.2.1. Livingston Cratering Theory. Researchers then began looking at the shockwaves that were generated by commercial explosives and how these effected rock blasting. This work began through the experimentation of Livingston (Livingston C. , 1950) and later developed into the work of Duvall and Atchison with the U.S. Bureau of Mines. The Livingston Theory was based on old cratering principals, which were defined from military work and blasting in permafrost to observe the crater size utilizing spherical charge principles. A spherical charge is a Swedish concept that stated that when a charge had a length less than six times its diameter that it would function as a point source, with the pressure from the charge being applied equally in all directions (Grant, 1964; Johnson S. , 1971). However, this spherical charge theory contains many flaws; the first of which being that blastholes utilized in the mining and construction industry are not spherical but are long, cylindrical charges that have a length much greater than six times their diameter and exert force outward from the charge. Therefore, should spherical charges be a valid theory, the assumption that the physics behind the spherical charge and a cylindrical charge are the same cannot be made and has been disproven in underwater testing by Cole (Cole, 1948).

Furthermore, the spherical charge theory is not a valid theory as soon as the charge deviates from spherical. The pressure of the charge is a function of the force and the surface area of the charge (Cooper, 1996). For a charge that has the same length as the diameter with a cylindrical shape approximately 67% of the charge's surface area is on the side of the charge. For a charge with a length six times the diameter 89.2% of the surface area is composed of the sides of the charge. A charge which is 2 inches in diameter and ten feet long, which is an example of a real charge scenario from blasting

has over 99.2% of its surface area off its side (Ash R. , 1974). It has been shown that the effects of the directionality of a charge has real world effects, even when the charge meets the criteria for a spherical charge based on the crater they break when the charge has a free surface off the side (Ash R. , 1973). The Livingston crater theory is then not defining breakage for a charge as would be seen from blasting; but instead from a charge which has no burden (free face) off of its largest surface area. This results in inefficient blasting in the form of cratering, which is not applicable to mining or construction.

While the Livingston theory has been shown to be based on false principles, it is still important to address the theory and actual findings of Livingston's work as they form the basis for all modern shockwave theory today. Livingston believed that when blasting craters, the explosive had two effects on the rock. The first effect was the shockwave which caused breakage to occur. The second effect was the gas pressure produced by the explosive, which could cause additional breakage and move the material. Livingston believed that each of these played an important role in breakage. He conducted numerous studies in permafrost and found that when a charge was deeply buried it would produce radial fractures and a conical shaped breakage around the borehole (Figure 2.4). As the charge was brought closer to the surface the crater would break finer and material could be ejected from the borehole. He believed that this showed that the shockwave had larger effects than the gas pressure because the gas ejection of material occurred at a reduced depth of burial and the shockwave showed effects at deeper burial.

However, Livingston never actually looked at the shock breakage or the energy and time of these breakage planes. When reviewing pictures of the breakage observed in Livingston's crater studies it is now understood that this is not 'shock breakage' but

circular breakage around a borehole from lifting and bending of the upper layer of material. For example, the author observed this same feature when blasting sandstone in Saudi Arabia. In this situation, a large cave was present in the middle of the material to be blasted and the mine loaded the material underneath the cave. When the explosive detonated, the gas pressure filled this cave, causing lifting and bending of the surface. This cave made the availability of the shockwave to rise to the surface impossible, yet the same breakage patterns are observed. These features which were observed in Livingston's case are not because of the shockwave, but because as the explosive detonated a large high-pressure gas is present in the borehole. If no free surface is present and this gas is deep within the ground to where it is not of enough pressure to break out and be released a large, high pressure gas sphere is formed. This causes the material above the gas sphere to lift slightly causing bending of the material, which leads to this circular breakage. This breakage is easily seen in the field by a large circular breakage line at some distance from the borehole, following by fractures from the borehole to this circular failure. This breakage pattern also has increased breakage around the borehole where the material is lifted further, leading to increased strain. It was not the shockwave that Livingston was observing but the effects of deeply confined charges.

Livingston also began the development of a new theory of failure of materials, which was not based strain but on energy transfer. This energy transfer theory was not only to look at the total magnitude of pressure or stress on an object but also the time that this stress was applied (Livingston C. , 1956). For example, phenomena such as "creep" and "relaxation," which are slow moving deformation and strain of objects, which depend on a large amount of time and lower stresses (Jeremic, 1994).

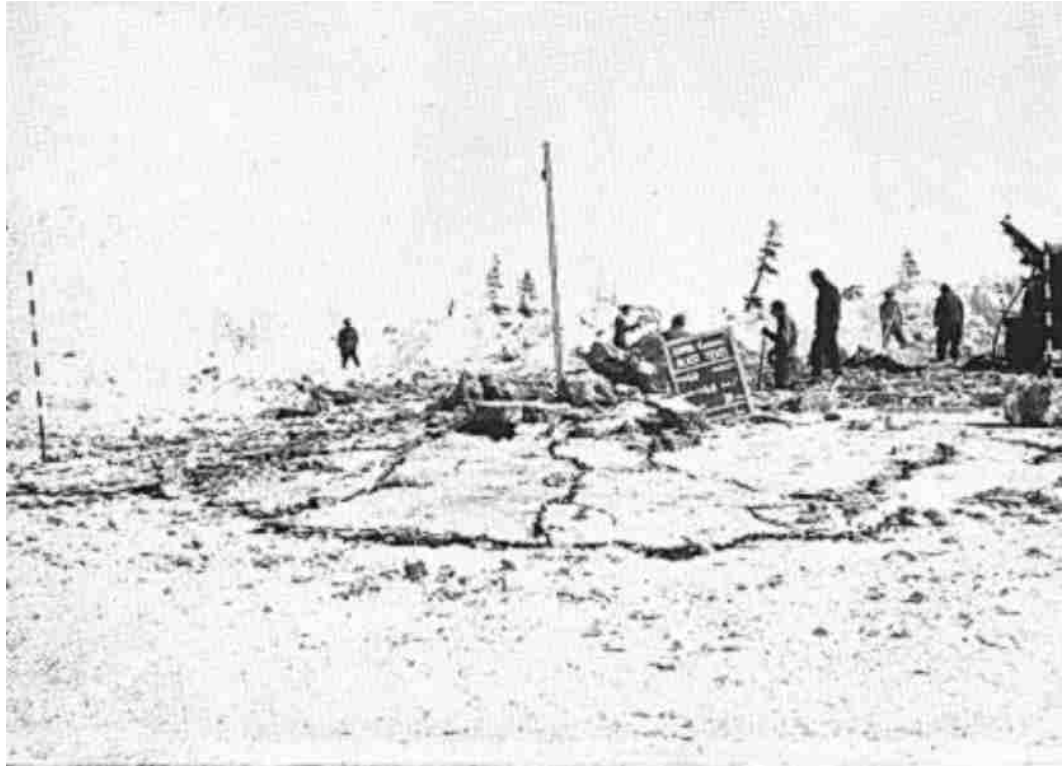


Figure 2.4 - Crater after Livingston (erroneously) showing shock breakage (Livingston C. , 1956)

As the speed of loading decreases from years to minutes, the properties of the rock change and a much larger stress field is required to cause breakage (Goodman, 2014). Livingston then states, “The hypothesis advanced here is that failure of solids is dependent upon energy transfer, and that fundamentals of energy transfer do not differ greatly for solids, liquids, and gases.” Therefore, as the time of loading was decreased to milliseconds or microseconds the rock needed very large stresses to cause sufficient strain to facilitate breakage. This idea is also contrary to the shock energy causing breakage as a large pressure is exerted over a very short range of time; which contributes to approximately 5% to 15% of the total energy of the explosive (Person, Holmberg, &

Lee, 1994). Livingston's two theories, the shock breakage of rock and energy transfer, directly disputed each other.

However, at this time the Livingston crater theory was the new method, which was quickly put into use through the Livingston crater theory equations. The base Livingston crater theory used a strain-energy factor, which was dependent on the explosive and material being blasted, to determine the maximum depth of burial that breakage would be obtained. However, this widely varied and had to be determined through experimentation for each rock type, structural region at a mine, and explosive type. Case studies of this show that this was a complicated process, which resulted in lengthy on-site studies and was entirely empirical based in application; relying minimally or not at all on his base theoretical assumptions (Bauer, Harris, Lang, Preziosi, & Selleck, 1965).

2.3.2.2. U.S. Bureau of Mines Cratering Theory. Livingston's research acknowledged the fact that the gas pressure played an important role in the rock breakage process, further facilitating breakage and leading to throw of material. However, others took his new theory and began studying this new field of shockwave breakage. Perhaps the most famous of this research was that of Duvall et. al. (Obert & Duvall, 1949; Obert & Duvall, 1950; Duvall W. , 1953; Duvall & Atchison, 1957; Duvall & Petkof, 1959), which was instantly spread and accepted, as these authors were part of the U.S. Bureau of Mines researchers.

Basing their research off Livingston's earlier work, crater formation was observed from both holes vertically drilled into the rock mass and horizontal holes drilled into a face with a bench off the side to observe directionality of breakage from the charge with

variations to the scale depth of burial of the charge. This carried on the same errors that were present in the Livingston research, including the spherical charge assumptions and misdiagnosis of breakage patterns.

Throughout nearly a decade of this research dozens of configurations of craters was shot in various rock types. It was noted that in each case that when the depth of burial was large enough that the gas could not break through and throw rock on the surface, that breakage occurred near the surface. This was thought to be the shockwave breaking along the surface after the effects of gas had been minimized, leading researchers to believe that the shockwave was the primary breakage mechanism. This theory was further propagated to assume that since the shockwave causes breakage at deep burial, that when the burial is reduced to see gas effects, the shockwave had much larger effects (Leet, 1960). In all reports of this time it was noted that the breakage from this deep burial was minimal compared to actual breakage when the depth was reduced, and the gas pressure could perform work on the rock. This was a confusing topic at the time for many engineers and researchers not involved, as they believed the U.S. Bureau of Mines but noted that in many situations topics such as stemming of a borehole, which increased gas pressure but did not have any effect on the shockwave, were extremely important for rock breakage (Johnsson & Hofmeister, 1961; Ash R. , 1963a; Ash R. , 1963b).

2.3.2.3. Shockwave Spallation Theory. Concurrently with the Duvall and Atchison work, Hino was working on the theoretical proof of the shock breakage theory. At this time, high-speed photography was just being invented, which could capture these breakage mechanisms.

The basis of Hino's research was founded on observing columns of concrete, which contained a charge on one side (excerpt from his book shown in Figure 2.5). Hino then observed how the column broke to prove the existence of the shockwave. From studying under Livingston, Hino understood that for the shock breakage theory to be true a spallation, or breakage from the side away from the charge, needed to be observed. Hino ran his experiment and found this to occur; combining this high-speed proof and using Livingston's previous work Hino then developed his Shock Breakage Theory (Hino, 1959).

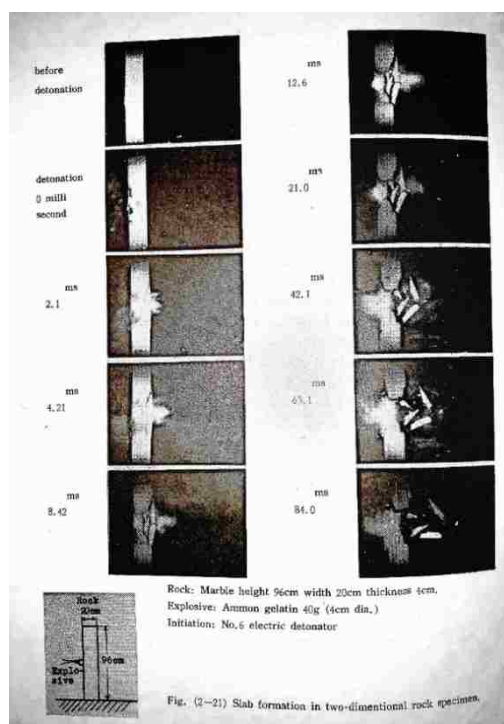


Figure 2.5 - Hino research on unconfined charges

Hino then concluded that a blast functioning under the shock breakage theory would have the following breakage mechanisms:

- (1) The detonation of an explosive produces a crushed zone around it so far as the intensity of shock wave produced by an explosive is greater than the compressional strength of the rock
- (2) Beyond the crushed zone there can be no breaking by compression due to shock wave, however, the shock wave is reflected as a tension wave at a free face. As the tensile strength of rock is much smaller than the compressional one, rock can be broken by this tension wave, the range of breaking extending from a free face inwards to the center of the charge.
- (3) Only a part of the total energy of an explosive goes into shock wave and the gases from detonation at high pressure expand doing additional work against the resistant force of rock and against inertia of the big mass of rock previously detached by shock wave from the ground. However, the contour of the crater in time and space is primarily determined by shock wave.

This new theory overstated the shockwave from the explosive as the major breakage mechanism in rock blasting and that the gases simply moved the broken rock forward. This was radically different than previous schools of thought on rock breakage. However, Hino had a few major problems with his experimental set-up and the accompanying theory.

- (1) The burden Hino used for his columns was approximately 15% of what is used for that charge load in mine and quarry blasting. This error in improperly scaling the charge to match the burden led to an overestimation of the shockwave breakage mechanism. While this uncovered that the shockwave was a breakage mechanism at a significantly reduced burden, it did not prove

that the shockwave was a major breakage mechanism at normal burdens in field blasting.

- (2) Hino's research solely used unconfined explosive charges, where the pressure from the gas is not withheld and was applied to the models. Therefore, it could not be proven that the shock breakage was greater than the gas pressure. Furthermore, with having to have a reduced burden to see the shock breakage occur, it is likely that had this been a confined charge, the gas pressure would have blown the model apart and across the room.
- (3) In Hino's proof of the shock breakage through compression around the borehole (to generate the crushed zone) he takes into account attenuation of the shockwave as it moves through the rock, assuming decay factors that are favorable to the shock breakage argument. However, when Hino calculates the maximum pressure from an explosive charge, he generates a detonation pressure of 550,000 psi. Hino then uses the lowest compressional strength for granite on record to show that this would be sufficient to break out to 4.76 charge diameters under compression.
- (4) Hino is using the static compressive strength of granite, the dynamic compressive strength of rock is typically much higher, where minimum dynamic compressive strength of granite is around 58,000 psi (Qian, Qi, & Wang, 2009; Livingston C. , 1956). This would change the crushed zone to a maximum of 3 charge diameters for breakage under compression, which in typical design accounts for less than 10% of the total burden.

- (5) The crack speed of rock is 20% to 30% of the sonic velocity of the rock. If crack tips are not stressed, they will not continue to grow. By the time the cracks are one charge diameter away from the charge, the shock wave would be 3 charge diameters away; causing no breakage to occur further out. This would reduce the range that the shockwave could effectively break in compression to less than one charge diameter due to the stress duration on the crack tips.
- (6) Hino also did not consider the attenuation of the shockwave as it moves through a medium, losing energy both due to an increased volume it effects and losses caused by friction (Cole, 1948). Using Hino's graphs (Figure 4-1, page 98) and the attenuation at a typical burden which is used in rock blasting with commercial explosives, the shockwave would have a magnitude below 1000 psi when it reaches the free face. Further work has shown that the attenuation of the shockwave in rock is much greater than Hino predicted and would result in minimal shockwave pressure reaching the face (Spathis & Wheatley, 2016).
- (7) Hino updates the Livingston cratering theory with the shock breakage model to develop design equations for a 90° conical crater. His powder factor for this crater is 8 pounds per cubic yard; where traditional rock blasting would be between 0.5 lbs/cyd and 2.0 lbs/cyd.

Later in his work Hino states that “only a part of the total energy available of explosive goes into shock and a bigger part of it is consumed as work done by expansion of gas.” At the end of his theory Hino states that a much larger portion of the energy goes

into gas than into the shock breakage; yet at the time he was trying to justify the understanding of the day and developed a bias in his experimentation and further analysis.

2.3.2.4. Strain Wave Theory. The work by Livingston, Duvall et. al., and Hino was then developed into the Strain Wave Theory by Starfield (Starfield, 1966; Ben-Dor & Takayama, 1992). This theory extended these principles and stated that crater formation is solely based on the shock (strain) wave that is generated by the explosives and that gas breakage is a minimal factor. This theory also introduced Hino's work on slabbing as the primary mechanism of rock breakage in this crater formation. This theory was based on a series of theoretical craters that was physically tested, these craters are:

1. A gas crater which is formed through the effect solely of gas pressure
2. A strain crater which is formed through the effect solely of the strain wave
3. A combined crater which is formed from both the gas and strain crater

Starfield then theorized that if a strain wave crater could be fired without effects of the gas crater, and this showed breakage at a depth deeper than the combined shock and gas crater then it could be assumed that the strain wave was the primary breakage mechanisms.

This was the same conclusion as the Duvall et. al. work, where the breakage was mis-interpreted for studies ranging over a decade. Further authors later attempted to expand the Strain Wave Theory including for application at weak seams and joints in the rock mass. The Strain Wave Theory was widely refuted through its existence for inability to match field conditions and improper theoretical development. Large grant funding went into proving the theory; however, it was never successfully proven.

2.3.2.5. Refutation of the application of shockwaves in blasting. These theories and research were heavily disputed based on several inconsistencies, including the inability to use with ANFO explosives (Ash R. , 1974), the inability to have a true shockwave nature even in high shockwave producing explosives (Cook M. A., 1974), and the inability to apply theory to real, practical blasting scenarios (Langefors & Kihlstrom, 1973).

The existence of the shockwave was not disputed, and further researched went into the understanding of how the shockwave affects the rock breakage process. Through a series of testing it was determined that the shock wave had a total of between 5% to 15% of the total energy of the blast (Persson, Lundborg, & Johansson, 1970). Model and full-scaled studies showed that breakage of the face in blasting did not occur from shockwave spallation in blasting but instead the first face movement occurred at five to ten times longer than it would take the shockwave to reach the free face (Persson, Ladegaard-Pedersen, & Kihlstrom, 1969; Noren, 1956). Further studies showed that for a typical borehole to experience shockwave spallation on the face, the borehole would have to be loaded to 8 lbs/cyd (5kg/m³) or higher depending on the rock type, over eight times the typical explosive load in rock blasting (Lang & Favreau, 1974; Persson, Lundborg, & Johansson, 1970). Typical loads for bench blasting are around 1lbs/cyd (0.6 kg/m³).

Researchers have utilized high speed photography with physical models to compare the effects of shock breakage with powder factors near 8 lbs/cyd (5kg/m³). Figures 2.6 through 2.10 contain previously unpublished photographs taken by Dr. Calvin J. Konya that show one of the time sequences of the physical models. These models are cubic blocks of plexiglass with a ruler put behind them to determine scale. When a

shockwave moves through plexiglass the density of the plexiglass is increased which results in a darkening of the area of the shockwave. This then allows for determination of the location of the shockwave.

Figure 2.6 shows this plexiglass model before any detonation has occurred. It can be seen that this model has a hole drilled directly into the center, which is filled with PETN explosives. The top of the hole is stemmed with molding clay to retain the gas pressure. Figure 2.7 shows the initial 'fire-in-the-hole' where the explosive begins to detonate. Figure 2.8 shows the explosive fully detonated, and the shockwave can be seen as a dark ring advancing from the hole. The breakage around the hole is not a result of the shockwave but is the gas pressure already breaking through the material. Figure 2.9 shows the moment the rebound of the shockwave and the spallation occurred, it can be seen that the spallation is very small, even when utilizing a burden of 15% of typical field loads, as was done in this experiment. Figure 2.10 shows the final frame before the model was blown apart, the internal breakage from the borehole outward is a result of breakage from the gas pressure and the external breakage on the walls is breakage from the shockwave spallation.

This simple model proves that when the burden of the blast is extremely small, around 15% of typical field burdens, some shockwave spallation may occur, but the magnitude of the spallation is minimal. When this occurs, it is also evident that the breakage from the gas pressure is extreme and would throw rock to a much greater extent than would be desired in practical application. This implies that the shockwave is a very minor breakage mechanism at powder loads much higher than what is utilized by industry today, and for typical blasting is not a breakage mechanism.

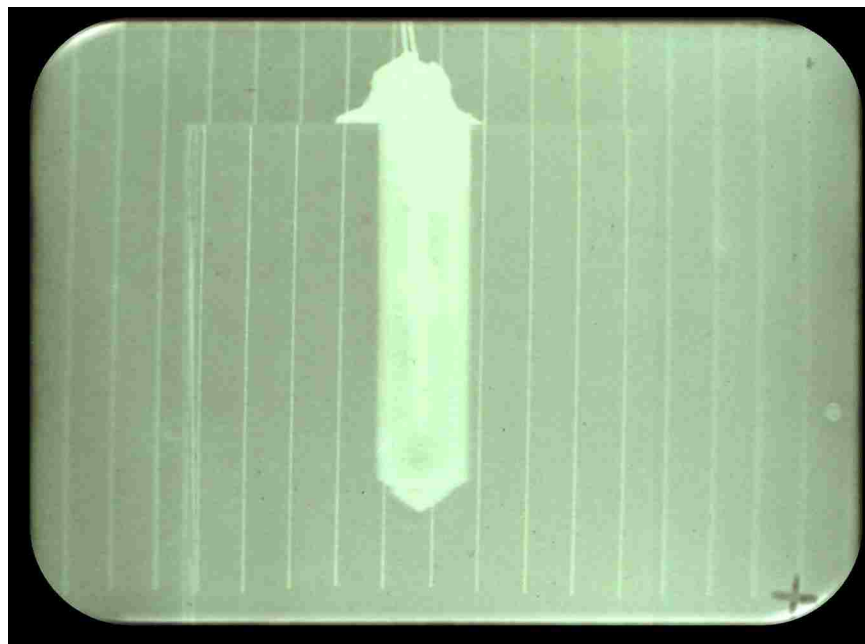


Figure 2.6 – Initial conditions of shockwave breakage model

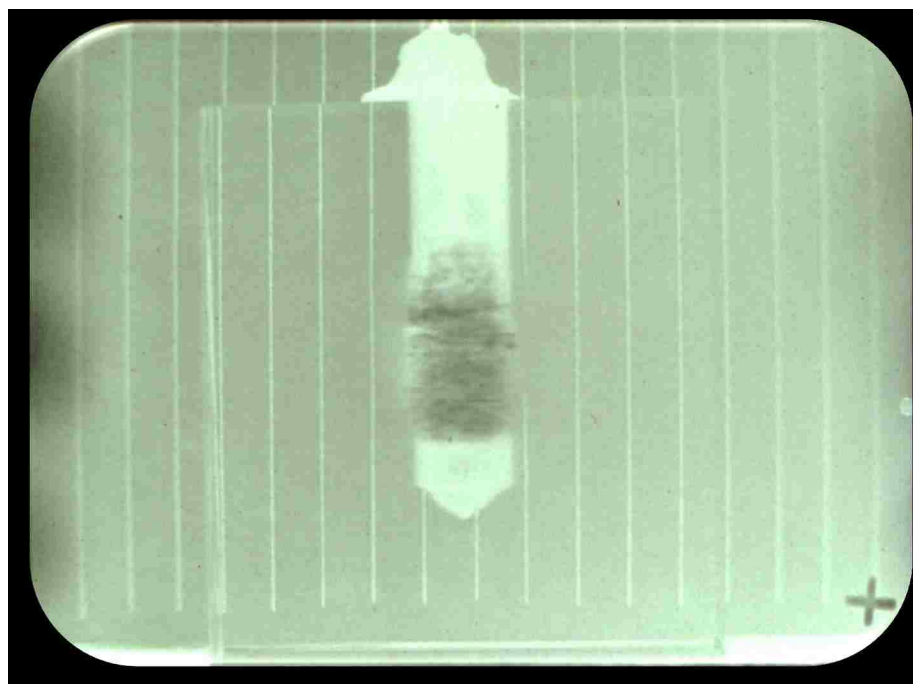


Figure 2.7 – Detonation for shockwave breakage model

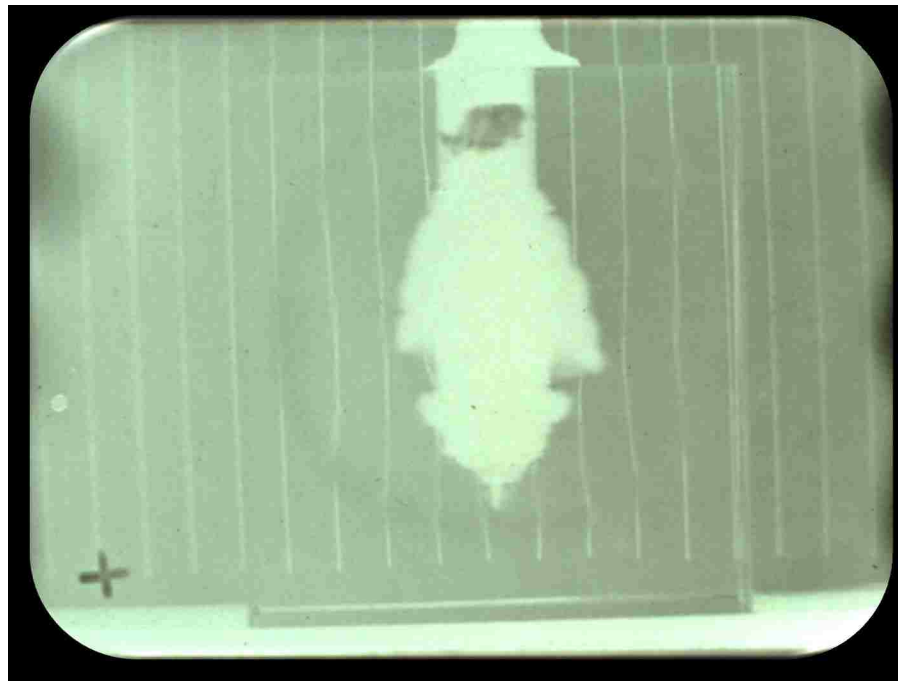


Figure 2.8 – Shockwave can be seen in plexiglass as darkened ring



Figure 2.9 – Shockwave spallation occurring at 15% of typical burden

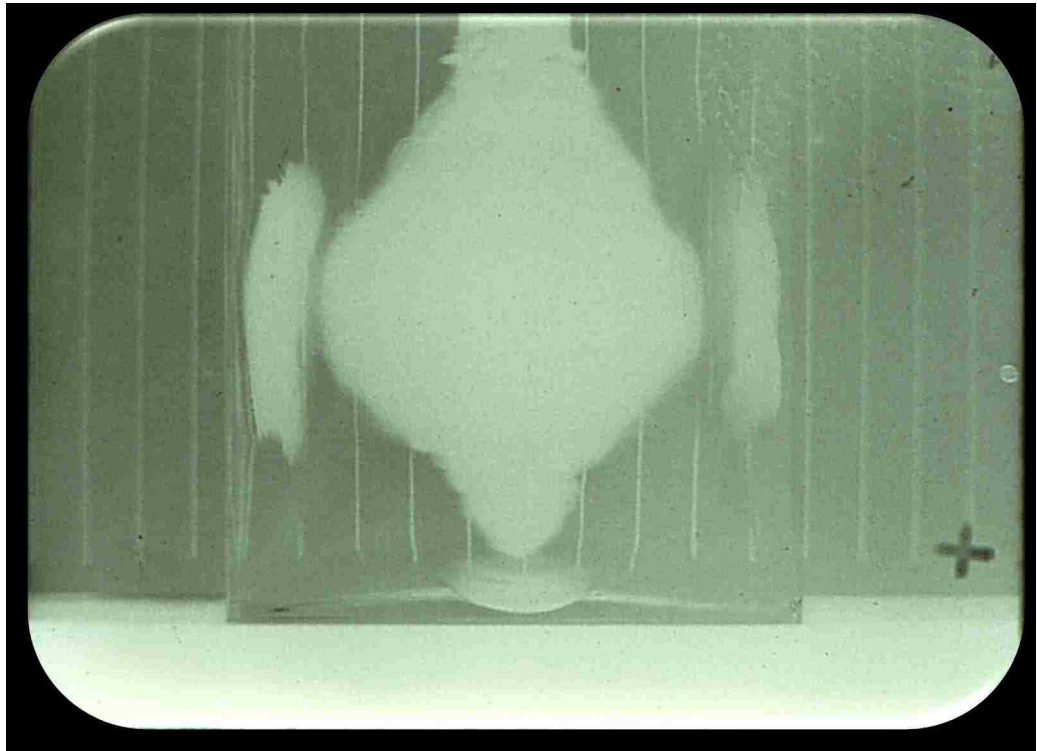


Figure 2.10 – Final frame of test series showing magnitude of gas breakage (internal) versus shock breakage (external)

2.3.3. Shockwave Theory and Mathematical Concepts. The first full theory of shockwaves from explosives was developed in the late 1800's to incorporate the concepts of the time, based on modifications to the acoustic laws (Mikhel'son, 1893). As new technology progressed, this theory was later updated (Rayleigh L. J., 1910) and expanded upon (Taylor G. I., 1939; Taylor G. , 1940a; Taylor G. , 1940b; Taylor G. I., 1950a; Taylor G. I., 1950b) to incorporate updates to the theory as additional research was completed including that of nuclear weapons. This theory is known known as Classical Shockwave Theory. Classical Shockwave Theory is still applied today in many situations as it presents an easy method of calculating parameters around a shockwave. It is also applied in many of today's Computational Fluid Dynamics models.

Classical Shockwave theory has been greatly expanded to incorporate numerous mathematical models for various materials and conditions. Modern shockwave theory has been thoroughly explained in other texts (Cooper, 1996; Zel'dovich & Raizer, 2002) and is beyond the purview of this dissertation. Instead this dissertation will focus on explaining the basic concepts of shockwaves and introducing the mathematical formula which will be used later in this discussion.

A shockwave is a wave which has a very rapid rise in pressure causing a compression in a material. This shockwave is followed by a decay of the wave, which is often discussed as a rarefaction wave. This shockwave can be formed in many ways including impacts, supersonic events, or detonations of explosives. The event causing the shockwave will determine how the shockwave is developed and the original and final form. Regardless of the formation, a shockwave is a wave that has a very large pressure and due to the large pressure travels faster than the speed of sound in the material.

Acoustical approximations can begin to be used to develop the principals behind a shock wave. The basis of this would then rely on a term known as Impedance (Z), which is presented in Equation 3.

$$Z = \rho V_s \quad (3)$$

where Z is the impedance of a rock in kilograms per square meter seconds, ρ is the density in kilograms per cubic meter, and V_s is the sonic velocity of the material in meters per second.

When a shockwave is travelling through one medium and hits a boundary between that medium and another, part of the shockwave is transmitted into the second medium and part of the shockwave is reflected back into the original medium traveling in

the opposite direction. For example, if a right moving shockwave in air hits a granite ledge, part of the shockwave will be transmitted into the granite as a right moving shockwave and part of the shockwave will be reflected in the air as a left-moving shockwave. The intensity of the shockwave which is transmitted or reflected can be calculated using equations 4 and 5, respectively (Worsey P. , 2016).

$$I_t = \frac{4Z_1Z_2}{(Z_1+Z_2)^2} \quad (4)$$

$$I_r = \frac{(Z_1-Z_2)^2}{(Z_1+Z_2)^2} \quad (5)$$

where I_t is the intensity of the shockwave transmitted, I_r is the intensity of the shockwave reflected, Z_1 is the impedance of the originating material, and Z_2 is the impedance of the receiving material.

The following discussion will focus only on those waves which are planar and interaction boundaries which are at a 90° angle. Furthermore, it will be assumed that at no point will a medium be defined as being thinner than the wavelength of the shockwave.

The pressure of the detonation wave can be estimated using the Chapman-Jouguet (CJ) pressure equation. While more advanced models have been given to determine the pressure to a more exact level, for explosives with a specific gravity of 1.0 to 1.8 a simplified equation has been proposed (Cooper, 1996) and will be used to estimate the detonation shockwave pressure for various explosives. This equation is:

$$P_{CJ} = \frac{\rho D^2}{4} \quad (6)$$

where P_{CJ} is the Chapman-Jouguet shockwave detonation pressure in GPA, ρ is the density of the explosive in grams per cubic centimeter, and D is the velocity of detonation in meters per second.

2.4. GAS PRESSURIZATION BREAKAGE IN COMMERCIAL BLASTING

Combustion, (fire), has been one of the fundamental principles that drove humanity out of the dark ages and to the top of the food chain (Harari, 2011). Aristotle and Heraclitus of Ephesus viewed combustion as the universal force of creation and these philosophers, along with humankind, pondered the phenomena of combustion (Jaffe, 1930). Originally it was believed that combustion was a special element that was found within materials, and it wasn't until the 1600s that scientific theory was applied to the thought of combustion. Fire was eliminated as an element and instead the Theory of Phlogiston was developed (Becher, 1667). The phlogiston theory stated that all material had a component, called phlogiston, which was released when the item was burned, as burning wood and other materials caused a loss in mass. This theory had many challenges brought on early, including that some compounds such as metals gained mass when burned, yet the theory was defended.

The concept of phlogiston and the misunderstanding of combustions and generation of gases led to researchers incorrectly attempting to quantify the force of propellants and explosives. The first published mention of the force of gunpowder stated that the force produced from gunpowder was due to increased elasticity in the air between grains of black powder, which was caused by heating as the gunpowder burned (Hire,

1702). At this time, it was believed that the pressure of gunpowder was approximately 75 psi.

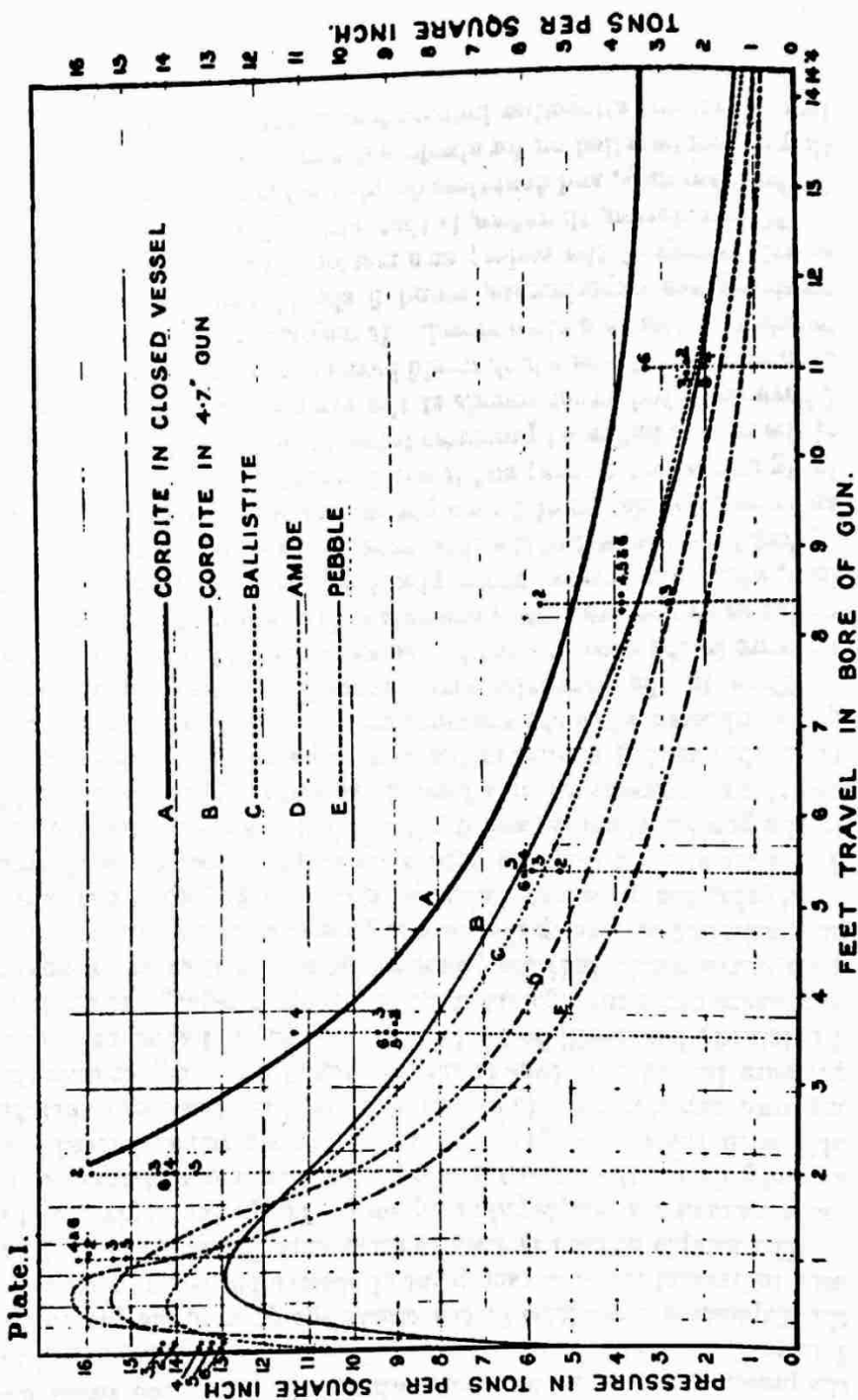
As understandings of combustion and gas generation advanced, new theories of the force of gunpowder emerged. The first concept of gunpowder forming gases was developed in 1743 (Robbins, 1743) where it was believed that black powder, when combusted, would turn into gas which would take up 236 times the original volume of the charge. It was then assumed with increases in temperature of these gases a pressure of 15,000 psi could be achieved in the bore of a gun. New research later showed that gunpowder could reach up to 30,000 psi (Hutton, 1778). The first direct measurements of the pressure associated with gunpowder were made using very small charges, typically under one gram, to fire projectiles of varying weights. With this experimentation it was determined that gunpowder could have a pressure of upwards of 426,182 psi with theoretical calculations of 1,485,600 psi (Count of Rumford, 1797).

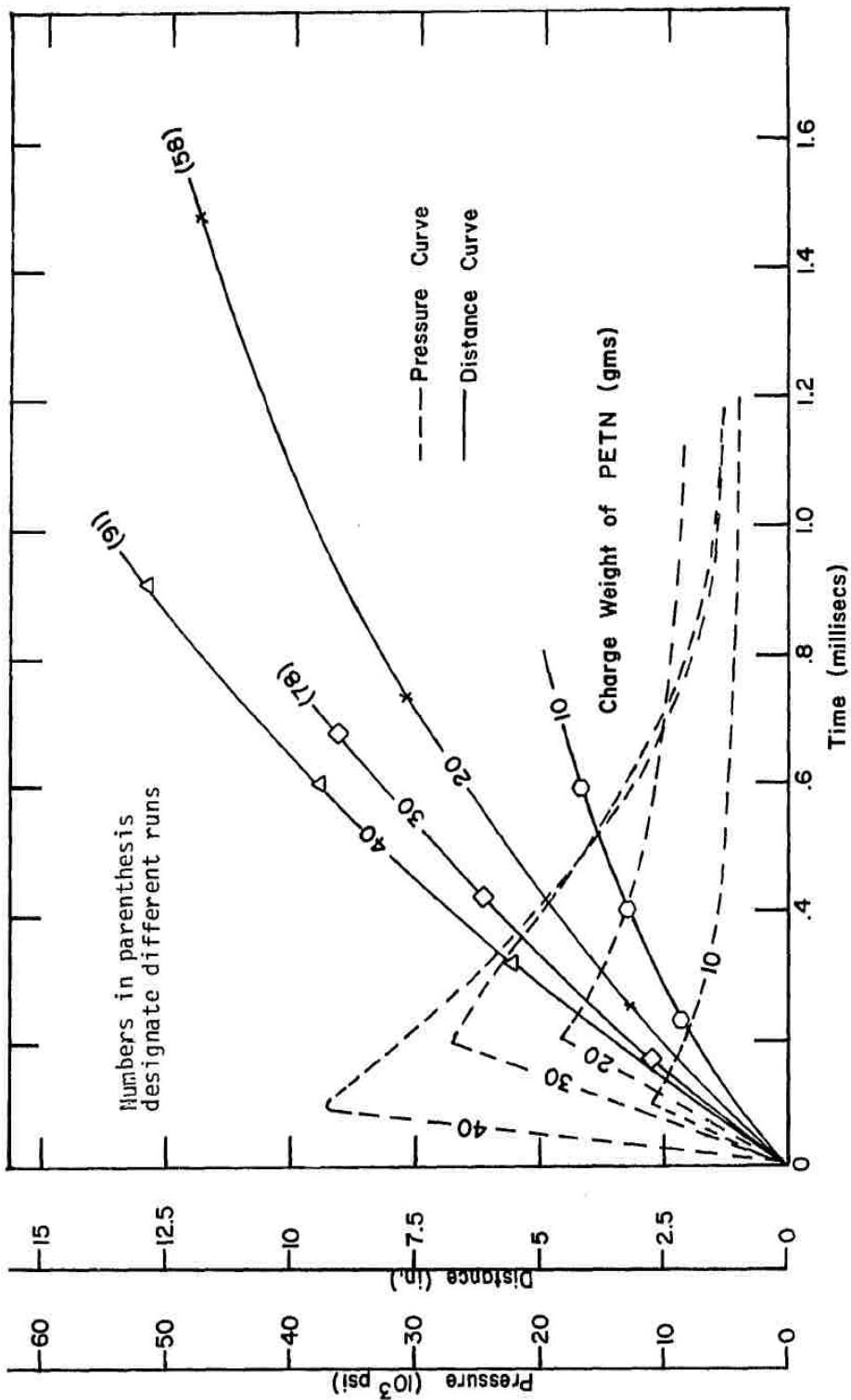
Theoretical and model testing of gunpowder continued with numerous authors making claims for the final products of the combustion and the pressures associated with gunpowder in the bores of guns. However, the majority of the work that can still be considered today to hold accuracy was completed by Sir Andrew Nobel in the late 1800s defining both the products of the combustion (Nobel & Abel, 1875) and the associated pressures (Nobel S. A., 1892). This testing concluded that in testing of artillery with Pebble Powder, Cannon Grade Black Powder, the pressure from 12 pounds of propellant was 31,800 psi, which is approximately 2,650 psi per pound or 6 psi per gram of black powder. A reproduction of Sir Andrew Nobel's graph is shown in Figure 2.11, which shows the pressure profile of black powder.

Work completed by Otuonye then advanced the understanding of pressure profiles of explosives, but this time the borehole dynamics and effects of pressure on stemming material was studied (Otuonye, 1981). This is the only research which has attempted to quantify the pressure inside of a borehole from a decoupled charge. The pressure profiles of the borehole filled with a decoupled charge of high explosives has many similarities to that of Nobel's work; with the main difference being the magnitude of the pressure. The high explosive produced much greater pressures than the low explosive. This research does not consider the shockwave, only the gas pressure in the device affecting these pressures. This shows that high explosives, due to a combination of the gases, rate of combustions, the temperature of combustion, and gas volume produced lead to an increase in borehole pressure. Figure 2.12 shows a reproduction of Otuonye's work and Table 2.1 has some of the results obtained by Otuonye for peak pressure based on charge weight. Otuonye's work is the only measurement of borehole pressures for a decoupled hole and will be relied upon for this work as no other data exists.

At this time, it had been shown that the variation of density of the explosive will affect the velocity of detonation and the total pressure developed in the bore. It was also understood at this time that depending on the speed of combustion the pressure profile could rapidly change, even when the same theoretical gas volume was produced in a certain diameter bore (Berthelot, 1892).

This work was proven theoretically and experimentally, and Table 2.2 is a reproduction of the table produced by Nobel showing pressure in both closed vessels and in a gun with variations in density and propellant type (Nobel S. A., 1892).





The theory for the actual pressure of the gas produced by explosives was also expanded from a theoretical standpoint. Another theory was that the differences in pressure between explosive types was the result of the different gaseous products that were formed from the explosives, which would change the total pressure due to the intermolecular forces (Quinan, 1912). This early work was known as dissociation and looked at the type of molecule developed in the detonation process and the effects of the high-density effects of the explosive gases. Sarran's Theory also added further to the development of gas pressure from an explosive charge by introducing the heat of the explosion (Sarran, 1884). While the magnitude of the heat of detonation was dramatically overemphasized in Sarran's work, it did give the explosive industry another tool to incorporate into explosive gas pressure models.

Low density gases can be accurately modeled using the ideal gas law, however for high-density gases, new equations of state needed to be developed. This is due, in part, to the fact that when a gas is at high pressure and high densities the co-volume of the gas begins to become a substantial part of the total volume. At extreme pressures the molecules are in contact or nearly in contact with one another and the pressure is then mainly due to the contact forces between molecules (Johansson & Persson, 1970).

2.4.1. Becker-Kistiakowsky-Wilson (BKW) Equation of State. Becker developed an early equation of state for the detonation gases, assuming that the co-volume was an exponential (Becker, 1922b; Becker, 1922a). His equation is:

$$P_e = \rho nRT_e [1 + b\rho e^{b\rho} - \alpha\rho^2 + \beta\rho^7] \quad (7)$$

Where P_e is the explosive pressure, ρ is density, n is number of moles, R is the universal gas constant, T_e is the temperature of detonation, and b is co-volume.

Table 2.1 – Measured peak pressure for PETN in borehole simulation device after Otuonye (Otuonye, 1981)

Weight of PETN (Grams)	Maximum Pressure (PSI)
10	9,000
10	11,000
10	10,000
10	10,000
20	19,500
20	17,000
20	18,000
20	15,000
20	19,500
20	19,500
20	19,500
20	13,500
30	27,000
30	28,000
30	27,000
30	26,000
30	27,000
30	25,000
30	30,000
40	37,000
40	37,000
40	36,000
50	50,000
50	51,000

Table 2.2 – Pressures from propellants pressure edited to psi (Nobel S. A., 1892)

Peeble Power			Amide Powder		
Density	Pressure (PSI)		Density	Pressure (PSI)	
	Closed Vessel	Gun		Closed Vessel	Gun
0.65	35,360	31,640	-	-	-
0.6	31,100	29,100	-	-	-
0.55	27,240	23,680	0.55	51,000	31,000
0.5	23,700	18,620	0.5	44,000	27,500
0.45	20,460	16,240	0.45	38,200	24,200
0.4	17,460	14,000	0.4	33,000	20,000
0.35	14,700	12,220	0.35	28,000	16,680
0.3	12,140	10,420	0.3	23,800	14,100
0.25	9,760	8,400	0.25	19,600	11,760
0.2	7,540	5,900	0.2	15,500	9,100
0.15	5,460	3,640	0.15	10,000	6,200
0.1	3,520	1,400	0.1	7,100	2,640
Ballistite			Cordite		
0.26	41,600	26,900	0.26	43,500	25,000
0.24	38,000	25,400	0.24	39,600	23,900
0.22	34,200	23,660	0.22	35,600	22,560
0.2	30,600	21,540	0.2	32,000	21,200
0.18	26,800	19,500	0.18	28,400	19,700
0.16	23,400	17,400	0.16	24,600	18,200
0.14	20,000	15,000	0.14	21,000	16,320
0.12	16,800	13,040	0.12	17,400	14,160
0.1	13,200	10,580	0.1	14,200	11,400
0.08	10,000	8,160	0.08	10,800	8,020
0.06	7,000	5,080	0.06	7,600	4,660
0.05	5,600	3,280	0.05	6,000	3,140

The terms α and β were empirical constants to be determined by experimentation. These were later determined to be 0.25 and 0.3, respectively (Kistiakowsky & Wilson Jr., 1941a). The last two terms of Becker's equations are the terms for the long-range interaction forces between molecules and later were removed from the calculation. This equation was also updated to include temperature as an explicit variable (Kistiakowsky & Wilson Jr., 1941b; Brinkley & Wilson Jr., 1942). This resulted in the development of Equations 8 and 9:

$$P_e = \rho n R T_e [1 + x e^{\beta x}] \quad (8)$$

$$x = \rho k (T + \theta)^{-\alpha} \quad (9)$$

where P_e is the explosive gas pressure, ρ is the density of the explosive, n is the moles of gas, R is the gas constant, T_e is the temperature of detonation, and β , k , θ , and α are all experimentally determined constants. It has been suggested that acceptable values for these constants are $k = 1$; $\theta = 0$; $\alpha = 0.25$; and $\beta = 0.3$.

These variables are all experimentally determined constants. It was later shown that these constants vary based on the explosive being utilized and experimentation is needed to validate the best fitting set of constants (Mader, 1963). This equation of state of determining the explosive pressure became known as the Becker-Kistiakowsky-Wilson (BKW) Equation of State.

This Equation of State is an older, empirical equation which has recently fell out of literature due to more advanced models which do not use empirical constants.

2.4.2. Cook's Equation of State. The work of Nobel and Abel was adapted to determine a pressure equation based on the co-volume and termed "Abel's Law" (Nobel & Abel, 1875; Cranz, 1926). Dr. Cook added to, then modified this based on Van Der

Waals equation of state, assuming that the co-volume was a function only based on density (Cook M. , 1947; Cook M. , 1958). This developed the Cook Equation of State shown in equations 10 and 11:

$$P_e = \frac{\rho n R T_e}{[1 - \rho * b(\rho)]} \quad (10)$$

$$b(\rho) = e^{-0.4\rho} \quad (11)$$

where b is the co-volume of the gas mixture, which Cook assumed to be a function of only density, P_e is the explosive gas pressure, ρ is the density of the explosive, n is the moles of gas, R is the gas constant, T_e is the temperature of detonation.

2.4.3. Taylor's Equation of State. Taylor developed an equation of state for the detonation gases based on the Maxwell-Boltzmann's kinetic theory and Boltzmann's virial expansion theories. In this way, Taylor's equation of state utilized the mean co-volume of all gas produced in the detonation and was then only a function of temperature. This explosive pressure model is considered a simple to use model that is typically not as accurate as other models but can easily be used when complex, extremely accurate calculations are not required. Taylor's equation is presented in equation 12:

$$P_e = \rho n R T_e [1 + b\rho + 0.625b^2\rho^2 + 0.287b^3\rho^3 + 0.193b^4\rho^4] \quad (12)$$

where b is the co-volume of the gas mixture, which Cook assumed to be a function of only density, P_e is the explosive gas pressure, ρ is the density of the explosive, n is the moles of gas, R is the gas constant, T_e is the temperature of detonation.

2.4.4. Outoynne-Skidmore-Konya (OSK) Equation of State. Outoynne et. al analyzed explosive pressures from PETN and commercial explosives in both model scale and full scale blasts looking to quantify borehole pressures and develop an equation of state to match real pressures generated from commercial explosives (Otuonye, Skidmore,

& Konya, Measurements and Predictions of Borehole Pressure Variations in Model Blasting Systems, 1983). This method began with a basic analysis of the chemical combustion of the explosive, mainly the gases which are produced as a result of combustion. It was typically assumed that the product was oxygen balanced or fuel-rich, not containing enough oxygen to convert all carbon to CO₂ and did not considered oxygen-rich explosives. The enthalpy of the reaction can then be calculated using equation 13:

$$Q_e = n_{H_2O} \lambda_{H_2O} + n \int_{T_0}^{T_a} C_p dT \quad (13)$$

where Q_e is the heat of explosion in KJ per mole, n is number of moles, λ is the thermal conductivity, C_p is the Specific Heat at constant pressure, and T is the temperature in Kelvin.

The OSK system then calculated the temperature of the explosion using equation 14:

$$T_e = \frac{Q_e}{\sum n_i C_v} + T_1 \quad (14)$$

where T_e is the temperature of the explosion in degrees Kelvin, Q_e is the heat of explosion in kilojoules per moles, n is moles of a specific gas, C_v is Specific Heat at Constant Volume of a Specific Gas, and T_1 is set at 298° K. For equation 12, T_1 is a constant which is set equal to 298 K.

This developed the first assumption of temperature, which would be used to then individually calculate the n_i and C_v for each gas product and then the system would be re-run to develop a second temperature. This simulation would occur until the variations in the temperature between runs was within appropriate error.

Following the determination of the explosive temperature, the explosive pressure could be calculated using equation 15:

$$P_e = \frac{N_g RT_e}{V_e - \alpha} \quad (15)$$

The specific volume of explosive gases could be calculated using equation 16:

$$V_e = \frac{1}{\rho} \quad (16)$$

where P_e is the explosive gas pressure in atmospheres, N_g is the moles of gas per kilogram, R is the universal gas constant, T_e is the temperature of detonation, V_e is the specific volume of the explosive gases in liters per kilogram, and α is the co-volume factor in liter per kilogram, and ρ is the density of the explosive.

2.4.5. Theoretical Borehole Pressure Calculations. All the previously presented explosive pressure equations are for determination of the explosive pressure when the gas is at the same volume as the original charge. However, the interest for the application of presplitting with decoupled charges is not in the explosive pressure at the diameter of the original charge, but instead the explosive pressure with the gases filling the entirety of the borehole. In the past some rudimentary methods have been proposed to determine the borehole pressure, but most have lacked through analysis of the average compressibility of the gas mixture.

Methods of calculation are presented in the OSK Equation of State for determination of the pressure in the borehole. This has been proposed as an acceptable method for use with decoupled charges. This is presented in equation 17:

$$P_g = \frac{Z_c nRT}{V_b} \quad (17)$$

where P_g is the borehole pressure in psi, Z_c is the compressibility, n is the moles of gas, R is the universal gas constant, T is the temperature in Kelvin, and V_b is the borehole volume in liters.

Under this method it is assumed that there is no loss in temperature, thus $T = T_e$. Equations 18 and 19 will also need to be utilized to find the reduced temperature and reduced pressure of the process.

$$T_r = \frac{T}{T_c} \quad (18)$$

where T_r is the reduced temperature, T is the temperature of the gas in Kelvin, T_c is the critical temperature in Kelvin.

$$P_r = \frac{P}{P_c} \quad (19)$$

where P_r is the reduced pressure, P is the gas pressure in psi, P_c is the critical Pressure in psi.

The compressibility then is solved through a process of simulations, where the initial pressure is assumed to develop the first reduced pressure and reduced temperature. The total mixture of reduced temperature and reduced pressure can then be calculated, and compressibility curves can be used to calculate the compressibility (Wark, 1988). The chamber pressure can then be updated with the new compressibility and the process begins again, running multiple simulations until a steady state is obtained.

2.5. PRESPLITTING

The mechanisms of production rock blasting are critical to understand because the same forces that apply to rock blasting also apply to presplit blasting. The ways an explosive applies force and causes breakage to a rock do not change. Just as controversy

existed in the mechanisms of a production blast, the theories behind a presplit mechanism have not been well defined and relatively few studies have been completed on presplit formation. In today's blasting industry both shock breakage (Zhang, 2016) and gas pressurization of the borehole (Konya & Konya, 2017a) is presented in modern technical papers as mechanisms of presplitting. Many have also argued that the mechanism behind the presplit is unimportant or academic, which may be true for the traditional case of presplitting, which remains the same under almost all circumstances. However, with the advent of Precision Presplitting the mechanism behind a presplit is of importance, as changes to dimensions such as the spacing of boreholes and explosive load in a hole are designed to meet the structural geology and rock properties. Without an understanding of the mechanisms behind a presplit formation, a strategic design to eliminate overbreak while allowing for smooth breakage is impossible.

The first large scale explosive presplit was produced on the Niagara Power Project, which was completed in 1962 (Paine, Holmes, & Clark, 1961; Paine, Holmes, & Clark, 1962). This project was based in dolomite and limestone with a single layer of shale near the bottom of the excavation. It was required to have smooth walls to pour concrete against. During the project, numerous methods of controlled blasting were attempted including line drilling, line drilling with explosive loads in every third hole, modified cushion blasting, decks of dynamites throughout the borehole, and finally presplitting. It was reported that the only method that produced satisfactory results to minimize overbreak was the presplitting, which was accomplished by taping 1 ¼" by 4" sticks of dynamite on Primacord every 12 inches. The boreholes were 2 ½" to 3" in diameter, spaced 24 inches apart and stemmed with crushed gravel. This resulted in an

increased rock excavation rate and a reduction in scaling by a factor of 10. Additionally, the project had significant savings on concrete costs and increased safety as the walls were cleaned smooth (Paine, Holmes, & Clark, 1961). Following the project presplitting was widely accepted as the best and most cost-effective method of overbreak control.

Based on this work, researchers of presplitting both in a laboratory and in a practical setting began looking into the decoupling of charges, or the reduction of the diameter of the explosive compared to the diameter of the borehole. This was done to decrease the dynamic gas flow on the borehole wall and to reduce the gas pressure in the borehole (Konya, Britton, & Lukovic, 1987) preventing large compressive strengths which would lead to overbreak (Day, 1982). However, this increase in decoupling ratio also led to minimal shock pressure transmission into the rock mass due to large impedance mismatches between explosives and air, then air and rock.

With the large increase in research of shock breakage in rock blasting, many authors began to investigate possible effects of shockwave collision between boreholes to develop tensile zones and causing presplit formation (DuPont, 1975; Crosby & Bauer, 1982). This theory was widespread due to the popularity of the DuPont Blasters Handbook, and it is still circulated amongst many leading organizations today (International Society of Explosive Engineers, 2016) and researchers (Salmi & Hosseinzadch, 2014). This theory was heavily disputed and shown in numerous studies of the day and it was shown that no correlation exists between the dynamic shockwave and the presplit formation, with numerous studies showing that the quasi-static gas pressure in the borehole was responsible for presplit formation (Konya C. , 1973; Worsey P. , 1981; Worsey, Farmer, & Matheson, 1981; Daehnke, Rossmanith, & Kouzniak, 1996).

Additional studies were conducted utilizing a propellant charge, Pyrodex, to fire a presplit blast. These propellant charges produce no shockwave, as they deflagrate, not detonate (Akhavan, 2011), which completely isolated the gas pressure as the only working energy. Using the same principles as in traditional presplit design (Konya C. , 1980), the propellant charges produced the exact same results as a presplit blast that was fired with detonating explosives (Konya, Barret, & Smith, 1986). This proved that presplit mechanisms on a full-scale blast had no reliance on the shockwave generated by detonating explosives.

This led to the development of a Precision Presplit style of blasting, where extremely light loads of detonating cord are utilized to prevent all breakage around the borehole while forming the presplit fracture (Konya C. , 1982). This design utilized closely spaced boreholes of 24 inches or less to minimize the impacts of rock structure on the presplit (Worsey P. , 1984; Worsey & Qu, 1987; Tariq & Worsey, 1996). As this design methodology has begun widespread use, new empirical research into the explosive loading based on the rock properties has been developed (Konya & Konya, 2015; Konya & Konya, 2017b; Konya & Konya, 2016).

This method of Precision Presplitting has effectively zero shock energy to form a fracture after accounting for impedance mismatches (Cooper, 1996), non-ideal detonation (Cook M. A., 1974), and attenuation of the shockwave in the rock mass (Spathis & Wheatley, 2016). It has then been theorized that the mechanism behind the presplit formation is due to large hoop stresses which are generated between the boreholes causing a fracture, with no advancement of the fracture from gas penetration (Konya & Konya, 2017a). The hoop stress field for a thick-walled pressure vessel has been one

proposed method for the determination of the stresses from the gas pressurization of the borehole, using the spacing between boreholes as the thickness (Konya & Konya, 2017a).

This is shown in equation 18:

$$\sigma_c = \left[\frac{p_i r_i^2 - p_o r_o^2}{r_o^2 - r_i^2} \right] - \left[\frac{r_i^2 r_o^2 (p_o - p_i)}{r^2 (r_o^2 - r_i^2)} \right] \quad (18)$$

where σ_c is the circumferential hoop stress in psi, p_i is the internal pressure in psi, r_i is the internal radius in inches, p_o is the external pressure in psi, r_o is the outside diameter in inches, and r is the distance the stress is being analyzed at in inches.

These hoop stresses are concentrated towards areas of least thickness and in normal rock blasting this is the free face. However, in presplitting when the burden is essentially infinite in all directions, these hoop stresses cannot act to the free face and instead concentrate between boreholes. Therefore, the mechanisms of presplitting (Konya & Konya, 2017a) are:

1. The explosive detonates, causing a shockwave to propagate into the rock. This shock wave may cause initial micro-fractures on the borehole wall. This shockwave is of insufficient magnitude to cause major fracturing of rock, and with the almost infinite burden, will not cause any tension spalling.
2. The gases within the borehole begin to expand, putting a pressure on the borehole walls. With the proper explosive load, this pressure will cause hoop stresses to form between two boreholes, causing a fracture to form.
3. The expanding gases will extend into the fractures, causing an opening of the fractures and expansion of the fractures to the drilling surface as the gas begins to blow-out.

4. If the proper amount of explosive and stemming is used, the explosive will blow the stemming out of the borehole and the gas pressure will be released through the top of the borehole (Choked Flow Gas Theory)

By analyzing the steps of a presplit, one can quickly begin to see the importance of many variables including:

1. Explosive Load – this will directly influence the total gas pressure inside of the borehole. The large gas pressure in the borehole can lead to overbreak around the hole through various mechanisms, including:
 - a. A fractured zone due to too great a gas pressures (compressional breakage) if no free face is available
 - b. Too large of a gas volume to easily flow through the borehole, leading to failure at the crest (cratering) and enlargement of cracks
 - c. Too little of an explosive load can also be a problem, as insufficient gas build-up will not form large enough hoop stresses to fracture from borehole to borehole.
2. Stemming – If the stemming creates a stemming plug (Konya & Walter, 1990) then the stemming will lock into the borehole. This will cause the highly pressurized gases to:
 - a. Crater the borehole, causing backbreak at the top of the resulting face
 - b. Open and expand cracks, potentially causing additional breakage or opening existing cracks, joints, or bedding planes.

- c. If the stemming is insufficient to momentarily hold the gas pressure, the pressure inside of the borehole will be of insufficient magnitude to form a large hoop stress, resulting in no fracture between boreholes.
3. Spacing – if the spacing is too large, the hoop stresses will be insignificant to cause the proper fracture to form resulting in a rough face. If the spacing is too small, the hoop stresses will be so large that additional fracturing will occur extending outward from radial cracks and multiple radial cracks will connect between blastholes

2.5.1. Traditional Presplitting. Traditional Presplitting will be defined as a method of presplit blasting which utilizes presplit powder, or other explosives, in which the load in the borehole is, at minimum, 0.30 pounds per foot. The typical case of traditional presplitting would be using a 7/8” presplit powder, which has a load per foot of 0.3 lbs/ft of borehole length, a spacing of 36” (3 feet), and a stemming length of 30” (2.5 ft). These presplits can have the charge weight expanded and/or the spacing increased or decreased. The traditional presplitting techniques have not incorporated geologic factors into the design criteria and instead rely on basic rules of thumb for the design.

These rules of thumb are shown in Equations 21 and 22 (Konya & Walter, 1990):

$$EL = \frac{d_h^2}{28} \quad (21)$$

$$S = 10d_h \quad (22)$$

where EL is the explosive load in pounds per foot, S is the spacing in inches, and d_h is the diameter of the borehole in inches. The constant in the equation 22 can be modified and typically falls between 8 and 14 but is set as 10 for the first test blasting in an area.

In the past, changes to the design of a traditional presplit were based on the split-factor, which is the load per square area of face. A blaster may have a presplit that works in a certain situation and attempt to increase the explosive load and modify the spacing. The blaster would then compute how many pounds of explosive were being used to split a certain square footage of wall. They would then assume that this split-factor would hold for presplitting that rock type and change the spacing between boreholes based upon changing explosive weight to fit the split factor. This improperly assumed that the relationship was linear and was known to perform very poorly for design purposes, except in rare cases. Recent work has shown that the function is not linear, and it has been shown why split-factor was a poor method of design (Worsey P. , 1981; Konya & Konya, 2017a).

2.5.2. Precision Presplitting. Precision Presplitting is a method of presplitting which utilizes extremely light charge loads, along with the borehole spacing and rock properties to develop a design which will cause a fracture to form without overbreak. The spacing of the borehole will be a function of the desired control, the structural geology, and the cost of blasting.

This method is commonly used in weak, or heavily jointed rock where normal presplit blasting does not work. This method of presplitting uses the proper amount of explosive load to cause a smooth fracture to form between boreholes, without causing overbreak or excessive shattering of the wall.

In previous years, Precision Presplitting utilized 18” to 24” spacing and the explosive load was determined through test blasts. These test blasts would be detonated, and the back wall would be exposed. It then took an experienced engineer or blaster who

has worked extensively with presplitting to determine what explosive load was ‘optimal’ for the presplit. If the proper explosive load was not used in the test blast, in many cases the blaster or engineer would say that the geology was not proper for presplitting. This occurred in many cases when using the common presplit powders because of the overloading of explosives. This method of Precision Presplitting has been used on projects such as Highway 28 in Pennsylvania, Folsom Dam, Kentucky Locks, Panama Canal, Grundy Virginia Remediation Project and many other large construction projects and in mines worldwide and is the primary presplitting technique used by the Army Corp of Engineers (U.S. Army Corp of Engineers, 2018).

In recent years, Anthony Konya and Dr. Calvin Konya have derived methods to calculate the optimal explosive load for a precision presplit with a spacing of 24” (0.61m) center to center based on the Young’s Modulus of the rock with tests shown in Figure 2.13. (Konya & Konya, 2016). The ‘typical’ method of Precision Presplitting utilizes 24” (0.61m) of spacing with a 3” (75mm) diameter blasthole and 30” (0.75m) of stemming. This simplifies design to having the rock type be the only consideration for the explosive load.

This was then expanded upon to include equations to determine the explosive load required to cause a fracture to form based on the rocks Young’s Modulus, the Konya Presplit Factor, and the spacing between boreholes. The calculation of the Konya Presplit Factor is shown in Equation 23:

$$K = \left(\frac{40579}{E} \right)^{0.625} \quad (23)$$

where K is the Konya Presplit Constant and E is the Young’s Modulus in GPa.



Figure 2.13 - First test of a Precision Presplit completed in 1980 (Konya & Konya, 2017a)

This presplit factor has been tested on numerous rock types and is assumed to hold true for almost all rocks and rock types, however, certain rocks (super brittle and extremely elastic-plastic) have not been tested but are expected to follow different mechanics due to the difference in the release and consumption of energy. This presplit factor may also change with excessive jointing, and methods to account for jointing are discussed below. Table 2.3 has values for the presplit factor for the average rock of different rock categories.

The next consideration in the design of the Precision Presplit is the spacing that will be used between boreholes, center to center. This is of extreme importance, as even properly varying the explosive load with the spacing will produce different fracturing. This is because the rock is non-homogenous and has joints and fractures that will cause fractures to deviate and stop fracture growth.

Furthermore, the increase in spacing results in an increased explosive load, which can lead to over-pressurization of the borehole. This can result in additional breakage around the borehole. The spacing must then be chosen for each site to provide the desired wall characteristics based on the local geologic structures. This can also dramatically increase the cost for overbreak control, as decreasing the spacing significantly increases cost, especially in drilling and initiation.

The effects of the structural geology in a local area been studied in the past to determine how presplits behave in non-homogenous rock. It is now understood that jointing and other discontinuities between two boreholes of a presplit will cause increased backbreak and a worse wall, and the joint frequency between boreholes will be one of the major limiting factors of the maximum spacing.

In a study by Syed Tariq and Dr. Paul Worsey (Tariq & Worsey, 1996), the effects of discontinuities on presplit spacing was analyzed. This work was completed for a traditional presplit and it was concluded that:

1. Increased discontinuities can help facilitate a presplit, however, a worse presplit fracture is produced
2. A larger joint frequency between boreholes enhances the effects of cratering of the borehole, a worse presplit fracture is produced

3. For a single joint between boreholes, cratering occurs when the joint is farther than 8% of spacing and up to 20% of spacing between holes

Table 2.3 – Konya Presplit Factor for various rocks

<i>Rock Type</i>	<i>Konya Presplit Factor</i>
Granite	76
Limestone	86
Shale	116
Sandstone	127
Siltstone	201

From this research, one can see that the joint frequency between two boreholes is critical for the production of a smooth fracture. High jointing frequency decreases the explosive load needed and it increases the potential for backbreak and cratering. In cases of high joint frequency, spacing should be reduced in order to reduce the effects of fracture widening and deviation based on the jointing. This can be done by limiting the actual number of joints between boreholes to a maximum of three and varying the spacing and the explosive load.

In another paper by Dr. Paul Worsey (Worsey P. , 1984), it is stated that “Of the most importance; the presence of discontinuities at less than 60 degrees to the proposed pre-split line tends to cause poor line definition. If the angle is less than 15 degrees, pre-split blasting has no visible effect on slope profile over bulk blasting.”

Dr. Worsey also states that the pre-split fractures will intersect discontinuities at approximately right angles. This demonstrates not only the importance of spacing, but also the orientation of the presplit in relation to the natural jointing of the rock mass.

If a smooth presplit fracture must be obtained in extremely jointed rock, the author has used a spacing of 12” (0.30m) to reduce the effects of the discontinuities. In rocks that are extremely massive, with minimal jointing or other discontinuities, the spacing of the pre-split can be expanded much further to decrease the cost and maintain similar walls.

Increasing the spacing on a Precision Presplit can be done in rock with a low joint frequency, however considerations must be taken towards final wall conditions and distance to free burden. The presplit mechanism works because the distance between holes (spacing) is very small. As the spacing increases and the explosive load is increased. This can result in breakage to other production holes within the blast pattern, along geologic seams, and at the crest of the borehole.

Spacing can be properly expanded and a similar fracture can be maintained, as long as the spacing is within reasonable distance, the rock is competent, and the explosive load and decoupling ratio are adjusted accordingly. This will also cause a benefit by reducing the cost of presplitting which is beneficial to the mining industry, which is often in competition with other miners.

Decoupling ratio is defined as the ratio of the diameter of the drillhole to the diameter of the explosive charge. Decoupling is used to minimize the pressure on the borehole walls and prevent the micro-fracturing on the boreholes wall from the shock wave (Konya, Britton, & Lukovic, 1987). Decoupling charges will also decrease the

density of gas in a borehole and reduce the pressure exerted on the borehole walls. This helps to maintain control of a presplit and is a common technique used for wall control.

The borehole pressure is inversely proportional to the square of the decoupling ratio (Figure 2.14) (Konya, Britton, & Gozon, 1985). Choked Gas Mass Flow is proportional to the discharge area of the borehole. For applications of presplitting, such as Precision Presplitting, where the decoupling ratio is large, the borehole must be momentarily confined to create the proper hoop stress and fracture. This momentary hold should last approximately 8ms or slightly less and then blow out, quickly allowing the release of pressure from the borehole to avoid overbreaking the rock. In order to do this, the borehole is generally stemmed using a stemming plug, along with drill cuttings to a depth of 10 to 12 times the borehole diameter. This will allow proper decoupling of the borehole to prevent excessive breakage while allowing the gas pressure to quickly be released.

With the ability to calculate the presplit factor of different rocks one can now approach the design of a precision presplit with an engineering approach. The explosive of choice for a Precision Presplit is detonating cord. This is because detonating cord provides a consistent, controllable amount of energy throughout its length. Detonating cord fires reliably at small diameters whereas other commercially available explosives cannot be used in small diameters. Detonating cord is also easy to work with, with proper techniques it is simple to load, and explosive load variations can be made throughout the borehole to account for different rock types in a single blast (example in Figure 2.15).

The explosive load with detonating cord, is calculated in grains per foot where 7,000 grains is equivalent to one pound of explosive. Using the Konya Presplit Factor (K)

and the spacing between boreholes, one can then calculate the explosive load (EL) to be used from Equation 24.

$$EL = 7000 * \left(\frac{S}{K}\right)^2 \quad (24)$$

where EL is the explosive load in grains per foot, S is the spacing in inches, and K is the Konya Presplit Constant for the specific rock type. The use of the presplit factor takes into account the variations in rock types. This equation has been run for the average type of rock from multiple different classes and has been graphed in Figure 2.16.

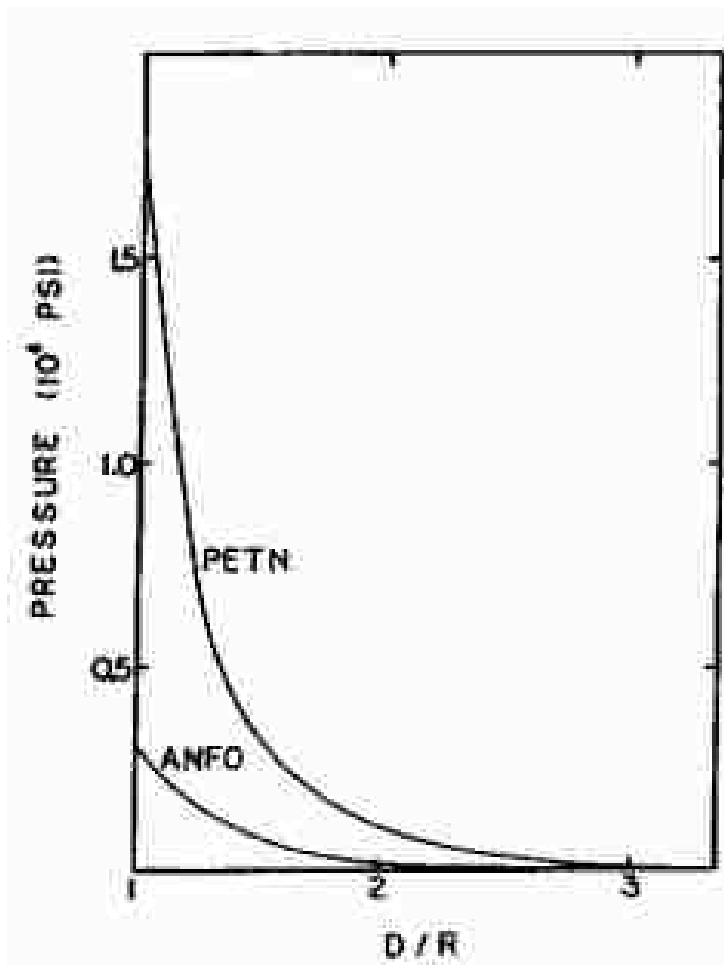


Figure 2.14 – Decoupling ratio to borehole pressure

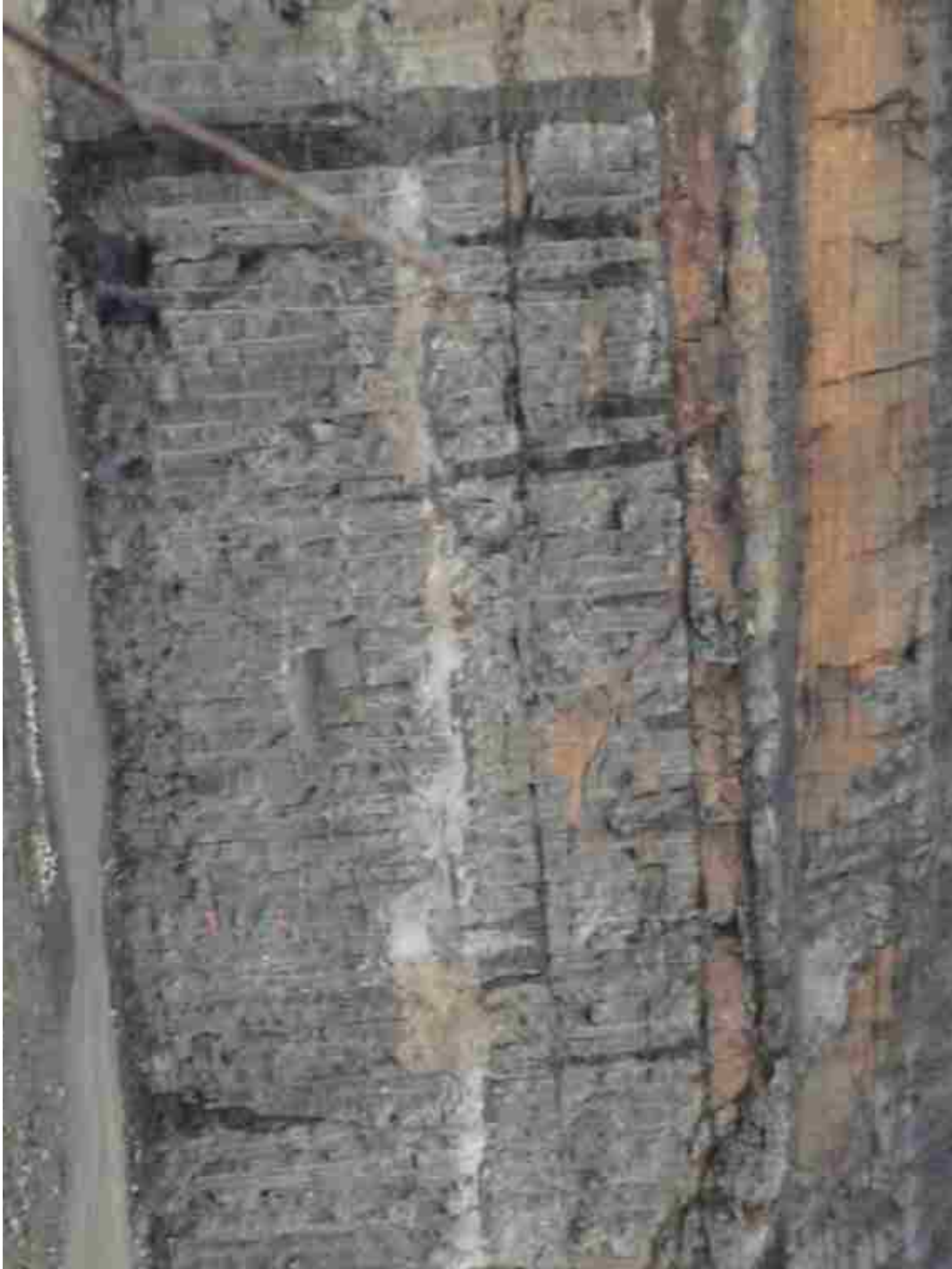
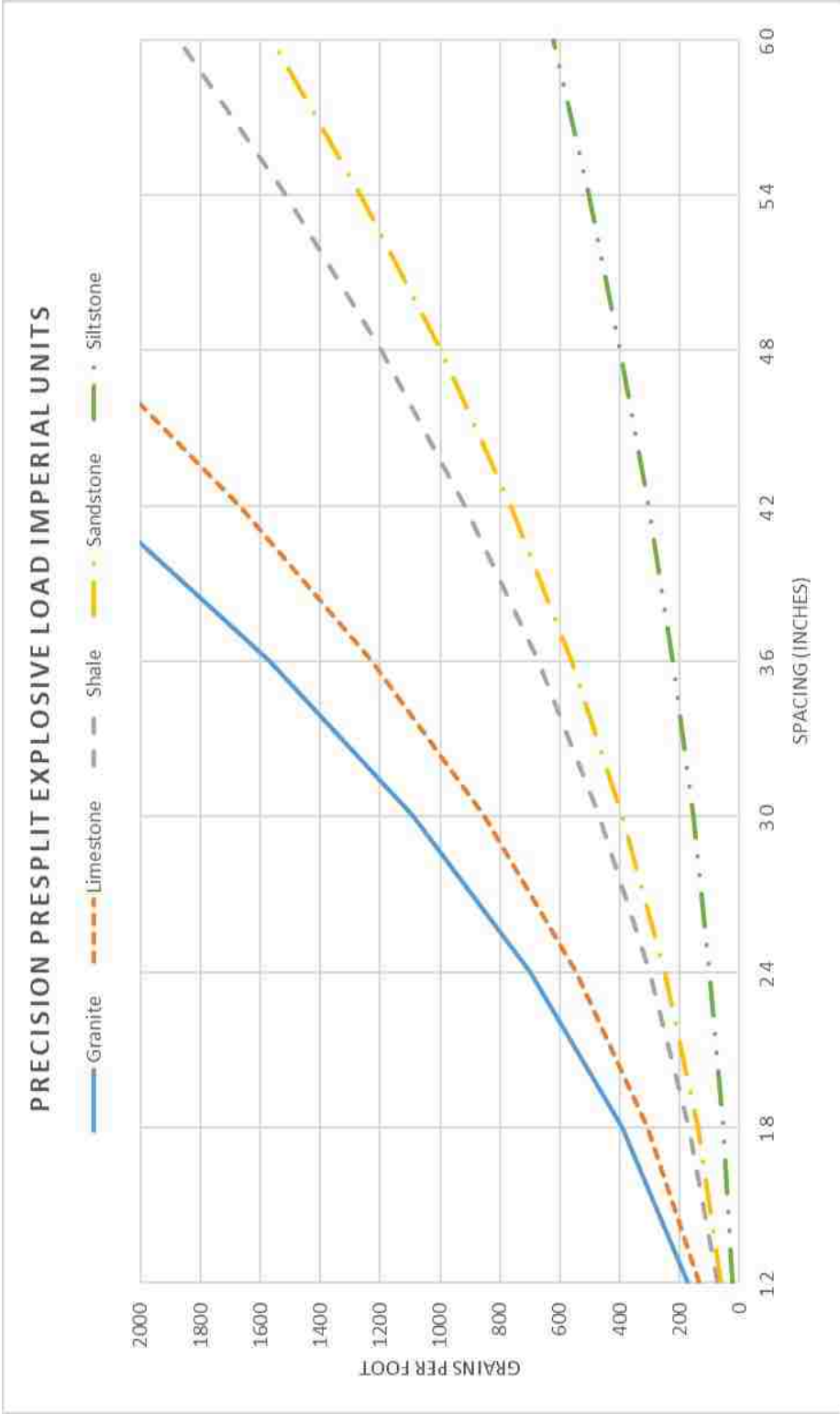


Figure 2.15 – Precision Presplit blast completed in 4 different rock types in Grundy, Virginia (Konya & Konya, 2017a)



2.5.3. Propellant Presplitting. Propellant presplitting is a method of presplitting which was tested to determine if propellants could be used to cause a presplit (Konya, Barret, & Smith, 1986). This testing was completed to observe if the shockwave was an important consideration for presplit blasting and was directly compared to presplits completed with dynamite. These were full scale tests, which were completed in a granite quarries in Georgia using a propellant known as Pyrodex. A comparison of Pyrodex to Black Powder has been reproduced in Table 2.4. The results of various tests with the dynamite versus the propellant have also been reproduced in Table 2.5.

The testing also utilized both loaded and unloaded holes with variations to the hole diameter and the spacing of the holes. While the ‘split-factor’ was not used for design on this project, it was used to compare the two explosives to determine the economic feasibility of using the products. The split factors for the two explosives are nearly identical and range between 0.04 to 0.07 pounds per square foot of new face created. It was noted that once the borehole began to fracture, or in areas of weak rock, the Pyrodex could not build up to pressure as confinement was lost.

It is important to note that the authors of this study reported and included several pictures in the paper which show that the presplits performed the same between the dynamite and the Pyrodex. In the situation of the Pyrodex no shockwave was produced and the only force acting on the rock mass was that of the gas pressure. The formation of a presplit from a propellant charge would not be possible under the currently proposed theory of shockwave collisions. However, it is clearly evident that with no shockwave being produced the presplit still fully formed. This states that the presplit is not a function of the shockwave but of another mechanisms.

Table 2.4 – Properties of black powder compared to Pyrodex (Konya, Barret, & Smith, 1986)

	Black Powder	Pyrodex
<i>Heat of Combustion (K cal/Kg)</i>	684	722
<i>Gas Volume (cc/gm)</i>	271	230

Table 2.5 – Tests completed with propellant presplit v. dynamite (Konya, Barret, & Smith, 1986)

Product	Hole Diameter (in)	Hole Spacing (in)	Charge Per Hole (lbs)	Charge per foot (lbs/ft)	Split Factor (lbs/ft ²)
Dynamite	2.75	24	0.75	0.11	0.04
Pyrodex	1.63	8	0.56	0.11	0.07
Dynamite	2.75	44	2.44	0.27	0.07
Pyrodex	3.25	72	3.00	0.42	0.05

It is important to note that the split factors in Table 2.5 are directly from the authors paper. The test comprised boreholes of various heights and loading parameters which including skipping loading every-other hole for some shots. This leads to difficulties directly calculating the split factors shown and are relied upon from the original paper (Konya, Barret, & Smith, 1986).

3. EMPIRICAL ANALYSIS OF BOREHOLE PRESSURES

3.1. DEVELOPMENT OF AN EMPIRICAL BOREHOLE PRESSURE MODEL

The first method to determine the borehole pressure will be based on empirical development of research from borehole pressures which were measured by Otuonye and presented in Table 2.1 (Otuonye, Skidmore, & Konya, 1983). Otuonye presented the data from testing in terms of total explosive weight and pressure produced in the borehole, as his research was focusing on the movement of the stemming column and the pressure was the variable which was of importance.

In order for this data to be useful for the development of practical, empirically based equations to model the pressure from the explosive, quantity needs to be expressed in terms of the explosive load per foot, which is an industry standard measure for the design of blast rounds. The explosive load used to define a Precision Presplit is defined as in terms of grains per foot. The first step to develop this comparison is to convert the weight of the explosive from grams to grains.

Grains are a unit of measure for explosives where 7,000 grains are the equivalent to one pound. The chamber used by Otuonye measured 5 inches in length with the charge being spread over the length of the chamber. The load can then be transformed to be expressed in grains of explosive per foot of borehole (gr/ft) by assuming that the charge was evenly spread throughout the length of the borehole.

The data for this conversion is shown in Table 3.1. The equivalent loads in Otuonye's work ranged from 370 gr/ft to 1850 gr/ft. These are similar ranges which are found on Precision Presplits blasts in industry.

Table 3.1 – Borehole pressures (after Otuoyne) compared to charge weight per foot

Weight of Charge (Grams)	Charge Weight per Foot (gr/ft)	Pressure (psi)
10	370	9,000
10	370	11,000
10	370	10,000
10	370	10,000
20	740	19,500
20	740	17,000
20	740	18,000
20	740	15,000
20	740	19,500
20	740	19,500
20	740	19,500
20	740	13,500
30	1110	27,000
30	1110	28,000
30	1110	27,000
30	1110	26,000
30	1110	27,000
30	1110	25,000
30	1110	30,000
40	1480	37,000
40	1480	37,000
40	1480	36,000
50	1850	50,000
50	1850	51,000

The data in Table 3.1 can then be plotted and a linear regression can be completed to develop an empirical equation which relates the pressure to the explosive load in a borehole. This results in Equation 25

$$P_g = 26.4EL - 1372 \quad (25)$$

where P_g is the borehole gas pressure in psi; EL is the explosive load in grains of explosive per foot.

The decoupling ratio of the blast, defined as the diameter of the borehole divided by the diameter of the charge, will also affect the borehole pressure as previously discussed. Otuonye did not consider the effects of decoupling on his work, however the decoupling ratio of the charge would have effects on the total pressure. In order to determine the decoupling of Otuonye's work, it will be assumed that the PETN was at a density of 1.5 g/cc and the total volume of the charge can be calculated. With the charge being spread throughout the length of the chamber, it will be assumed that the diameter of the charge was consistent throughout. The decoupling ratio can then be calculated by determination of the diameter of the charge based on the volume of a cylinder. The diameter of the testing chamber was two inches. The decoupling ratio has been calculated for various charge configurations and is shown in Table 3.2.

Table 3.2 – Decoupling ratio for Otuonye work

Charge Weight (g)	Charge Volume (in ³)	Charge Radius (in)	Decoupling Ratio
10	0.4	0.2	12
20	0.8	0.2	9
30	1.2	0.3	7
40	1.6	0.3	6
50	2.0	0.4	6

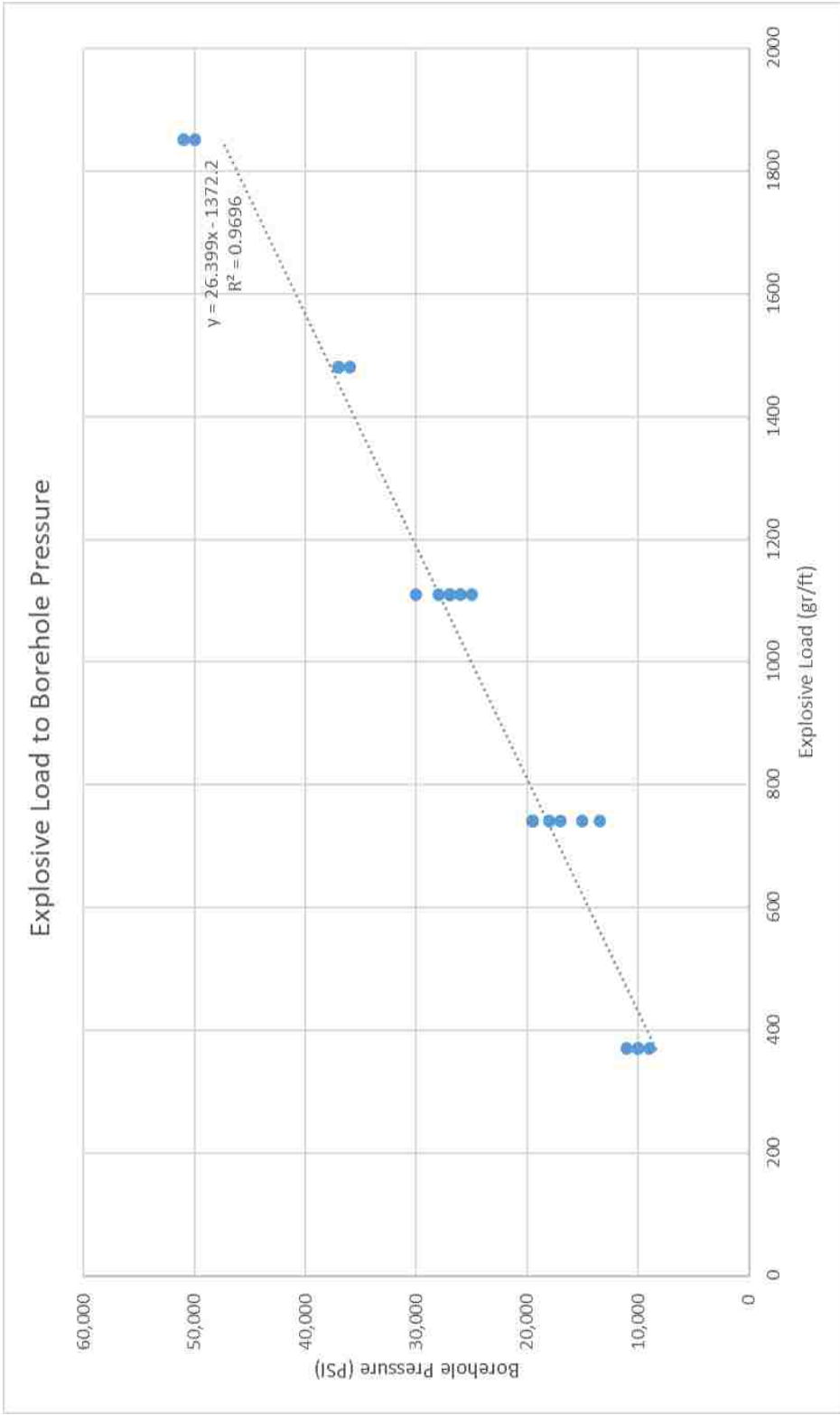
The effects of decoupling ratio have been previously discussed and it is understood that when the decoupling ratio is larger than three (3), the decoupling ratio has minimal effects on the changes in the borehole pressure. The data tested by Otuonye

varied between a decoupling ratio of six (6) through twelve (12). For the purposes of this dissertation, a decoupling ratio greater than three (3) will be considered a large decoupling ratio which has no effect on borehole pressure. Therefore, Equation 23 can be stated as being applicable to determine the borehole pressure for charges with a large decoupling ratio for a borehole which is two inches in diameter.

Equation 23 is graphed along with Otuonye's data in Figure 3.1 and is seen to have a R^2 value of 0.97, which implies an excellent fit of the data to be modeled by the developed equation. A close inspection of the data does show that there are some minor deviations at all the charge loads which can be considered some experimental error. Figure 3.1 shows a linear relationship between the borehole pressure and the explosive load. This proves that the previously made assumption about large decoupling ratios is correct and no effects of reducing the decoupling are realized within this range.

Furthermore, Otuonye's work was completed with PETN which is the same explosive that is used in Precision Presplitting. Different explosives will detonate with variations in temperature and gas products, which will lead to different borehole pressures. Equation 25 can only be used when the explosive being utilized is PETN.

This introduces the base form of the Empirical Model which can be used for estimating pressures in a borehole with a two-inch diameter. However, it is important to develop methods for changing this borehole diameter



3.2. MODIFICATION OF THE EMPIRICAL MODEL

Equation 23 has been shown to be applicable for the determination of the borehole pressure under large decoupling for a two-inch diameter borehole. In order to develop an equation that can accurately model the borehole pressure to be used in field loading conditions, a model will have to be developed which can calculate the borehole pressure with changing borehole diameter. The borehole pressure will have large changes based on the borehole diameter due to the accompanying volume changes. The gas volume generated by the explosive will have to occupy a larger space causing a reduction in the pressure. For example, a three-inch hole has a volume which is 229% of the volume of a two-inch hole. The detonation process and pressurization of a borehole is extremely rapid and is treated as an adiabatic process which has no change in temperature. Boyle's law is an accepted technique for analyzing variations of pressure with changes volume at a constant temperature and is shown in Equation 26.

$$P_1V_1 = P_2V_2 \quad (26)$$

where P_1 is the original pressure, V_1 is the original volume, P_2 is the final pressure, and V_2 is the final volume.

The original pressure would be that of the pressure in a two-inch diameter borehole, which is presented in Equation 25. The original volume will be the volume of a two-inch diameter borehole and the final volume will be the volume of the actual borehole. The volume of the borehole can be calculated based on the volume of a cylinder, which has been shown in Equation 27 in a modified form to include units typical in the blasting industry.

$$V_b = \frac{\pi}{4} d_h^2 PC \quad (27)$$

where V_b is the volume of the borehole in cubic inches, d_h is the diameter of the borehole, and PC is the length of the powder column in inches. It is important to note that by using the length of the powder column, it is assumed that the borehole will reach maximum pressure before the stemming begins movement. This has been verified to be a true assumption as maximum borehole pressure is not dependent on stemming movement or the loss of stemming (Otuonye, 1981). Rearranging Equation 26 to isolate the final pressure gives Equation 28

$$\frac{P_1 V_1}{V_2} = P_2 \quad (28)$$

Substituting Equation 25 for P_1 and Equation 25 for V_1 and V_2 gives Equation 29.

$$\frac{\left((26.4EL - 1372) * \left(\frac{\pi}{4} * 2^2 * PC \right) \right)}{\frac{\pi}{4} d_h^2 PC} = P_2 \quad (29)$$

where EL is the explosive load in grains per foot, PC is the length of powder column in inches, d_h is the diameter of the borehole in inches, and P_2 is the borehole pressure in psi.

Simplification of Equation 29 gives Equation 30, which is the Empirical Model for determination of the borehole pressure.

$$P_g = \frac{105.6EL - 5488}{d_h^2} \quad (30)$$

where P_g is the borehole pressure in psi, EL is the explosive load in grains per foot, and d_h is the diameter of the borehole. The error for this equation is 5% to 10% from measured values obtained by Otuonye, with an average of 8.8%.

Equation 30 can then be used to determine the borehole pressure based on the changes in the explosive load and borehole diameter, assuming the decoupling ratio is large, and the explosive is PETN. Equation 28 has been used to generate Figure 3.2 which shows changes in the borehole pressure based on changes to borehole diameter and

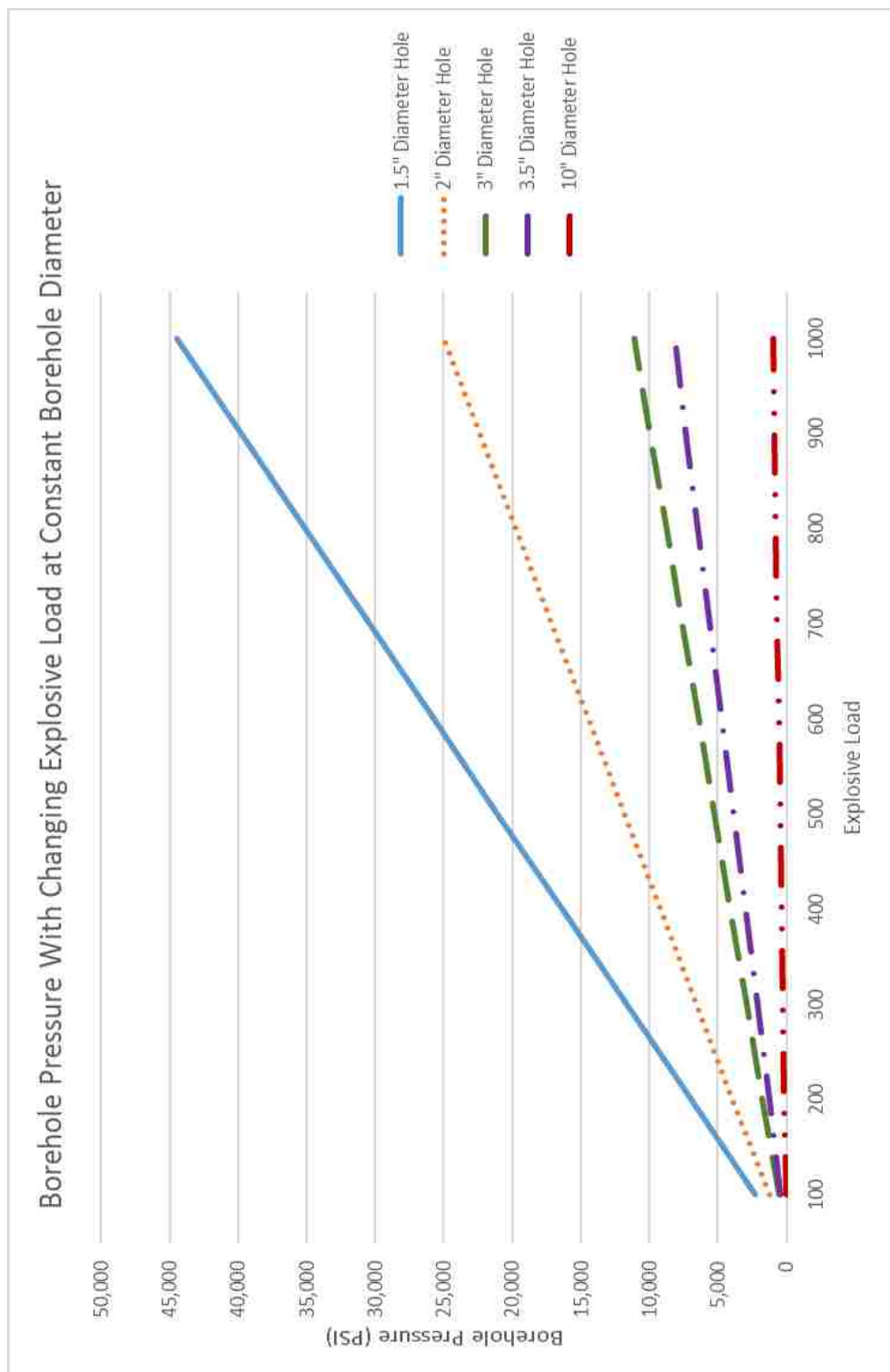
explosive load. The range of explosive load has been taken as 100 grains per foot to 1000 grains per foot, which is the explosive load typically found in Precision Presplitting.

Figure 3.2 shows, similar to Figure 3.1, that when the borehole diameter is set the borehole pressure varies linearly with the explosive load.

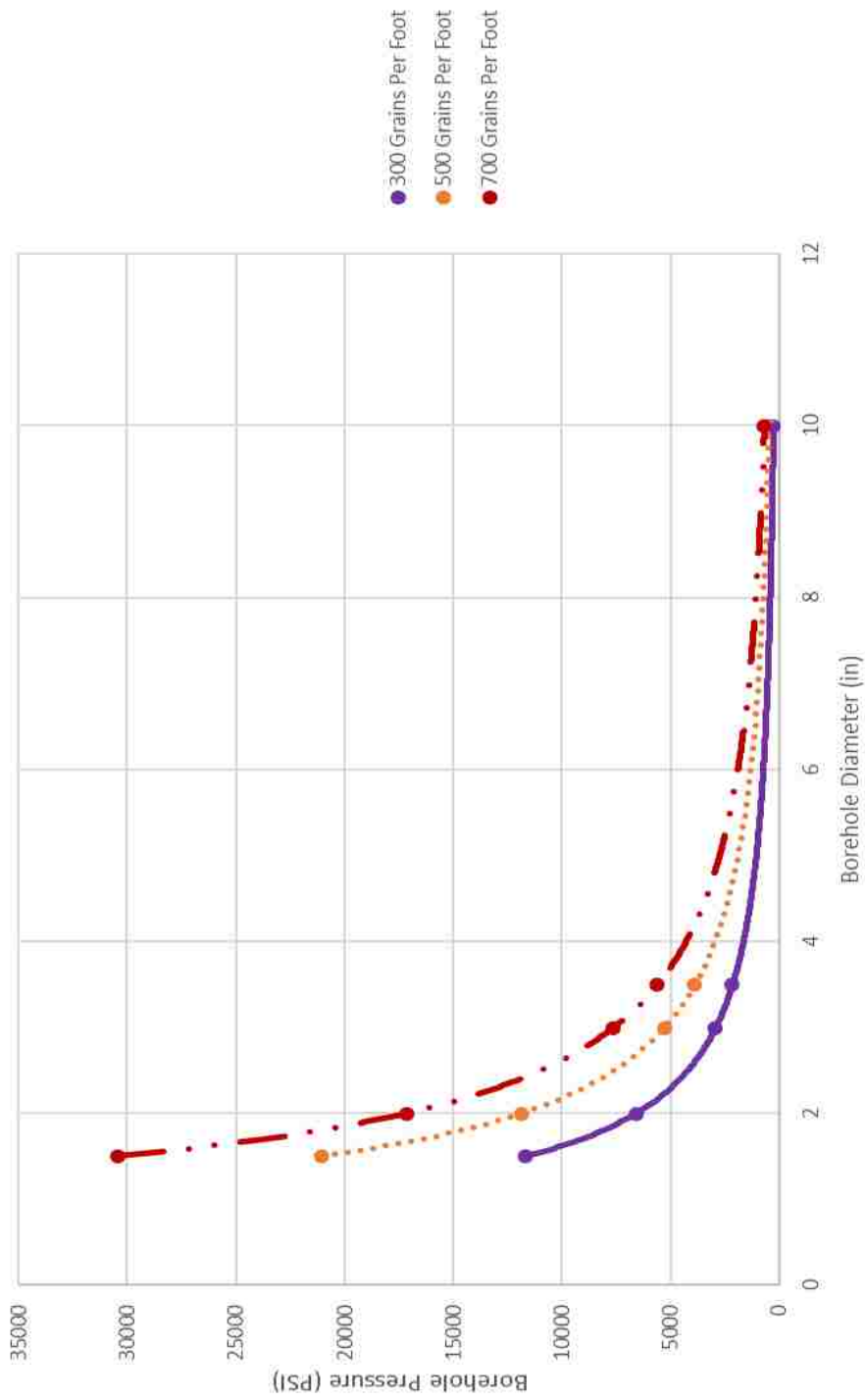
Figure 3.3 shows the effects of a changing borehole diameter while maintaining a constant explosive load. The three explosives loads shown here are commonly used in the field for various rock types with a 24" spacing between boreholes, such as Shale (300 grains per foot), Limestone (500 grains per foot), and Granite (700 grains per foot).

Figure 3.3 shows that the effects of the explosive load to borehole pressure are large at a borehole diameter under six inches, but when the borehole diameter exceeds six inches it is difficult to generate substantial borehole pressures from Precision Presplitting, which would be equivalent to a decoupling ratio of approximately 25. It would therefore be advised that the decoupling ratio remain below 25 on any presplit blast from a borehole pressure analysis.

Equation 30 is termed the Empirical Borehole Pressure Model which can be used to quickly determine the borehole pressure from a charge with large decoupling (greater than three) and a PETN based explosive. The benefit of this model is that it contains a low error and is a simple and straightforward calculations. This model cannot take into account different mixtures of detonation products, different densities of PETN, different temperatures of detonation, or different methods of combustion (i.e. detonation versus deflagration). Following sections of this dissertation will address these other topics from a theoretical standpoint for more advanced modelling.



Borehole Pressure with Changing Borehole Diameter at Constant Explosive Load



3.3. EMPIRICAL MODEL FOR TYPICAL PRECISION PRESPLIT

The previously presented equations can be used to determine the variations in the borehole pressure with variations to explosive load and borehole diameter. This was needed in order to be able to determine the explosive load from a standard Precision Presplit, which in a majority of situations will use a three-inch diameter borehole. Substituting in three inches for the borehole diameter and simplifying Equation 30 gives Equation 31 as a simplified borehole pressure equation for Precision Presplitting.

$$P_g = 11.7EL - 610 \quad (31)$$

where P_g is the borehole pressure in psi and EL is the explosive load in grains per foot.

This empirical equation allows for easy calculation of the borehole pressure based on the explosive load and will be applied later in this dissertation for the determination of the stress in the rock mass. This equation assumes that the borehole diameter is three-inches, the decoupling ratio is greater than three, and the explosive used is PETN. Table 3.3 shows the calculation of the borehole pressure from variations to explosive load from Equation 29.

Table 3.3 – Boreholes pressures for Precision Presplitting based on explosive load

Explosive Load (gr/ft)	Borehole Pressure (psi)
200	1730
300	2900
400	4070
500	5240
600	6410
700	7580

4. THEORETICAL ANALYSIS OF BOREHOLE PRESSURES

4.1. INTRODUCTION TO THEORETICAL MODELS

The empirical model presented in Equation 28 and 29 can be reliably used to determine the detonation pressure of a PETN based explosive charge in boreholes of varying diameter for a decoupling ratio above three. However, it would be beneficial to develop a model which could be used to determine borehole pressures for variations in explosive type and for decoupling ratios below three. This would give equations which could be used to determine the borehole pressure for any situation in which explosives are used to break rock. Without relevant empirical data for all scenarios, a theoretical model can be developed which would be derived from accepted theories in chemistry, thermodynamics, and hydrodynamics. The model would then be validated using the data from Otuonye.

Two models are presented in this dissertation as theoretical models for the determination of borehole pressure. The first model is derived from the detonation gas pressure of the explosive, relying on the equations of state previously discussed. This model can be considered a simplified model which has relatively little computational time. The first model presented would likely still only be valid for a decoupling ratio above three as it does not take into account compressibility of the gas at high pressures and temperatures; however, it is applicable to any type of high explosive. The second model is a more advanced model that relies on an iterative process. The second model is assumed to be a more accurate model as it accounts for items such as the compressibility of gases and could be used for low and high explosives at any decoupling ratio.

4.1.1. Temperature of Detonation. The first step in the use of either of these models will be to determine the temperature of the explosion or combustion. The determination of the temperature of the detonation can be done either through experimental testing or through equations previously presented (Otuonye, Skidmore, & Konya, 1983).

The measurements of a single crystal of unconfined PETN observe a temperature of detonation of 4140 ± 70 K (Yoo, Holmes, Souers, Wu, & Ree, 2000). The measurement of this detonation temperature is from a single crystal placed in an unconfined state using a nanosecond time-resolved spectropyrometric system. However, this data does not necessarily represent a comparison for the use of large amounts of PETN in a borehole.

Explosives typically have a rating of run-up distance, which is the distance away from the initiation point that the velocity of detonation reaches steady-state. This is different from a deflagration-to-detonation transition which is the point at which the explosive begins to detonate. PETN has a very short deflagration-to-detonation transition and is typically assumed to detonate immediately upon initiation.

An explosive is not at full energy until it reaches the proper run-up distance and the velocity of detonation is at the steady-state speed, even if it is detonating. The run-up distance for PETN has been shown to vary from 1mm to 10mm, or larger depending on the density and confinement of the charge (Reaugh, Curtis, & Maheswaran, 2017). It can then be assumed that until this run-up point is reached the pressure and temperature of the explosive will also not be at the maximum values. This implies that the temperature of

detonation for PETN would be greater than the previously measured value of 4140° K, as the small size measured was not at a steady-state detonation.

Theoretical modelling of the temperature of detonation would then need to be computed. Research has shown that Equation 14 is an acceptable and reliable model for the determination of the temperature of detonation (Akhavan, 2011). Equation 12 is re-introduced as Equation 32 below.

$$T_e = \frac{Q_e}{\sum n_i c_v} + T_1 \quad (32)$$

where T_e is the temperature of the explosion in degrees Kelvin, Q_e is the heat of explosion in kilojoules per moles, n is moles of a specific gas, C_v is Specific Heat at Constant Volume of a Specific Gas in J/mol/° K, and T_1 is set at 298° K.

Equation 32 is utilized by assuming an explosive temperature to begin with, for example for PETN one may assume a starting temperature of 4140° K. The specific heat of each gas is then determined based on this temperature. Equation 32 is run with the summation of the moles of a specific gas times the specific heat of that gas at the assumed temperature to develop a new temperature of detonation. This new temperature of detonation is then utilized to again determine the specific heat of the various gases, and the equation is run again to determine a new specific heat. This iterative process is run multiple times until the temperature reaches a steady point and changes in additional runs are minimal, for this dissertation that will be considered a temperature of 50° K.

4.1.2. Specific Heats for Explosive Products. The application of Equation 30 relies on the determination of the specific heats of various gases which are generated from the detonation of the explosion process. At standard temperature and pressure the specific heat for these various gases is well defined, for example water vapor (H₂O) has a

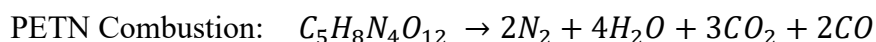
specific heat of $1.996 \text{ KJ/kg/}^\circ \text{K}$. This implies that to raise the temperature of steam one-degree Kelvin, 1.996 KJ of energy need to be applied per kilogram of steam. At temperatures below 1000°K the specific heat of gases minimally varies and as such many basic thermodynamic texts and solutions assume a constant specific heat for a certain gas. The major variations of specific heat below 1000°K comes from phase changes (Smith, Van Ness, & Abbot, 2005).

However, when the temperature is raised significantly above 1000°K the specific heat of substances begins to increase rapidly (Akhavan, 2011), for example at a temperature of 2500°K the specific heat of water vapor is $2.987 \text{ KJ/kg/}^\circ \text{K}$. The large increase in the specific heat must be accounted for when determining the temperature of the explosion due to the extremely high temperatures that are observed in a detonation. This must be found for each of the products that will be produced in the detonation, as each separate product has its own unique heat capacity. Currently minimal methods exist for the determination of the specific heats for the various products encountered, as such the author has developed equations based on a collection of data to determine the specific heats based on variations in temperature.

4.1.2.1. Dulong-Petit Limit. Specific heats at high temperatures for solids are typically determined based on the Dulong-Petit Law (Petit & Dulong, 1819) which states that the specific heat of a solid will vary between $22.5 \text{ J/mol/}^\circ \text{K}$ and $30 \text{ J/mol/}^\circ \text{K}$ with a value of $25 \text{ J/mol/}^\circ \text{K}$ as the standard constant. This was proven to apply as a maximum limit for the specific heat based on the temperature of the process for elemental solids (Einstein, 1906). Recent research has shown that solid compounds can exceed this limit value.

However, at a certain temperature, which varies based on the solid compound, the compound will reach a maximum heat capacity at which the heat capacity will stop increasing for any further increase in temperature. This maximum heat capacity is known as the Dulong-Petit Limit. K_2S , which is a solid compound produced by black powder, has a specific heat capacity which reaches a Dulong-Petit Limit of $70.226 \text{ J/mol/}^\circ \text{K}$ at a temperature of 1000°K .

4.1.2.2. PETN detonation products. The formula for the detonation of PETN can be found below. Using a simplified detonation product approach, the gases which are formed are Nitrogen, Steam, Carbon Dioxide, and Carbon Monoxide. This will be used to determine which products will need to have specific heat equations developed for use in Equation 32. The heat of combustion is shown in Table 4.1.



The heat of formation for PETN can be found below.

Molecular Weight of PETN: 316.2

Heat of Formation: $Q_e = -128.7 \text{ Kcal/mole}$ (Cooper, 1996)

Table 4.1 – Heat of combustion for PETN

<i>Products</i>	<i>Grams</i>	<i>Heat of Formation, Q_p (Kcal/mole)</i>	<i>Kcal</i>
$H_2O = 4*18.02$	72.08	$4 * (-68.4)$	-273.6
$N_2 = 2*28.02$	56.04	$2 * (0)$	0.0
$CO_2 = 3*44.01$	132.03	$3 * (-94.1)$	-282.3
$CO = 2*28.01$	56.17	$2 * (-26.4)$	-52.8
Total:	316.17	Heat of Combustion:	-608.7

Heat of Explosion (PETN) = -480.0 Kcal/mole or -1518 Kcal/kg

The four gases which are produced will also have to have specific heats determined based on experimentation with multiple data sets presented from various authors (Fenning & Whiffin, 1939; Otuonye, 1981; Klapotke, 2012).

4.1.2.3. Specific heat for nitrogen, N₂. The first gas that will be analyzed is Nitrogen, which has a total of 62 data points which ranged in temperature from 373° K to 5000° K. Figure 4.1 shows the graph of the data and the trendline which is determined through means of linear regression. The R² value is 0.99 which shows excellent fit of the data. Equation 33 is used to determine the specific heat, C_{vN₂}, for Nitrogen.

$$C_{vN_2} = 0.8605 * \ln(T) - 0.7056 \quad (33)$$

where C_{vN₂} is the specific heat of nitrogen in cal/mol/° K and T is temperature in ° K.

This allows for the calculation of the Specific Heat for Nitrogen with only variations in temperature.

4.1.2.4. Specific heat of water vapor, H₂O. The next gas that will be analyzed is Water Vapor, H₂O, which has a total of 56 data points which ranged in temperature from 373° K to 5000° K. Figure 4.2 shows the graph of the data and the trendline which is determined through means of linear regression. The R² value is 0.97 which shows excellent fit of the data. Equation 34 is used to determine the specific heat, C_{vH₂O}, for Water Vapor.

$$C_{vH_2O} = 2.271 * \ln(T) - 9.1272 \quad (34)$$

where C_{vH₂O} is the specific heat of water vapor in cal/mol/° K and T is temperature in ° K. This allows for the calculation of the Specific Heat for steam with only variations in temperature.

4.1.2.5. Specific heat for carbon dioxide, CO₂. The next gas that will be analyzed is Carbon Dioxide, CO₂, which has a total of 56 data points which ranged in temperature from 373° K to 5000° K. Figure 4.3 shows the graph of the data and the trendline which is determined through means of linear regression. The R² value is 0.97 which shows excellent fit of the data. Equation 35 is used to determine the specific heat, C_{vCO2}, for Carbon Dioxide.

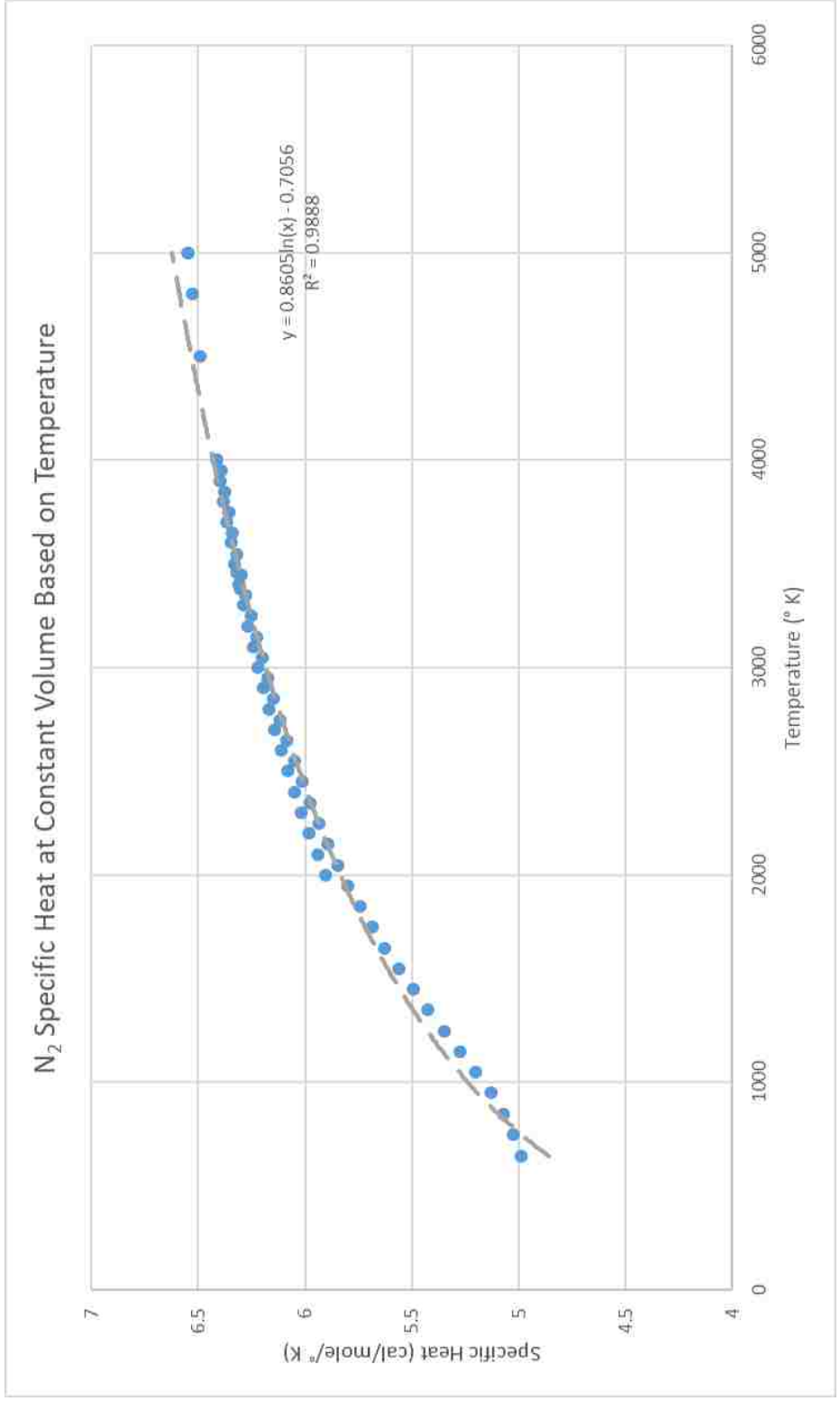
$$C_{vCO2} = 2.166 * \ln(T) - 5.8452 \quad (35)$$

where C_{vCO2} is the specific heat of Carbon Dioxide in cal/mol/° K and T is temperature in ° K.

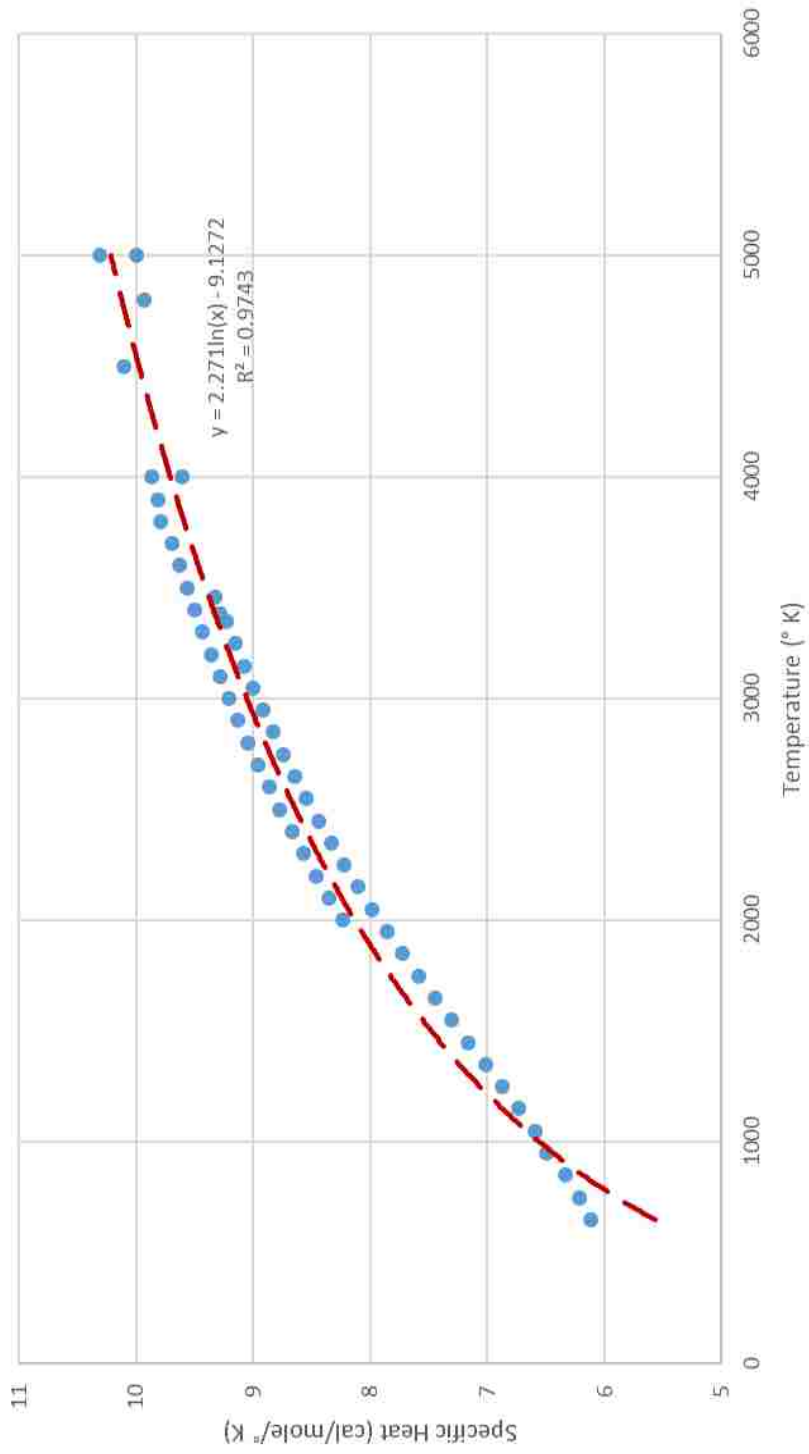
4.1.2.6. Specific heat for carbon monoxide, CO. The next gas that will be analyzed is Carbon Monoxide, CO, which has a total of 35 data points which ranged in temperature from 373° K to 5000° K. Figure 4.4 shows the graph of the data and the trendline which is determined through means of linear regression. The R² value is 0.99 which shows excellent fit of the data. Equation 36 is used to determine the specific heat, C_{vCO}, for Carbon Monoxide.

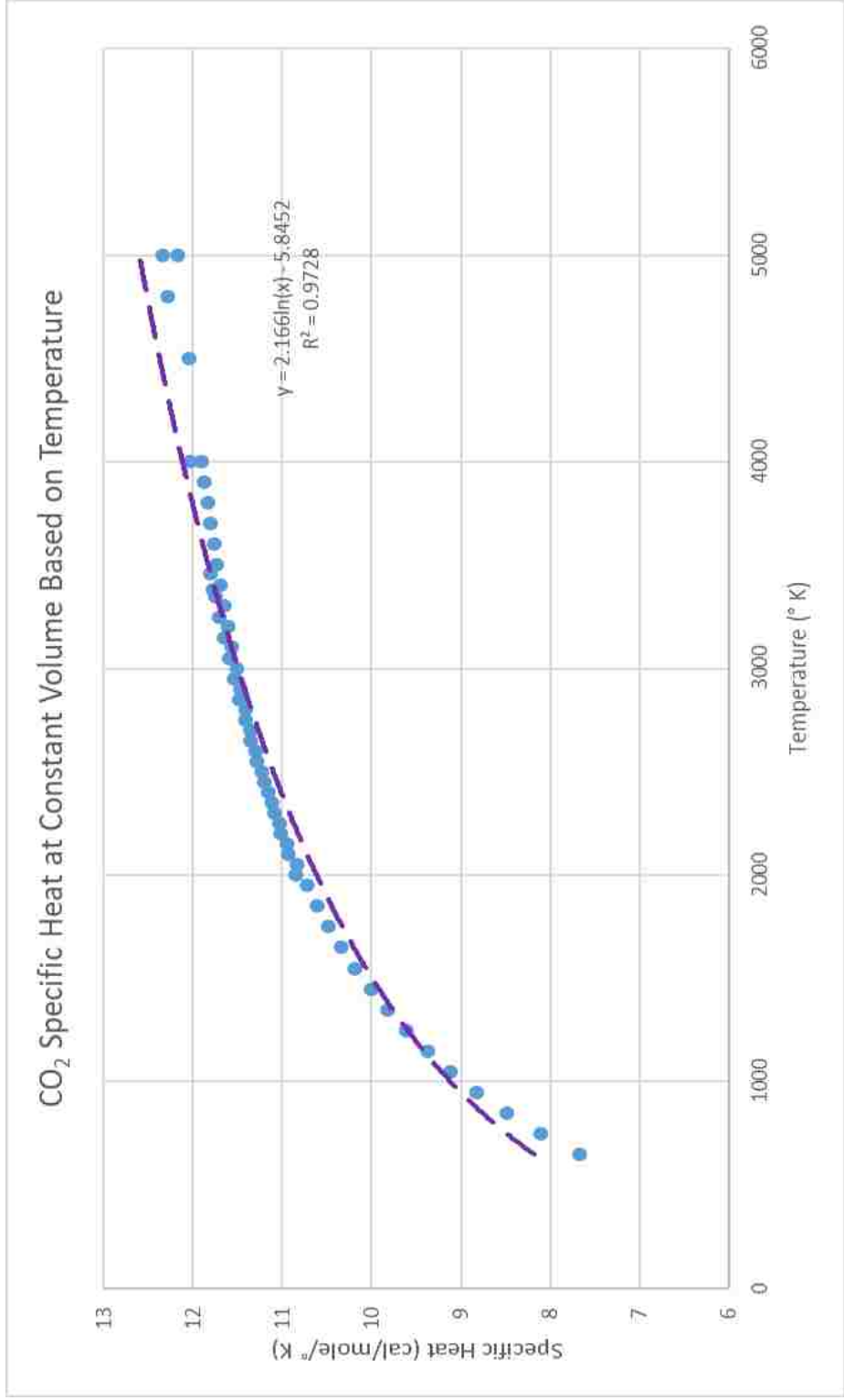
$$C_{vCO} = 0.8656 * \ln(T) - 0.6896 \quad (36)$$

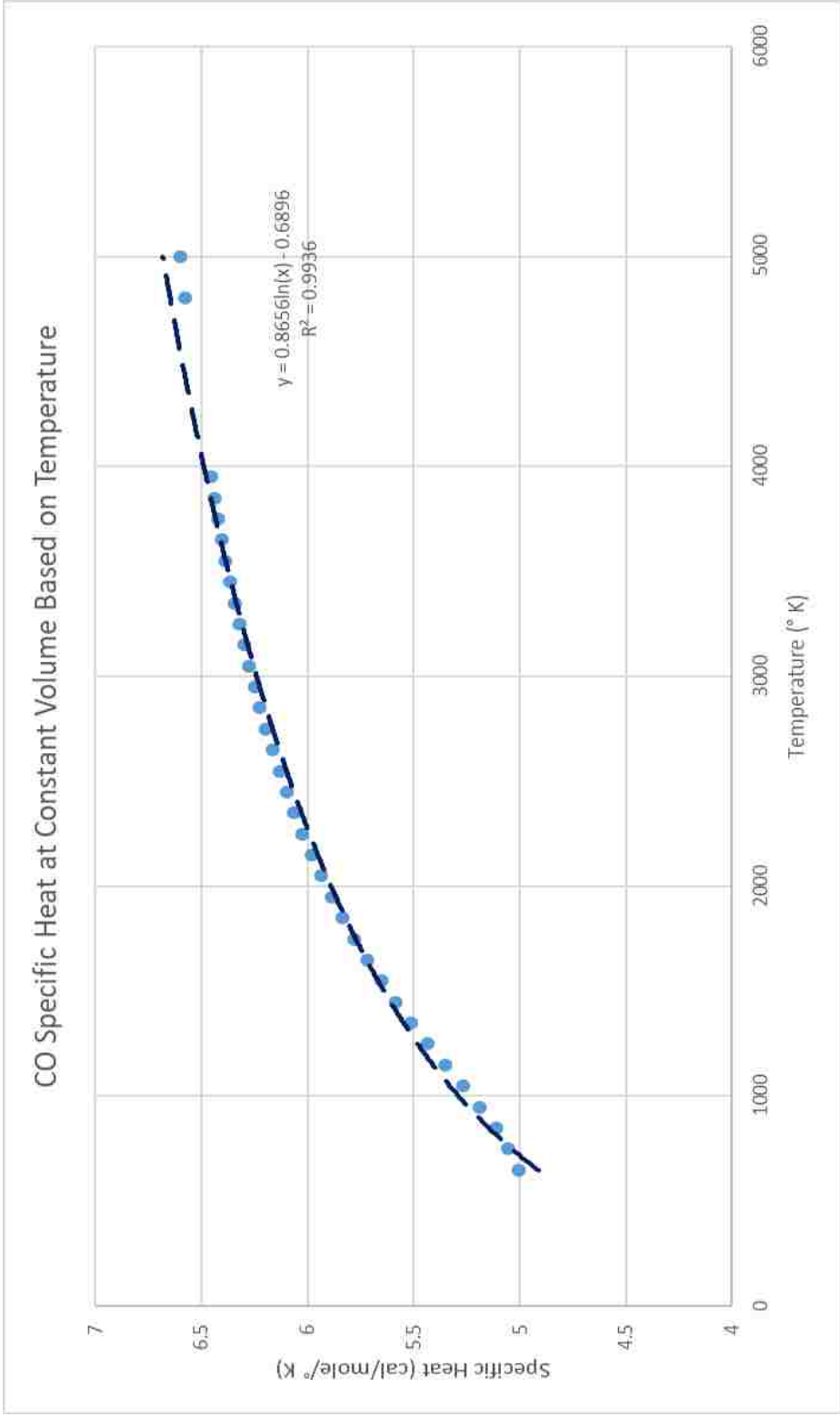
where C_{vCO} is the specific heat of Carbon Monoxide in cal/mol/° K and T is temperature in ° K. The use of Equation 33 through Equation 36 then give all the parameters to calculate the temperature of detonation for PETN. These can be utilized with other energetic materials, but the formation of different gases would require new models to account for specific heat of the specific gas being analyzed. Research has suggested that solid products should not be analyzed for pressure but do affect temperature for unconfined detonations (Needham, 2018).



H₂O Specific Heat at Constant Volume Based on Temperature







4.1.3. Calculation of the Temperature of the Explosion. With the methods presented above, the specific heat at constant volume for the various products which are produced from the detonation of PETN can be determined. The heat of explosion is computed in section 4.1.2.2 and is 1518 kcal/kg. The original temperature, T_1 , is set at 298° K. Equation 30 is then used for the determination of the borehole temperature. The first step in the computation is to assume a temperature of explosion, for this situation a temperature of 4140° K is assumed.

The specific heats, C_v are then computed using Equation 33 through Equation 36 in Table 4.2 with an assumed temperature of 4140° K.

Table 4.2 – Calculation of specific heat for first run of explosive temperature

Gaseous Product	Equation Used	Specific Heat (cal/mol/° K)
H ₂ O (Equ. 33)	$C_{vH_2O} = 2.271 \cdot \ln(4140) - 9.1272$	9.787
N ₂ (Equ. 34)	$C_{vN_2} = 0.8605 \cdot \ln(4140) - 0.7056$	6.461
CO ₂ (Equ. 35)	$C_{vCO_2} = 2.166 \cdot \ln(4140) - 5.8452$	12.194
CO (Equ. 36)	$C_{vCO} = 0.8656 \cdot \ln(4140) - 0.6896$	6.520

Following the calculations of the specific heat for each gaseous product, the summation from the denominator in Equation 32 can be calculated by multiplying the moles of each gaseous product produced per kilogram of explosive by the specific heat at constant volume. This is shown in Table 4.3 below.

Table 4.3 – Calculation for temperature of explosion for the first run

Product	Moles of Gas per Kilograms of Explosive, n_i , (mole/kg)	Specific Heat, C_v , (cal/mol/° K)	$n_i \times C_v$ (cal/kg/° K)
H ₂ O	12.65	9.787	123.80
N ₂	6.326	6.461	40.87
CO ₂	9.489	12.194	115.71
CO	6.326	6.520	41.24
Summation in Denominator of Equ. 32			321.62

The summation in the Denominator is 321.62 cal/kg/° K or 0.32162 kcal/kg/° K to arrive at proper units for the equation. Equation 30 with the above numbers gives:

$$T_e = \frac{1518 \frac{\text{kcal}}{\text{kg}}}{0.32168 \frac{\text{kcal}}{\text{kg} \cdot \text{K}}} + 298^\circ \text{K} = 5,017^\circ \text{K}$$

An accuracy of 50° K between assumed and calculated temperature will be used to determine successful runs. The first run of Equation 32 results in a temperature of explosion of 5,017° K. This is then compared to the assumption of 4140° K. The difference between the assumed temperature and the calculated temperature is 877° K, which is greater than the accepted tolerance of 50° K. This large difference implies that the assumption previously made was too low. The assumed temperature is relied upon to determine the specific heats for each of the gaseous products and is incorrect, as such the process is run again. The second iteration in the process will now assume a temperature of explosion of 5000° K, which is close to what was found from the previous run.

The specific heats, C_v are then computed using Equations 33 through Equation 36 in Table 4.4 with an assumed temperature of 5000° K.

Table 4.4 - Calculation of specific heat for second run of explosive temperature

Gaseous Product	Equation Used	Specific Heat (cal/mol/° K)
H ₂ O (Equ. 33)	$C_{vH_2O} = 2.271 \cdot \ln(5000) - 9.1272$	10.215
N ₂ (Equ. 34)	$C_{vN_2} = 0.8605 \cdot \ln(5000) - 0.7056$	6.623
CO ₂ (Equ. 35)	$C_{vCO_2} = 2.166 \cdot \ln(5000) - 5.8452$	12.603
CO (Equ. 36)	$C_{vCO} = 0.8656 \cdot \ln(5000) - 0.6896$	6.683

Following the calculations of the specific heat for each gaseous product, the summation from the denominator in Equation 32 can be calculated by multiplying the moles of each gaseous product produced per kilogram of explosive by the specific heat at constant volume. This is shown in Table 4.5 below.

The summation in the Denominator is 332.99 cal/kg/° K or 0.33299 kcal/kg/° K to arrive at proper units for the equation. Equation 32 with the above numbers gives:

$$T_e = \frac{1518 \text{ kcal/kg}}{0.33299 \frac{\text{kcal}}{\text{kg} \cdot \text{K}}} + 298^\circ \text{ K} = 4,857^\circ \text{ K}$$

The computed temperature from the second run is 4,857° K, which is a difference of 160° K from the previously computed 5000° K. This is outside the acceptable error of 50° K; therefore, a third iteration of the equation is run starting with an assumed temperature of explosion of 4,850° K.

Table 4.5 – Calculation for temperature of explosion second run

Product	Moles of Gas per Kilograms of Explosive, n_i , (mole/kg)	Specific Heat, C_v , (cal/mol/° K)	$n_i \times C_v$ (cal/kg/° K)
H ₂ O	12.65	10.215	129.22
N ₂	6.326	6.623	41.90
CO ₂	9.489	12.603	119.59
CO	6.326	6.683	42.28
Summation in Denominator of Equ. 32			332.99

The specific heats, C_v are then computed using Equations 33 through Equations 36 in Table 4.6 with an assumed temperature of 4850° K. The calculated specific heats show less deviation from the previous run, showing that the process is converging.

Table 4.6 - Calculation of specific heat for third run of explosive temperature

Gaseous Product	Equation Used	Specific Heat (cal/mol/° K)
H ₂ O (Equ. 33)	$C_{vH_2O} = 2.271 \cdot \ln(4850) - 9.1272$	10.146
N ₂ (Equ. 34)	$C_{vN_2} = 0.8605 \cdot \ln(4850) - 0.7056$	6.597
CO ₂ (Equ. 35)	$C_{vCO_2} = 2.166 \cdot \ln(4850) - 5.8452$	12.537
CO (Equ. 36)	$C_{vCO} = 0.8656 \cdot \ln(4850) - 0.6896$	6.657

Following the calculations of the specific heat for each gaseous product, the summation from the denominator in Equation 32 can be calculated by multiplying the moles of each gaseous product produced per kilogram of explosive by the specific heat at constant volume. This is shown in Table 4.7 below.

Table 4.7 – Calculation for temperature of explosion third run

Product	Moles of Gas per Kilograms of Explosive, n_i , (mole/kg)	Specific Heat, C_v , (cal/mol/° K)	$n_i \times C_v$ (cal/kg/° K)
H ₂ O	12.65	10.146	128.35
N ₂	6.326	6.597	41.73
CO ₂	9.489	12.537	118.96
CO	6.326	6.657	42.11
Summation in Denominator of Equ. 32			331.16

The summation in the Denominator is 331.16 cal/kg/° K or 0.33116 kcal/kg/° K to arrive at proper units for the equation. Equation 32 with the above numbers gives:

$$T_e = \frac{1518 \text{ kcal/kg}}{0.33116 \frac{\text{kcal}}{\text{kg}^\circ\text{K}}} + 298^\circ \text{ K} = 4,882^\circ \text{ K}$$

The temperature of detonation after the third iteration of Equation 32 yields a temperature of 4,882° K, which is a difference of 25° K from the second iteration temperature of 4857° K. This is within the acceptable tolerance of 50° K. The temperature of detonation for PETN is 4,900° K.

This method of determining the temperature of the explosion is a reliable method which works for high explosives. From the author's previous work, this system does not seem to work as well for low explosives which deflagrate dramatically over-estimating the results. This would then only be recommended for detonating explosives. The major challenge with this system is the proper computation of the specific heat for all products as information is scarce for the specific heats at these temperatures.

4.2. DETONATION PRESSURE MODEL

The detonation pressure model will utilize a base equation of state from previous research to determine the borehole pressure for variations in explosives.

4.2.1. Validation of Equations of State from Experimental Data. The development of the temperature of the explosion gives the ability to analyze the previously presented Equations of State (EOS) for the determination of the explosive pressures when the gas is in the same volume as the original explosive. These are presented below to facilitate easy referencing as Equations 37 through Equations 43. The BWS Equation of State is:

$$P_e = \rho n R T_e [1 + x e^{\beta x}] \quad (37)$$

$$x = \rho k (T_e + \theta)^{-\alpha} \quad (38)$$

where P_e is the explosive gas pressure atmospheres, ρ is the density of the explosive, n is the moles of gas, R is the gas constant, T_e is the temperature of detonation in degrees Kelvin, x is a constant based on a function of the temperature of detonation, and β , k , θ , and α are all experimentally determined constants. It has been suggested that acceptable values for these constants are $k = 1$; $\theta = 0$; $\alpha = 0.25$; and $\beta = 0.3$.

The Cook Equation of State is:

$$P_e = \frac{\rho n R T_e}{[1 - \rho * b(\rho)]} \quad (39)$$

$$b(\rho) = e^{-0.4\rho} \quad (40)$$

where b is the co-volume of the gas mixture in liters per kilogram, which Cook assumed to be a function of only density, P_e is the explosive gas pressure in atmospheres, ρ is the density of the explosive, n is the moles of gas, R is the gas constant, T_e is the temperature of detonation in Kelvin. The Cook equation of state has a specific calculation for the co-volume which will be used, other EOS will utilize published values of co-volume.

Taylor's Equation of State is:

$$P_e = \rho n R T_e [1 + b\rho + 0.625b^2\rho^2 + 0.287b^3\rho^3 + 0.193b^4\rho^4] \quad (41)$$

where b is the co-volume of the gas mixture in liters per kilogram, P_e is the explosive gas pressure in atmospheres, ρ is the density of the explosive, n is the moles of gas produced, R is the universal gas constant, T_e is the temperature of detonation in Kelvin.

The OSK Equation of State is:

$$P_e = \frac{N_g R T_e}{V_e - \alpha} \quad (42)$$

$$V_e = \frac{1}{\rho} \quad (43)$$

where P_e is the explosive gas pressure in atmospheres, N_g is the moles of gas per kilogram, R is the universal gas constant, T_e is the temperature of detonation, V_e is the specific volume of the explosive gases in liters per kilogram, and α is the co-volume factor in liters per kilogram, and ρ is the density of the explosive.

With an explosive temperature of 4,900° K, the pressure based on the various equations of state has been calculated and is shown in Table 4.8.

Table 4.8 – Explosive gas detonation pressure calculations for various EOS

<i>Temperature</i>	<i>BWK</i>	<i>Cook</i>	<i>Taylor</i>	<i>OSK</i>
4,900° K	218,305 psi	557,627 psi	401,765 psi	578,228 psi

These equations of state must be analyzed and compared with experimental data in order to determine which is the most accurate. With no current data available in the industry for the pressure on the borehole wall from a bulk explosive, which would most closely model this pressure, other methods of verification must be used. This can be accomplished by using Otuonye's data in combination with Boyle's Law to determine the actual gas pressure of detonation.

The volume of Otuonye's charges can be computed by assuming a density of 1.5 g/cc and dividing the weight of the charge (in grams) by this density to get the cubic centimeters of volume for each charge configuration. This has been completed in Table 4.9 and the charge volume is converted to liters to facilitate easy comparison to the volume of the chamber. The volume of the chamber is reported as 0.257 liters.

Table 4.9 – Charge volume calculations

Charge Weight (g)	Charge Volume (cm³)	Charge Volume (L)
10	6.7	0.0067
20	13.3	0.0133
30	20.0	0.0200
40	26.7	0.0267
50	33.3	0.0333

Re-arranging Boyle's Law to determine the final pressure after the gases expand to fill the chamber results in Equation 44. Equation 44 will be run for each of the charge configurations and compared to the average of the experimental results for that charge weight. This calculation is shown in Table 4.10.

$$\frac{P_e V_c}{V_b} = P_g \quad (44)$$

where P_e is the calculated explosive pressure from the various Equations of State in psi, V_c is the volume of the Charge in liters, V_b is the volume of the cannon chamber bore in liters, and P_g is the final pressure in psi.

Table 4.10 – Pressure calculations for decoupled charge from base equations of state

Charge Weight (g)	Charge Volume (L)	Chamber Volume (L)	BKS (psi)	Cook (psi)	Taylor (psi)	OSK (psi)	Experimental Result (psi)
10	0.0067	0.257	5,663	14,465	10,422	14,999	10,000
20	0.0133	0.257	11,326	28,930	20,844	29,999	17,500
30	0.0200	0.257	16,989	43,395	31,266	44,998	27,000
40	0.0267	0.257	22,652	57,860	41,688	59,998	37,000
50	0.0333	0.257	28,315	72,325	52,110	74,997	50,500

It will be assumed that the experimental result is the accurate pressure and the remainder of the pressures will be compared to the experimental result. The results of this analysis show that the BKS method of determination of the borehole pressure typically results in an underestimation of the actual measured experimental pressures, while the Cook, Taylor, and OSK methods typically overestimate the pressures. The BKS method has an average error of 40%, the Cook method has an average error of 54%, the Taylor method has an average error of 11%, and the OSK method has an average error of 60%.

The Taylor Equation of State will then be considered the most accurate of the four methods and will be used in further analysis.

As this analysis is completed, it is important to note that one of the reasons that other methods of pressure determination significantly overestimate the pressure is because this analysis has not taken the compressibility of the gases into account. As the decoupling ratio decreases, the gases are compressed to a larger degree which leads to an increase in pressure. This can be ignored for further analysis from the detonation pressure if the decoupling ratio remains large (which is defined as a decoupling ratio greater than three) but allows for determination of the borehole pressure from any explosive. The compressibility will dramatically increase pressure at small decoupling ratios.

4.2.2. Development of Detonation Pressure Model from Taylor EOS. In order to develop a model from the Taylor Equation of State for a charge of any explosive type which has large decoupling, the blasting process is extremely rapid and is assumed to be adiabatic. This results in no heat transfer of the explosive gases to the rock mass. Furthermore, due to the rapid expansion of gases and the stagnation temperature of gas collision on the borehole wall, it is assumed that the process is isothermal (Otuonye, Skidmore, & Konya, 1983) resulting in minimal change to the gas temperature.

The assumption that the process is isothermal does not represent actual field conditions but is a simplified modelling approach which presents minimal errors in the total magnitude of calculations. The temperature losses associated in the gas are minimal from the detonation, through expansion, to arrival of the maximum borehole pressure. This is due to the cooling effect of the gas during expansion being offset by the increase in the gas temperature from the stagnation of the gases at the borehole wall, which would

be assumed to be completed as the maximum pressure is reached. Following the maximum pressure, the process can not be treated as isothermal.

Furthermore, modelling of the process as an isothermal reaction for decoupled charges has shown a good fit to experimental data (Otuonye, Skidmore, & Konya, 1983). The theoretical treatment of this can also be completed using the mechanism of rarefaction gases cooling in a vacuum (Molmud, 1960). Under this modelling the rate of cooling would result in a change of temperature of approximately 100° K to 150° K, which is approximately 3% of the detonation temperature. The completion of a sensitivity analysis shows that a loss of temperature minimally effects the borehole pressure. For example, a loss of 100° K would result in a 2% change in the borehole pressure. Due to the minimal changes in temperature from a theoretical perspective, the accurate modelling of field data based on isothermal assumptions, and the minimal sensitivity of the changes in temperature to the pressure, the process will be modeled as an isothermal process. A full justification of the isothermal assumption can be found in appendix three.

Boyle's law can then be applied which relates initial pressure and volume to the final pressure and volume. Equation 45 is Boyle's Law (Equation 26) which has been modified to isolate the final pressure, or the borehole pressure, and had blasting specific terms substituted.

$$P_g = \frac{P_T V_e}{V_b} \quad (45)$$

where P_g is the borehole gas pressure in psi, P_T is the explosive pressure from Taylors Equation (Equation 41) in psi, V_e is the volume of the explosive charge in liters, and V_b is the volume of the borehole in liters.

The volume of the borehole can be modeled as the volume of a cylinder. Modifications to this equation to include blasting specific terms and facilitate common field units have been completed and are present in Equation 46.

$$V_b = 0.156d_h^2PC \quad (46)$$

where V_b is the volume of the borehole in liters, d_h is the diameter of the borehole in inches, and PC is the length of the powder column in feet.

The volume of the explosive can be calculated based on the total weight of the explosive in grams divided by the density in grams per cubic centimeter of the explosive. The weight of the explosive is equivalent to the explosive load in grams per meter of boreholes multiplied by the powder column.

This gives the volume of the explosive in the form of Equation 47.

$$V_e = \frac{EL*PC}{\rho} \quad (47)$$

where the V_e is the volume of the explosive is in cubic centimeters, EL is the explosive load in grams per meter, PC is the length of the powder column in meters, and ρ is the density of the explosive in grams per cubic centimeter.

Equation 46 can then be converted to typical field blasting units in the imperial system to facilitate ease of use. The conversion of Equation 47 leads to Equation 48.

$$V_e = \frac{0.454*EL*PC}{\rho} \quad (48)$$

where V_e is the volume of the explosive in liters, EL is the explosive load in pounds per foot, PC is the powder column length in feet, and ρ is the density of the explosive in grams per cubic centimeter. The density in Equation 47 is technically written in metric units and in imperial units would be termed the specific gravity of the explosive;

however, traditional blasting convention in the United States calls the Specific Gravity of the explosive the density of the explosive which has the units of grams per cubic centimeter.

The volumes which are calculated for the volume of the borehole and the volume of the explosive from Equations 46 and 48, respectively, can be used in Equation 44. This is presented in Equation 49.

$$P_g = \frac{P_T * 0.454 * EL * PC}{0.156 * d_h^2 * PC * \rho} \quad (49)$$

where P_g is the borehole pressure in psi, P_T is the explosive pressure in psi, EL is the explosive load in pounds per foot, PC is the length of powder column in feet, d_h is the diameter of the borehole in inches, and ρ is the density of the explosive in grams per cubic centimeter. Simplification of Equation 49 yields Equation 50. Equation 50 can be used to calculate the pressure in the borehole for a charge with large decoupling of any type of explosive from the Taylor Equation of State. Equation 48 will be termed the Detonation Pressure Model.

$$P_g = \frac{2.91 * EL * P_T}{\rho * d_h^2} \quad (50)$$

where P_g is the borehole pressure in psi, P_T is the explosive pressure from the Taylor EOS in psi, d_h is the diameter of the borehole in inches, and ρ is the density of the explosive in grams per cubic centimeter.

Equation 50 can be simplified for a traditional case of Precision Presplitting assuming a P_T for PETN of 401,765, a d_h of 3 inches, a density of 1.5 g/cc to develop an equation which determines the borehole pressure based on the explosive load. In addition

to this, the equation can be modified to facilitate the use of the explosive load in grains per foot. This is presented in Equation 51.

$$P_g = 12.32 * EL \quad (51)$$

where P_g is the borehole pressure in psi and EL is the explosive load in grains per foot.

Equation 50 can be compared to the actual measured borehole pressures by Otuonye. This shows an average error of 13.1% with some outliers over 25%. The empirically derived equation presented in Equation 30 can also be compared with Equation 50 and the measured values of the borehole pressure. A graph of this is shown in Figure 4.5. This shows that Equation 50 predicts slightly higher values for borehole pressure than Equation 30. Equation 50 falls slightly higher than the data set, which is due to the fact that Taylor's Equation of State introduces additional inaccuracies.

Equation 50, the simplified Precision Presplitting pressure equation based on the Taylor Equation of State, can also be compared to Equation 31, the simplified Precision Presplitting pressure equation based on empirical analysis. Figure 4.6 shows this comparison and Equation 51 typically predicts higher pressure values than Equation 31.

The major benefit of Equation 50 is in its ability to predict the borehole pressure for any type of explosive which has a decoupling ratio greater than three. For the case of Precision Presplitting, it seems a more accurate estimation may be made through the use of Equation 30 and 31.

4.3. DEVELOPMENT OF THERMODYNAMIC MODEL

The previously developed models in this dissertation can be used for situations where the decoupling ratio is above three for various types of explosives. As the

decoupling ratio is reduced under three, the pressure in the borehole rapidly increases. This can be modelled by using Equation 50 and observing the effects of a decreasing borehole diameter while keeping the explosive load constant. This effectively represents a decreasing decoupling ratio and is shown in Figure 4.7.

Figure 4.7 shows that once a decoupling ratio is less than three, the borehole pressure will rise dramatically while the pressure has a lesser reaction to changes in decoupling ratio over three. The changes in pressure, at steady temperature, also cause changes to the compressibility of the gas mixture. For example, at larger decoupling ratios the compressibility may change by 2% for a 1.0 decrease in the decoupling ratio. However, for an equivalent 1.0 decrease in the decoupling ratio at small values, the compressibility may change by 20%. In the previous methods of pressure determination, the compressibility of the gas mixture has been ignored, as it has minimal effects when the decoupling ratio is large and significantly increases the complexity of calculations. However, in order to develop a model which can be used for any decoupling ratio, the compressibility should be considered.

The compressibility of a gas will be denoted as Z and can be found from published compressibility curves for various reduced pressures and reduced temperatures (Wark, 1988).

The Ideal Gas Law is a method of calculating the pressure of a system based on the moles of gas produced, temperature, and volume of the container. This is a commonly accepted method to calculate the pressure of a system; however, it cannot be applied when the pressure and temperature are extreme because it does not consider the gas

compressibility. Therefore, thermodynamics has presented a simple modification to the Ideal Gas Law which incorporates compressibility and is shown in Equation 52.

$$PV = ZnRT \quad (52)$$

where P is the pressure in atmospheres, V is volume in liters, n is the moles of gas, T is temperature in Kelvin, R is the universal gas constant in liters-atm per mole degree Kelvin (this is a constant of 0.08206), and Z is the compressibility, which is unitless. The units presented here are different than in previous sections in order to properly scale with the compressibility.

The compression of a gas increases the pressure very rapidly as the packing density is significantly increased and other forces begin to take effect. This results in a high-density gas with large pressures, which is an uncommon occurrence and is rarely treated in explosive engineering.

In order to determine the compressibility at the set temperature and pressure, the temperature and pressure must be corrected to a reduced temperature and reduced pressure. The reduced pressure can be calculated with Equation 53.

$$P_r = \frac{P_g}{P_c} \quad (53)$$

where P_r is the reduced pressure in psi, P_g is the borehole pressure in psi, and P_c is the Pressure Compressibility Constant, which is different for each individual gas. The reduced pressure of the total gas mixture can be found from Equation 54.

$$P_{rMIX} = \sum n_i P_{ri} \quad (54)$$

where P_{rMIX} is the Reduced Pressure of the gas mixture, n_i is the moles fraction of gas per gram of explosive for an individual gas, and P_{ri} is the reduced pressure for an individual gas.

The reduced temperature of the mixture can be found using Equation 55.

$$T_r = \frac{T_e}{T_c} \quad (55)$$

where T_r is the reduced temperature in °K, T_e is the detonation temperature in °K, and T_c is the gas specific reduced temperature for each individual gas. The reduced temperature of the total gas mixture can be found from Equation 56.

$$T_{rMIX} = \sum n_i T_{ri} \quad (56)$$

where T_{rMIX} is the reduced temperature of the gas mixture, n_i is the moles fraction of each individual gas produced per gram of explosive, and T_{ri} is the reduced temperature for each individual gas.

The combination of the reduced temperature of the mixtures and the reduced pressure of the mixture is then used to determine the compressibility.

The pressure in the borehole can then be found from application of Equation 52. Equation 57 is the simplified form of Equation 52 to facilitate easier calculation of the borehole pressure. Equation 57 is termed the Thermodynamic Model.

$$P_g = \frac{14.7 * Z_c * n_g * R * T_e}{V_b} \quad (57)$$

where P_g is the borehole pressure in psi, Z_c is the compressibility of the gas mixture, n_g is moles of gas produced in moles, R is the universal gas constant which is taken as 0.08206 liters-atm per mole degree Kelvin, T_e is the detonation temperature in Kelvin, and V_b is the volume of the borehole in liters. The moles of gas produced can be calculated using Equation 58.

$$n_g = 454 * w_e * n_{MIX} \quad (58)$$

where n_g is the total moles of gas produced in moles, w_e is the weight of the explosive in pounds, and n_{MIX} is the moles of gas produced per gram of explosive.

The substitution of Equation 45 for the borehole volume and Equation 58 for the moles of gas into Equation 57 yields Equation 59.

$$P_g = \frac{3510 * Z_c * w_e * n_{MIX} * T_e}{d_h^2 * PC} \quad (59)$$

where P_g is the borehole pressure in psi, Z_c is the compressibility of the gas mixture, w_e is the weight of the explosive in pounds, and n_{MIX} is the moles of gas produced per gram of explosive, T_e is the detonation temperature in Kelvin, d_h is the borehole diameter in inches, and PC is the powder column in feet.

The explosive load can be written in terms of Equation 60

$$EL = \frac{w_e}{PC} \quad (60)$$

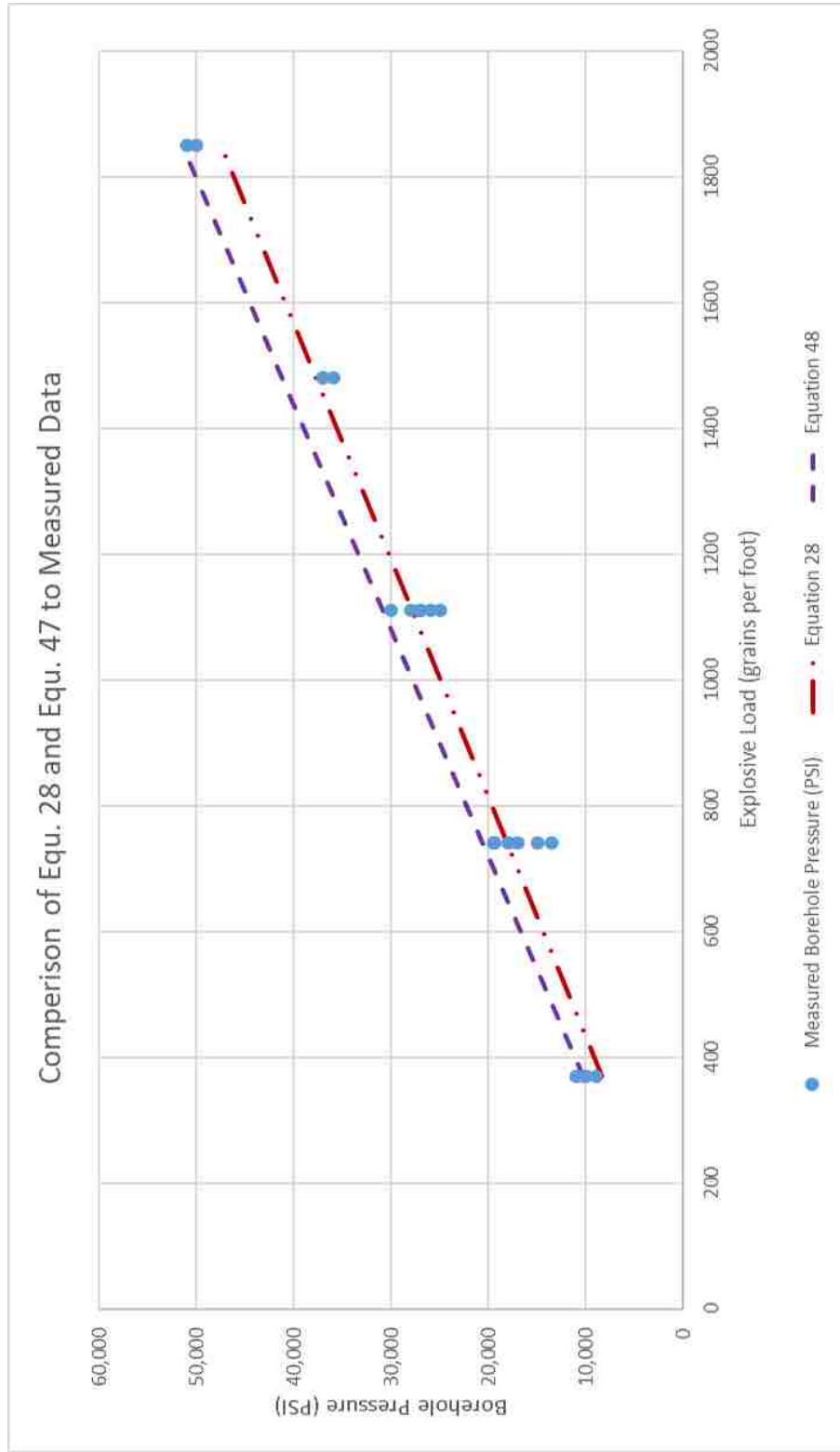
where EL is the explosive load in pounds per foot, w_e is the weight of the explosive in pounds, and PC is the length of powder column in feet.

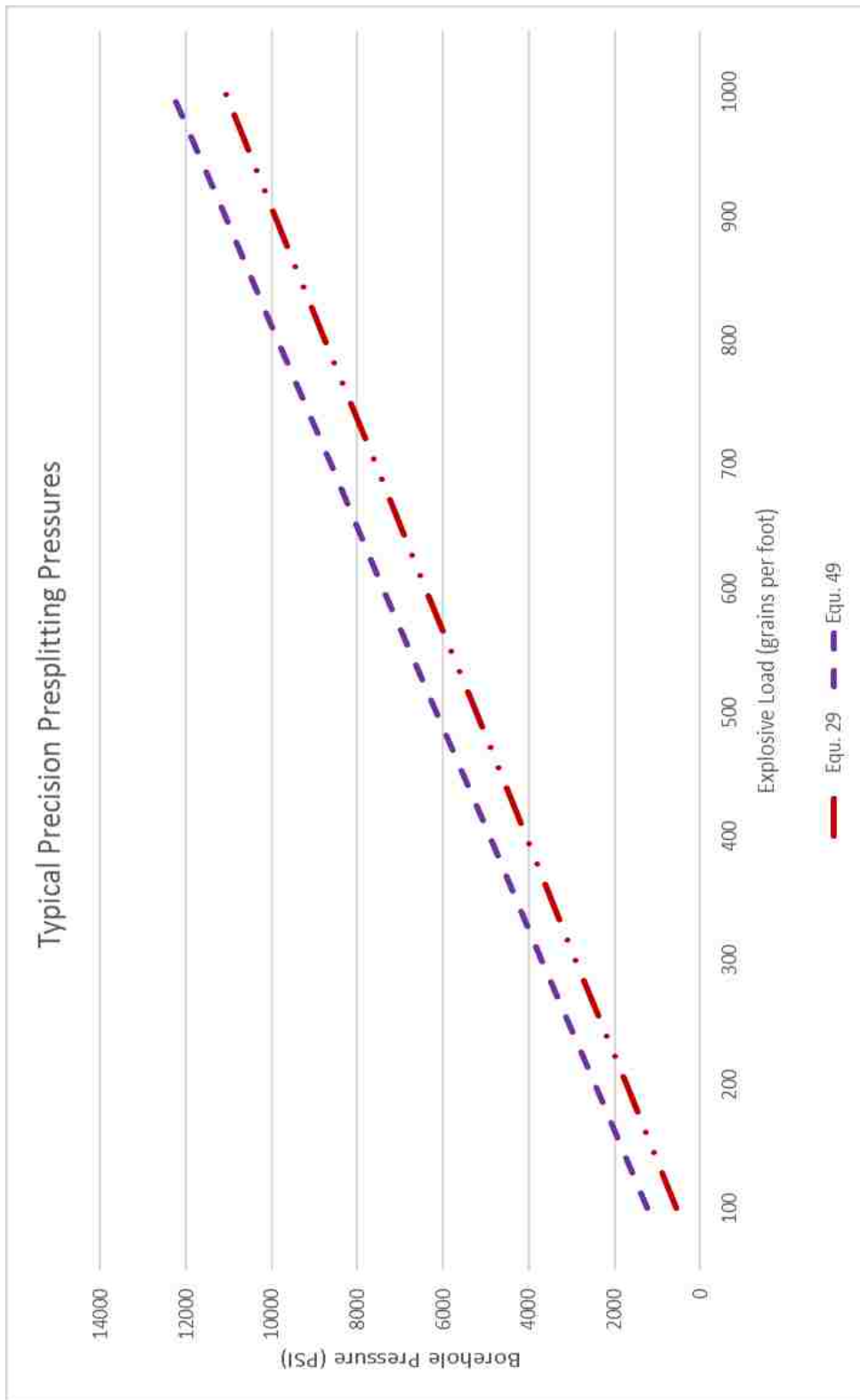
Equation 60 can then be substituted into Equation 59, producing Equation 61 giving an equation for the borehole pressure based on the explosive load used in the borehole.

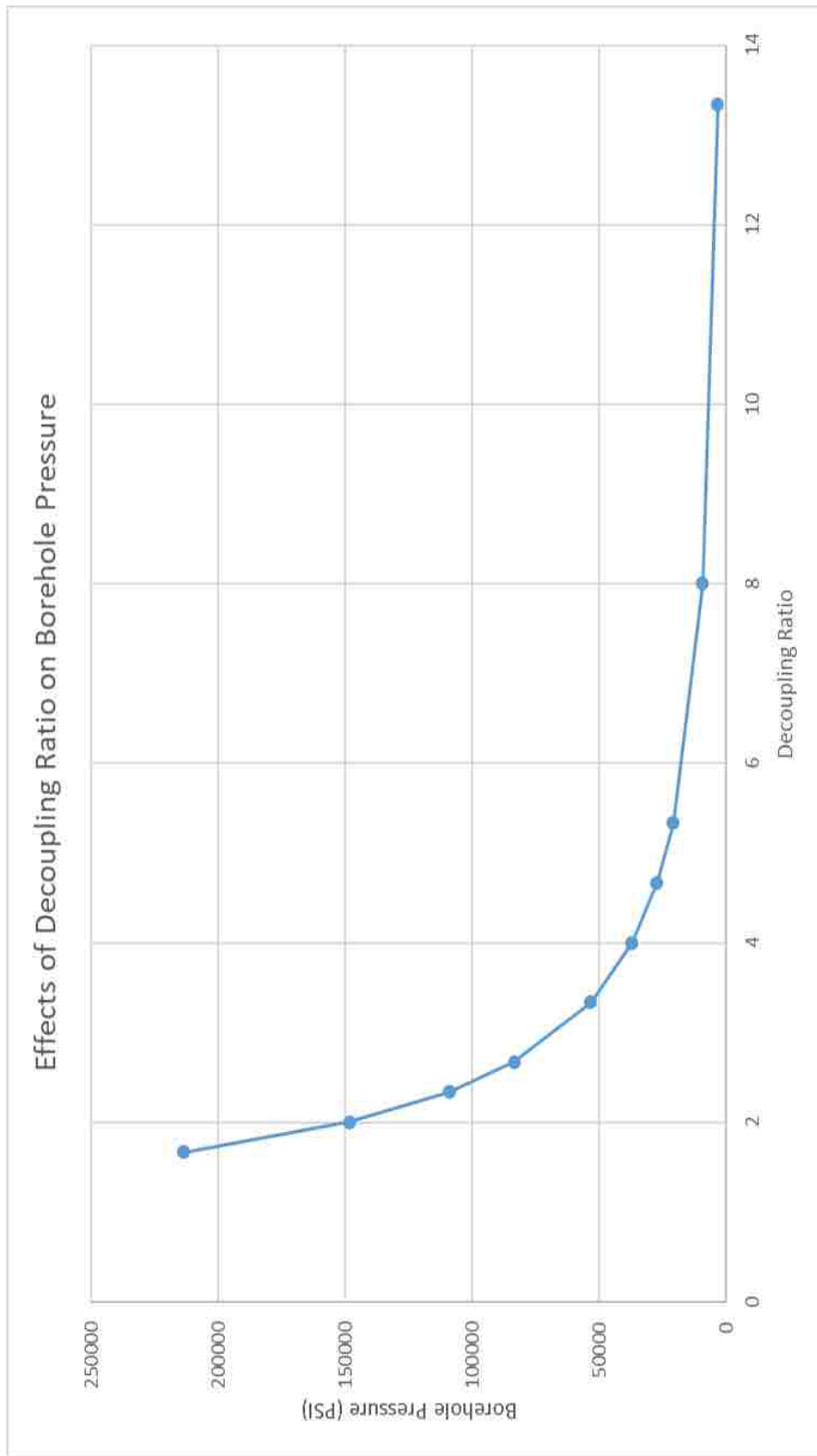
$$P_g = \frac{3510 * T_e * n_{MIX} * EL}{d_h^2} * Z_c \quad (61)$$

where P_g is the borehole pressure in psi, Z_c is the compressibility of the gas mixture, T_e is the detonation temperature in Kelvin, n_{MIX} is the moles of gas produced per gram of explosive, EL is the explosive load in pounds per foot, and d_h is the borehole diameter in inches.

Comparison of Equ. 28 and Equ. 47 to Measured Data







Equation 61 then allows for the determination of the pressure inside of a borehole for a charge of any explosive type with any decoupling ratio. To verify the accuracy of this equation, the various charges measured by Otuonye can be calculated with this system and compared to Otuonye's data. The first step of this will be to determine the mole fractions of various gasses produced by one gram of PETN and is shown in Table 4.11.

Table 4.11 – Mole fractions for gases produced from PETN

<i>Product</i>	<i>Mole Fraction</i>
<i>H₂O</i>	0.363
<i>N₂</i>	0.182
<i>CO₂</i>	0.273
<i>CO</i>	0.182

The critical temperature of PETN can then be computed using Equations 55 and 56 with a temperature of 4,900° K which was previously calculated as the detonation temperature for PETN.

Table 4.12 shows the calculation of the reduced temperatures for PETN detonation. This is set and will not change throughout the process and can be applied to all detonation of PETN gas mixtures under the current assumptions

Otuonye's data is in a form which can be easier applied to Equation 52, and as such it will be used in this analysis. This is because Otuonye's research was completed in a laboratory setting, whereas field data would be easier to apply to Equation 61.

Table 4.12 – Calculation of reduced temperature of PETN gas mixture

Product	Mole Fraction, n_i	T_c	T_r (Equ 55)	$n_i \times T_r$
H2O	0.363	647	7.573	2.749
N2	0.182	126	38.889	7.078
CO2	0.273	304	16.118	4.400
CO	0.182	133	36.842	6.705
T_{rMIX} (Equ. 56) =				20.933

For Otuonye's 10-gram charge, the number of moles of gas produced is 0.348 moles, the temperature of detonation has been calculated previously as 4,900° K, and the volume of the chamber is 0.257 liters. When these are input into Equation 52 and multiplied together it produces the relationship shown in Equation 62 (note this is only for this specific situation and must be calculated for changes in starting conditions).

$$P_g = 8004 * Z_c \quad (62)$$

where P_g is the borehole pressure in psi and Z_c is the compressibility. This example has extreme decoupling and as such the compressibility will be assumed to be equal to approximately one, this would assume a borehole pressure (P_g) of 8000 psi at a reduced temperature of mixture (T_{rMIX}) of approximately 21.

The reduced pressure of the mixture can then be calculated using Equations 53 and 54 and is shown in Table 4.13. The reduced pressure is only valid for the assumed pressure and will change through multiple iterations.

Table 4.13 – Calculation of the reduced pressure, iteration 1

Product	Mole Fraction, n_i	P_c	P_r (Equ 53)	$n_i \times P_r$
H2O	0.363	3205	2.496	0.906
N2	0.182	493	16.227	2.953
CO2	0.273	1072	7.463	2.037
CO	0.182	507	15.779	2.872
P_{rMIX} (Equ. 54) =				8.769

The mixture then has a reduced temperature (T_{rMIX}) of 21 and a reduced pressure (P_{rMIX}) of 8.77. These can be used in combination with a gas compressibility chart (Wark, 1988) to determine the compressibility of the gas mixture, Z_c . This computes a compressibility of 1.04, which is placed into Equation 60 and yields a borehole pressure of 8325 psi. For this dissertation, a pressure difference of 50 psi or less between iterations will result in a successful calculation.

The computed pressure of 8325 psi is a difference of 325 psi from the 8000 psi that was assumed for the first iteration. As such, the process is completed again using an assumed pressure of 8325 psi for the second iteration. The reduced temperature does not change, but the reduced pressure must be calculated again.

The changes to the reduced pressure will be observed in the calculation of P_r for each gas (based on the pressure change in Equation 53) and the summation of these numbers which is used in Equation 54. The second iteration of temperature is shown in Table 4.14.

Table 4.14 – Calculation of reduced pressure, iteration 2

Product	Mole Fraction, n_i	P_c	P_r (Equ 53)	$n_i \times P_r$
H2O	0.363	3205	2.598	0.943
N2	0.182	493	16.886	3.073
CO2	0.273	1072	7.766	2.120
CO	0.182	507	16.420	2.988
P_{rMIX} (Equ. 54) =				9.125

The mixture then has a reduced temperature (T_{rMIX}) of 21 and a reduced pressure (P_{rMIX}) of 9.125 which yields a compressibility of 1.05.

A compressibility of 1.05 in Equation 62 yields a pressure of 8400 psi. A calculated pressure of 8400 psi from iteration two is a 75 psi difference from the assumed pressure of 8325 psi.

For the purposes of this dissertation, a pressure difference of 50 psi or less between iterations will result in a successful calculation. As such a third iteration of the process is completed using an assumed pressure of 8400 psi.

The reduced pressure will be calculated again for the updated pressure assumption. The results of the reduced pressure calculation are shown in Table 4.15. The mixture then has a reduced temperature (T_{rMIX}) of 21 and a reduced pressure (P_{rMIX}) of 9.125 which yields a compressibility of 1.05. A compressibility of 1.05 in Equation 62 yields a pressure of 8400 psi which is equal to the starting assumed value. As such, the process is completed, and the borehole pressure is calculated to be 8,400 psi.

Table 4.15 – Calculation of reduced pressure, iteration 3

Product	Mole Fraction, n_i	P_c	P_r (Equ 53)	$n_i \times P_r$
H ₂ O	0.363	3205	2.321	0.951
N ₂	0.182	493	17.039	3.101
CO ₂	0.273	1072	7.836	2.139
CO	0.182	507	16.568	3.015
P_{rMIX} (Equ. 54) =				9.207

Table 4.15 contains the final iteration for the calculation of the borehole pressure. One iteration of this process has been shown here, with the remainder of iterations for comparison with the measured data by Otuonye shown in Appendix 1.

This method of analysis has an average error of 9.8% when comparing them to the measured pressures after Otuonye. This is a reduction in error of the previous method and this analysis can be completed for any explosive type or decoupling ratio.

Sources of error for this analysis include (1) the ability to accurately distinguish the compressibility factor based on interpolation of graphical compressibility curves, (2) this process assumes ideal and full detonation of explosives, (3) this process has severe limitations on the types of gas for which data is available, (4) the process assumes no heat loss to the surroundings, (5) calculation of theoretical temperature of explosion.

Additional error comes from the use of a significant amount of data through the process, such as compressibility factors, reduced pressure and reduced temperature of various gases, etc. which are developed based on experimentation and carry forward any errors.

While this method has appreciable sources of error, Figure 4.8 better illustrates that the model falls at approximate average values of the measured pressures found by Otuonye. This indicates that while some error is found in the model to actual field conditions, this model is excellent at predicting a typical borehole pressure for that charge type.

In order to simplify this method of calculation, a general formula is developed which applies to the traditional case of Precision Presplitting. Equation 58 can be simplified for the case of blasting with PETN explosives by substituting in the detonation temperature of 4,900° K and the moles of gas per gram of explosive produced as 0.0348. This results in Equation 63 for determination of the borehole pressure from a PETN based explosive.

$$P_g = \frac{85.5 * Z_c * EL}{d_h^2} \quad (63)$$

where P_g is the borehole pressure in psi, Z_c is the compressibility factor, EL is the explosive load in grains per foot, and d_h is the borehole diameter in inches.

The application of Equation 63 at the typical Precision Presplit design of a 3” diameter borehole can be modelled to determine the relationship between the compressibility and the explosive load of the charge. This has been completed in Figure 4.9 which shows that the compressibility varies linearly with the explosive load for Precision Presplitting and has an excellent coefficient of correlation with an R^2 factor of 0.98 and results in the development of Equation 64.

$$Z_c = 0.00008 * EL + 1.0 \quad (64)$$

where Z_c is the compressibility and EL is the explosive load in grains per foot.

Equation 64 can be substituted into Equation 61 and the borehole diameter can be set at three inches to simplify an equation to determine the borehole pressure based on the explosive load. This results in a simplified thermodynamic model for a typical Precision Presplit which is shown in Equation 65.

$$P_g = 0.00076 * EL^2 + 9.5EL \quad (65)$$

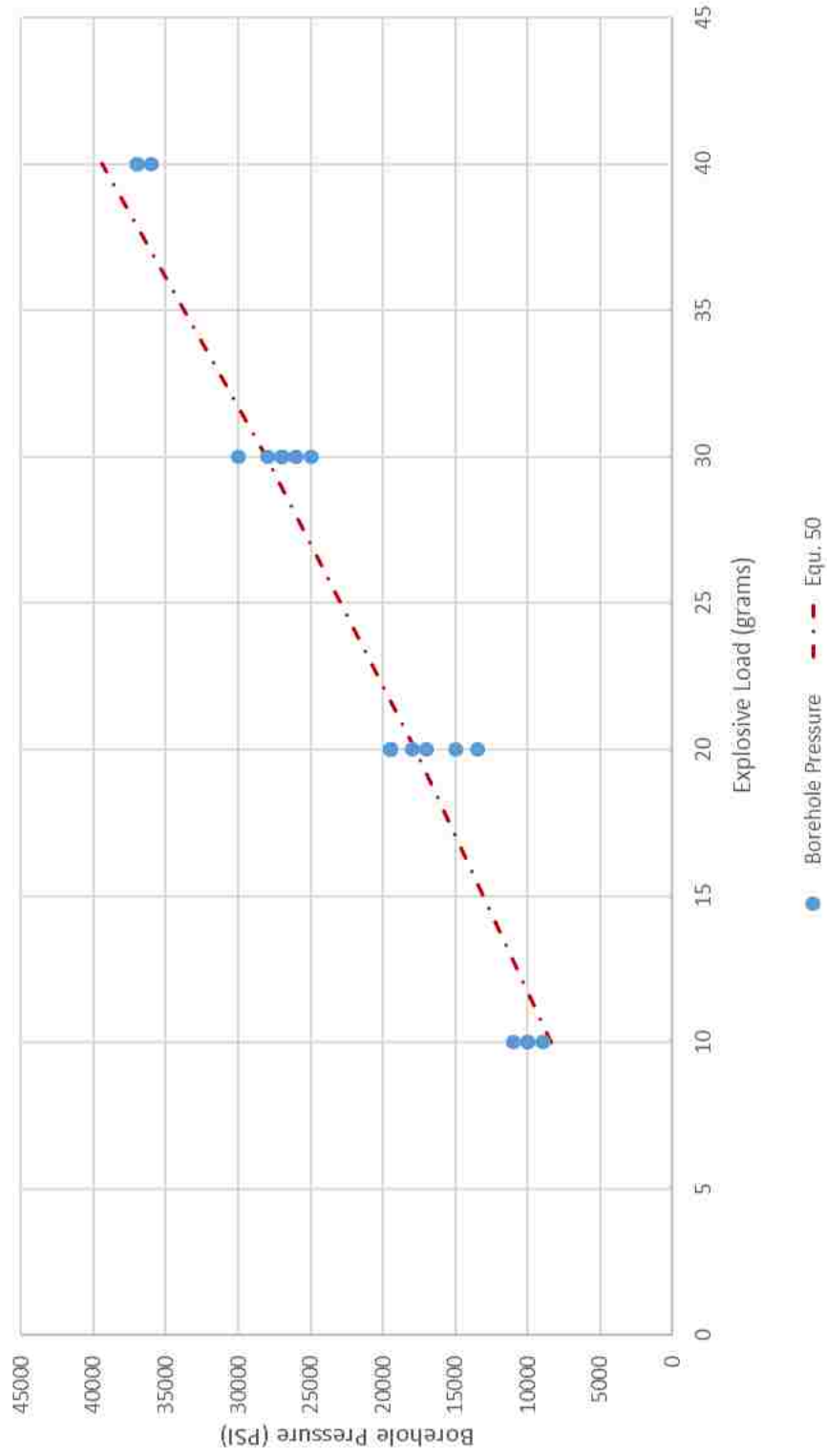
where P_g is the borehole pressure in psi and EL is the explosive load in grains per foot.

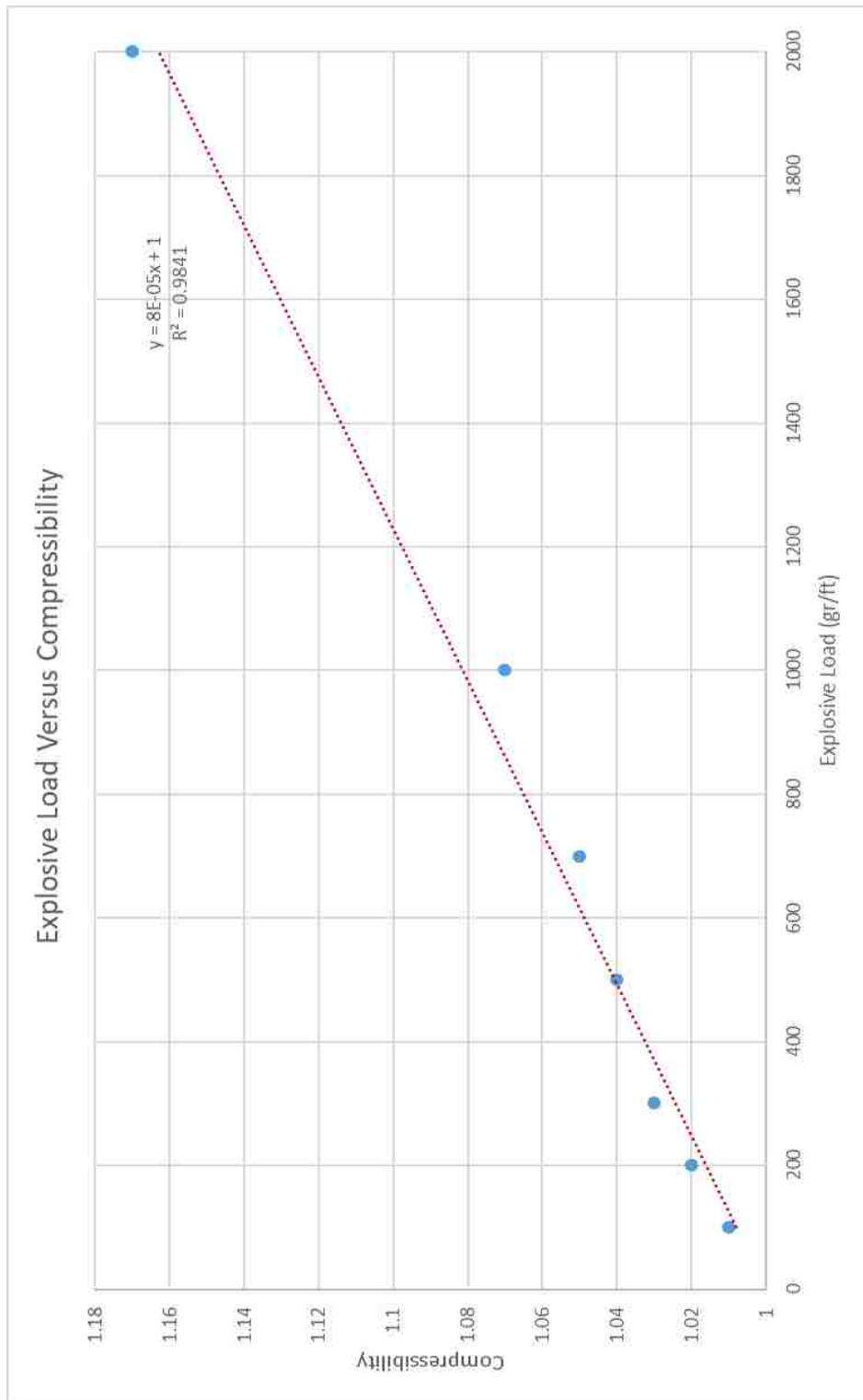
The Detonation Pressure Model is a theoretical model which can compute the borehole pressure based on variations in the explosive, which is one of the limitations of the Empirical Model. The Detonation Pressure model can only be used for large decoupling ratios, a decoupling ratio greater than three, as it does not take compressibility into account. The Detonation Pressure Model is more complex than the Empirical Model but is a straightforward calculation when assuming an appropriate co-volume factor.

The Thermodynamic Model is a complex model which revolves around numerous iterations and requires more complex information for various gases than the Detonation Pressure Model. The Thermodynamic Model can be used for variations in explosive type and decoupling ratio.

This gives the Thermodynamic Model the most flexibility of all the borehole pressure models presented. The flexibility of the model to apply for all field blasting situations is the most important consideration for the development of a general method of pressure predictions. This gives it the ability to be applied to all field loading situations for presplitting and over forms of blasting. The next important parameter is to determine how these models function with valid data and in comparison.

Thermodynamic Pressure Model to Measured Data





4.4. COMPARISON OF PRESSURE MODELS

Three borehole pressure models have now been developed and simplified for easy comparison in the traditional case of Precision Presplitting. The first model is an empirical model which was developed from empirical data and is applicable only for PETN based explosives in boreholes with large decoupling, which is defined as a decoupling ratio greater than three. This model has an average error of 8.8% and is the simplest of the models to use, relying solely on the explosive load.

The second model is developed based on the Taylor detonation pressure model which can be used with any explosive, but only for large decoupling as it does not take compressibility into account. This requires knowledge of the temperature of explosion and co-volume factors and is a more complex process than the empirical model. This model has an average error of 13.1%

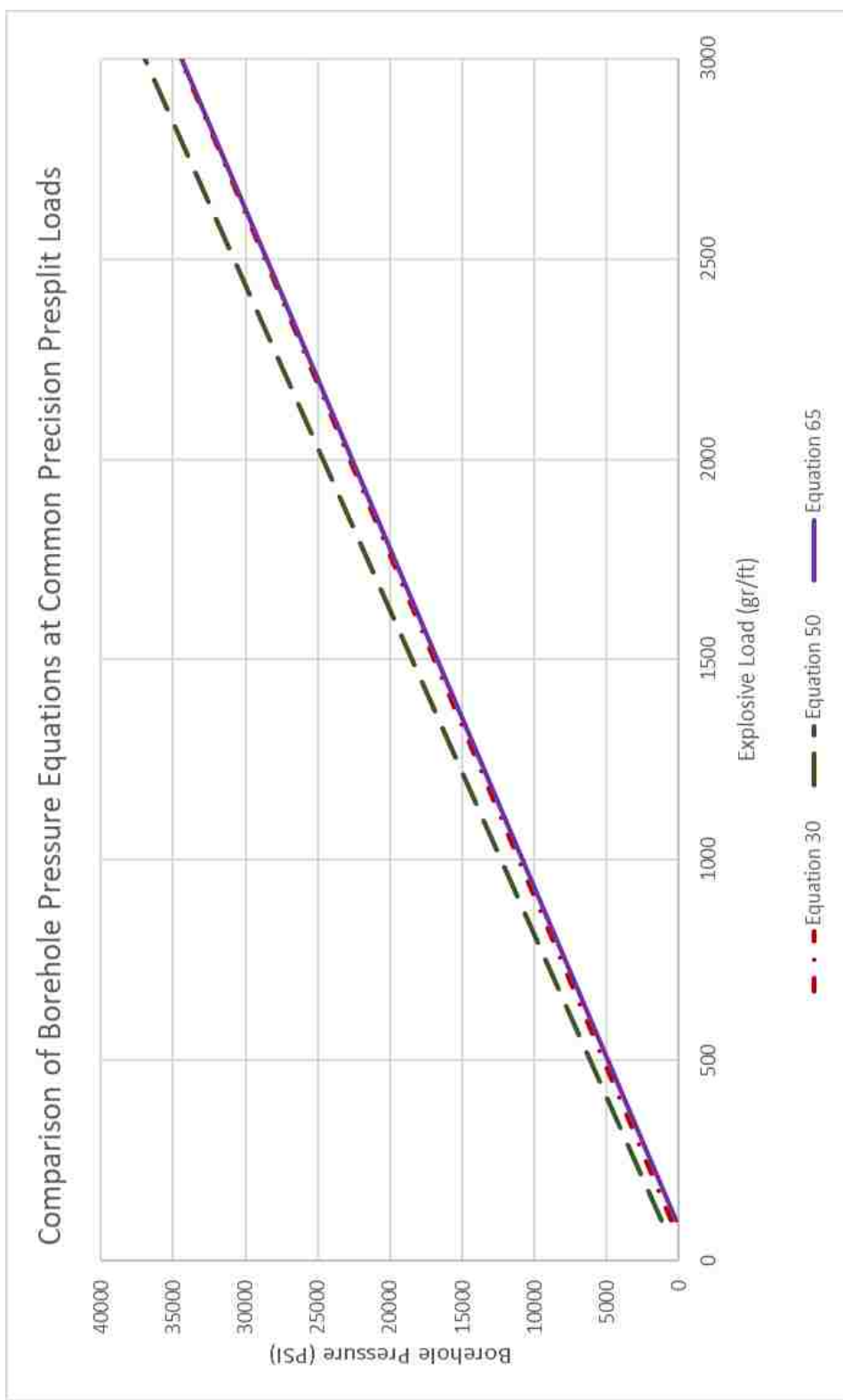
The final model is the most difficult model based on thermodynamic principles for gases at high temperature and pressure. This model is completed through an iterative process and requires all information from previous models, along with determination of the compressibility through compressibility curves. However, this model can be utilized for any type of explosive at any decoupling ratio giving the most flexibility of any of the models. The error of this model is 9.8% which is less than the model based off of Taylor's detonation pressure.

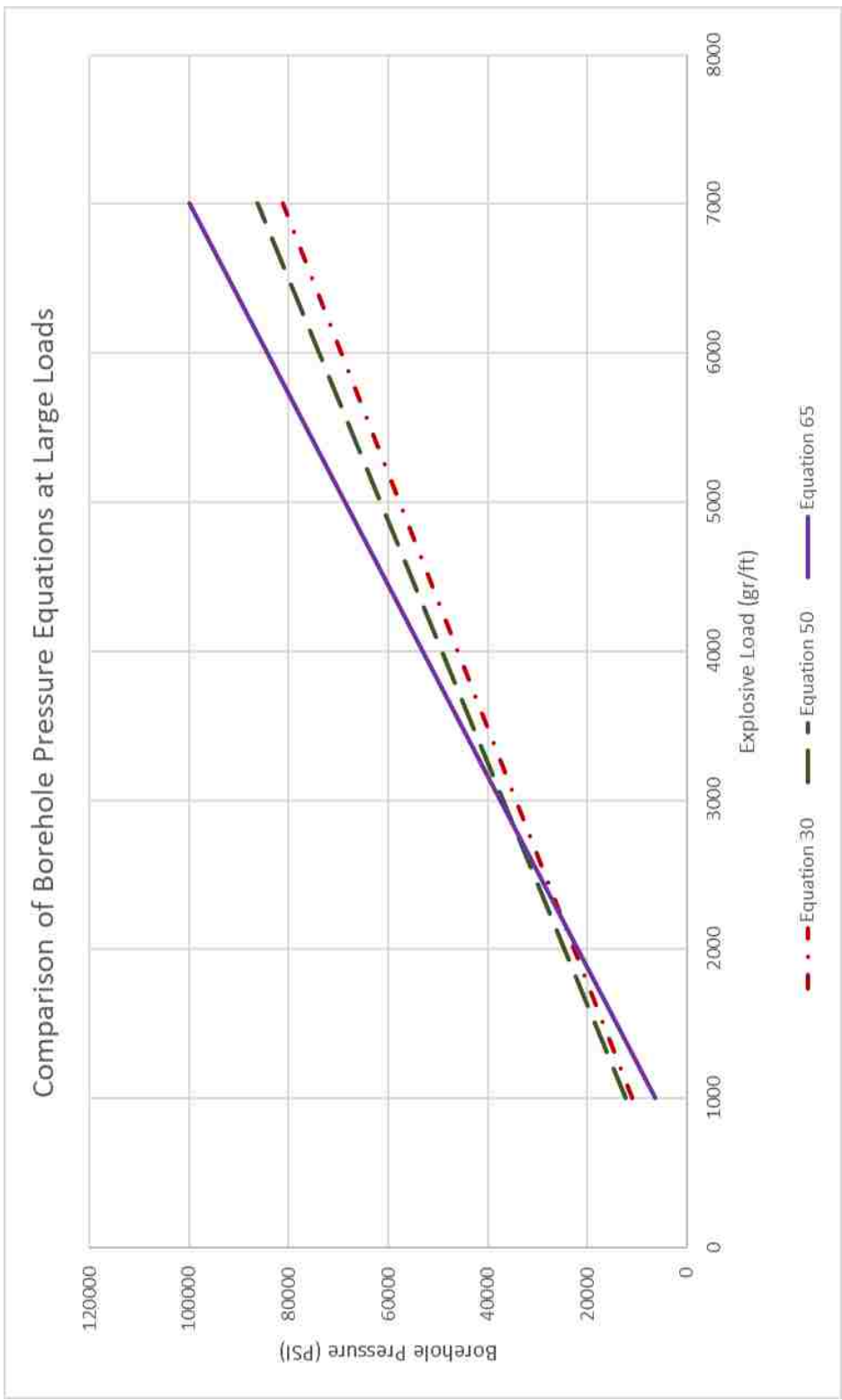
These three models can be analyzed in their simplified forms, which are found in Equation 31, Equation 51, and Equation 65. This analysis is developed to show the variations in predicted pressure between the models for various explosive loads. Figure 4.10 shows the three models from an explosive load range of 500 grains per foot to 3,000

grains per foot; this is the typical range of Precision Presplitting explosive loads. Once the explosive load has reached 3,000 grains per foot, the explosive would typically be switched to a presplit powder. At this range the pressure models are very similar, with Equation 30 (Empirical Model) and Equation 65 (Thermodynamic Model) being nearly identical. This shows that the Thermodynamic model accurately portrays the borehole pressure.

These equations can also be analyzed for much higher charge loads, such as that from 1,000 grains per foot to 7,000 grains per foot (one pound per foot), which represent a borehole with a small decoupling ratio. It can be seen in Figure 4.11 that Equations 30 and 50 dramatically underestimate the borehole pressure compared to Equation 65. This is because Equations 30 and 50 do not take into account the large rise in the compressibility of the explosive gases.

For this reason, it is recommended that the Thermodynamic Model be used when the borehole pressure determination is critical. The Thermodynamic Model has been shown to be the most accurate model of the three aforementioned pressure models. The Thermodynamic Model is also the most flexible of the models allowing for its application in numerous situations. Equation 65 will be used in all further analysis in this dissertation, as it is determined to accurately model the borehole pressure for all situations. Certain situations, which are not part of this dissertation, may require the use of the other pressure models. For example, when analyzing highly decoupled explosives which produce detonation products that lack the necessary information for advanced analysis.





4.5. BOTTOM CHARGE EFFECTS

A typical Precision Presplit load on a 24” spacing will utilize between 100 grains per foot and 700 grains per foot of detonating cord depending on the rock type. The typical loads at this spacing are shown in Table 4.16. As this spacing is expanded the explosive load is increased to typically a maximum of 1500 grains per foot; as the spacing is decreased the explosive load is decreased, with a minimum explosive load of 50 grains per foot. The typical borehole length that is used in industry is between 10 feet and 25 feet; with some Precision Presplit blasts having a borehole length of up to 50 feet. The reason the borehole length is typically kept short is that the drill deviation becomes severe as the boreholes increase in length and blasters often state that longer boreholes make it more difficult to presplit than shorter boreholes.

Table 4.16 – Typical explosive column load for various rock types

<i>Rock Type</i>	<i>Explosive Load through Borehole (EL_c)</i>
Granite	700 grains per foot
Limestone	500 grains per foot
Shale	300 grains per foot
Sandstone	250 grains per foot
Siltstone	100 grains per foot

The load which is brought throughout the entire borehole will be termed the ‘column load’ (EL_c) as it is the load that is continuous throughout the entire powder

column. The borehole will also contain a ‘bottom load’ which is a concentrate charge of explosives that is placed in the bottom of the borehole. This bottom load is used for two reasons, the first is that detonating cord can be difficult to place into a borehole. When a weight is placed on the bottom of the detonating cord, it simplifies the loading technique. The bottom load is simply lowered into the borehole and the detonating cord is pulled down. Secondly, although no studies exist showing this phenomena blasters and engineers often find that the bottom of the presplit is the most difficult to split. This could be for numerous reasons, including that the bottom of the presplit typically has less weathering than the top and therefore is more competent rock. This bottom load helps to increase the charge load at the bottom and ensures presplit formation in the bottom of the borehole.

The bottom load for the Precision Presplit is typically one pound, either in the form of emulsion, presplit powder, or a cast booster, which is a PETN based product. While the immediate effect of this charge may be at the bottom of the borehole, the maximum borehole pressure is considered to be equivalent throughout, as changes in the pressure of the bottom of the borehole will be transmitted upwards throughout the remainder of the borehole under the theory of choked gas flow. This bottom load is significant enough in relation to the column load that it greatly changes the borehole pressure. For example, a 10-foot borehole under typical stemming considerations, the bottom load is 65% of the total explosive load.

The bottom load can be scaled from a concentrated load, in pounds, to its equivalent distributed load using Equation 66.

$$EL_{be} = \frac{7000 * EL_b}{PC} \quad (66)$$

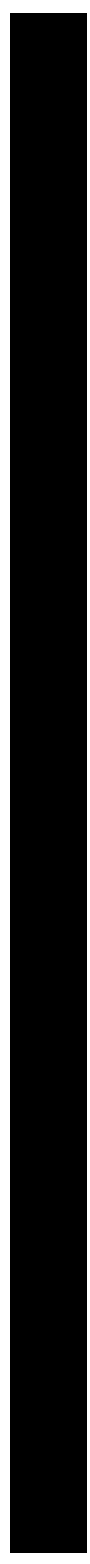
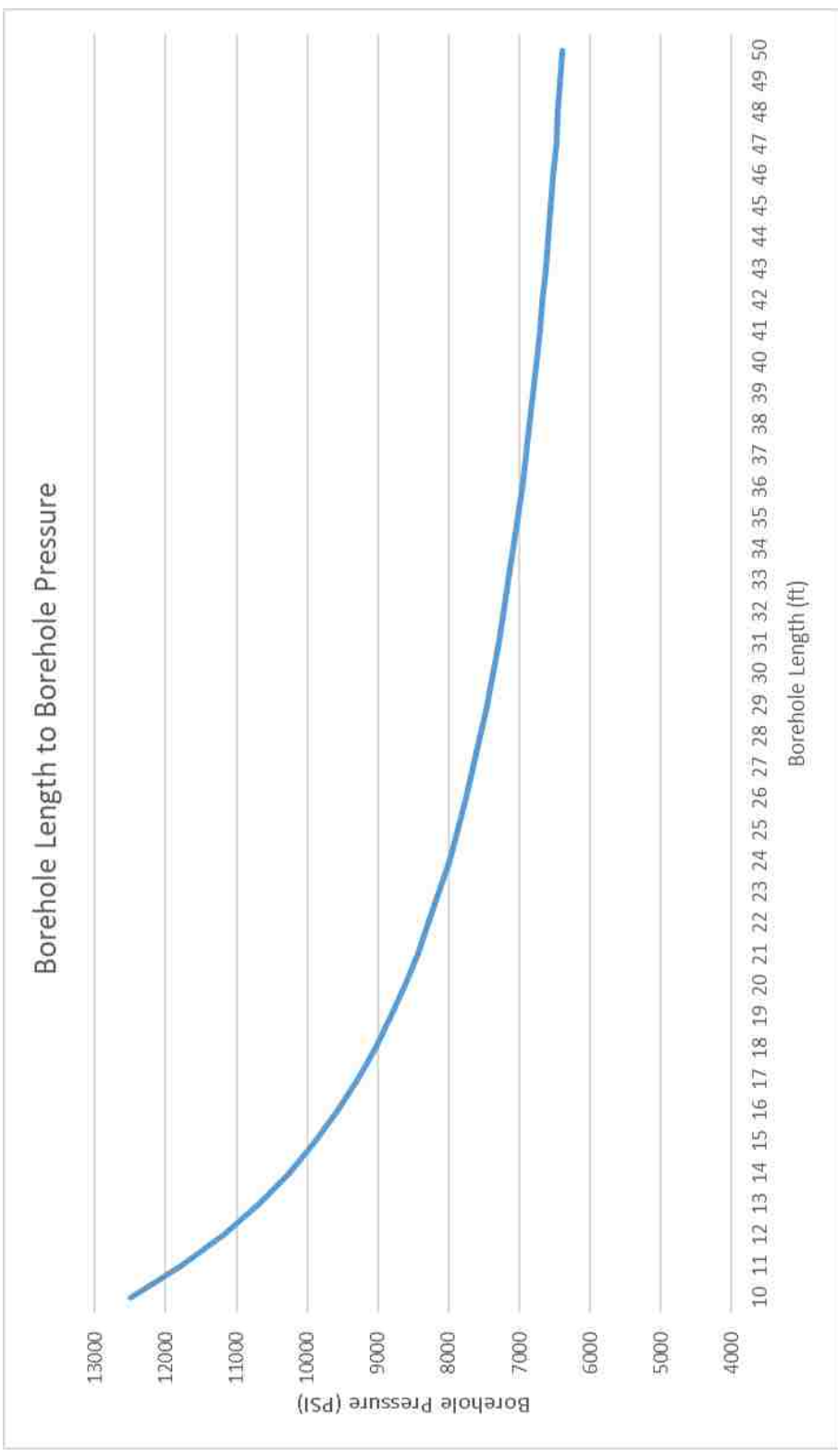
where EL_{be} is the Equivalent Bottom Load in grains per foot, EL_b is the bottom load in pounds, and PC is the length of powder column in feet. The total explosive load in the borehole is then the combination of the column load and the bottom load, which can be calculated using Equation 67.

$$EL_e = EL_c + EL_{be} \quad (67)$$

where EL_e is the Equivalent Explosive Load in grains per foot, EL_c is the column load in grains per foot, and EL_{be} is the equivalent bottom load in grains per foot. This equivalent explosive load would be used to determine the borehole pressure in the previously presented borehole pressure equations.

The current method of Precision Presplitting uses a set bottom load of one-pound of explosive product. Under this case, the borehole pressure then varies based on the length of the borehole. This can be modelled to show the differences in borehole pressure based on borehole length and is shown in Figure 4.12. This chart shows that as the borehole length exceeds 30 feet, the borehole pressure begins to reach a steady state and the effects of the bottom load are not as significant. The 10-foot borehole has double the borehole pressure of a 50-foot borehole. This would indicate that for boreholes which are greater than 25 to 30 feet, the column load would need to be increased to increase the overall borehole pressure.

The typical methods of Precision Presplitting have been analyzed for construction blasting on lock and dam projects by past authors. These situations use the short benches and bottom load considerations have not been previously analyzed. This indicates that the bottom load for these short benches is a major source of pressure and cannot be ignored in further analysis of the topic.



4.6. PRESSURE OF A TYPICAL PRECISION PRESPLIT

The borehole pressure for a Precision Presplit blast can then be found through the applications of Equations 65, 66, and 67. These equations will incorporate the bottom load as a function of the borehole length and the column load. For example, a common Precision Presplit blast in many U.S. Army Corp of Engineer's projects is to use a borehole length of ten-feet at the bottom of a project. Assuming that the rock is limestone the column load is 500 grains per foot, the bottom load is one-pound, and the blaster plans to use 2.5-feet of stemming, which results in a powder column of 7.5-feet, Equation 66 then yields:

$$EL_{be} = \frac{7000 * 1}{7.5} = 933.3 \text{ grains per foot}$$

The equivalent bottom load of 933.3 grains per foot is then incorporated into Equation 67, with a column load of 500 grains per foot, which yields

$$EL_e = 500 \frac{gr}{ft} + 933 \frac{gr}{ft} = 1,433 \frac{gr}{ft}$$

The equivalent explosive load is then used in Equation 65 to get the borehole pressure which yields

$$P_g = 0.00076 * 1433^2 + 9.5 * 1433 = 15,174 \text{ PSI}$$

The borehole pressure is then 15,174 psi for this example. This process can then be completed for any changes in the explosive load. If changes are to be made to the borehole diameter then Equation 63 can be used. With major changes to other variables such as the explosive type then the full Thermodynamic Model can be applied.

5. HOOP STRESS MODEL FOR BLASTING

5.1. DEVELOPMENT OF HOOP STRESS MODEL

The borehole pressure for various situations of blasting can now be determined from the application of either the Empirical Model, The Detonation Pressure Model, or the Thermodynamic Model. This is beneficial but does not give any insight into how the rock is actually breaking in a Precision Presplit. In order to determine how the rock is breaking, the magnitude of the stress field must be computed. The breakage process for a Precision Presplit breaking under the mechanisms of a Hoop Stress field has been previously discussed and the modelling method of a thick-walled pressure vessel has been presented in Equation 20. Equation 20 has been modified to include blasting specific terminology in Equation 68.

$$\sigma_c = \left[\frac{P_g d_h^2 - p_o S^2}{S^2 - d_h^2} \right] - \left[\frac{d_h^2 S^2 (p_o - P_g)}{d^2 (S^2 - d_h^2)} \right] \quad (68)$$

where σ_c is the Circumferential Hoop Stress in psi, P_g is the borehole pressure in psi, d_h is the diameter of the borehole in inches, p_o is the pre-existing rock stress, S is the spacing in inches, and d is the distance away from the center of the borehole in inches.

In a majority of situations for surface blasting where some excavation has already taken place, it will be assumed that the pre-existing rock stress is very small compared to the borehole pressure. This would treat the pre-existing rock stress as zero. This yields Equation 69.

$$\sigma_c = \left[\frac{P_g d_h^2}{S^2 - d_h^2} \right] + \left[\frac{d_h^2 S^2 P_g}{d^2 (S^2 - d_h^2)} \right] \quad (69)$$

The distance that the stress field is from the borehole, d , will be defined as a function of the spacing as shown in Equation 70.

$$A = \frac{d}{S} \quad (70)$$

where A is the distance constant, d is the distance away from the borehole in inches, and S is the spacing in inches. The constant 'A' will vary between a value of $\frac{d_h}{2S}$ and 1.

Equation 70 will be substituted into Equation 69, which yields Equation 71.

$$\sigma_c = \left[\frac{P_g d_h^2}{S^2 - d_h^2} \right] + \left[\frac{d_h^2 S^2 P_g}{A^2 S^2 (S^2 - d_h^2)} \right] \quad (71)$$

Simplification of Equation 71 yields Equation 72.

$$\sigma_c = \frac{P_g d_h^2 (A^2 + 1)}{A^2 (S^2 - d_h^2)} \quad (72)$$

where σ_c is the Circumferential Hoop Stress in psi, P_g is the borehole pressure in psi, d_h is the diameter of the borehole in inches, S is the spacing in inches, and A is the distance constant as defined in Equation 70. Equation 72 can now be utilized to calculate the magnitude of the Hoop Stress field at any distance in between two boreholes based on the explosive pressure.

Precision Presplitting functions with every borehole containing an explosive load. It will then be assumed that each borehole would cause a fracture to form to halfway between the boreholes, or half the spacing. This area results in an 'A' value of $\frac{1}{2}$ which will be called the maximum split distance. In situations where the second borehole is not loaded, the A value will reach a value of 1.0 to indicate that the fracture from the borehole would need to split the entire spacing distance, resulting in an increase to the explosive load.

The fracture formation of the presplit starts at the borehole wall and is modelled by a distance constant (A) of $\frac{d_h}{2S}$. Figure 5.1 shows that near the borehole wall the pressure is extremely large. As the distance away from the borehole increases, the magnitude of the hoop stress is rapidly reduced and is approximately 5% halfway between the boreholes when compared to what it is at the borehole wall. The hoop stress field at the adjacent borehole is less than 2% than the stress next to the borehole that fires.

The stress produced on the adjacent borehole produces a circumferential loading profile which is similar to what is found from overburden stresses on a mine opening. This creates a stress field around the borehole causing the sides of the borehole which are oriented towards the presplit line to have a stress of minus sigma ($-\sigma$) and at a 90° and 270° direction of the borehole to be in a stress state of three sigma (3σ). This places the borehole into differential loading, this differential loading causes the presplit to align between boreholes and prevents additional fracturing which can cause backbreak.

Furthermore, each borehole typically has one borehole being detonated on each side of the blast, which causes double the circumferential loading. This would signify that the borehole has 12% of the stress found at the borehole wall, which is acting in compression to prevent overbreak at 90° and 270° around the borehole, and 4% of the total pressure, which helps to align the presplit fracture between boreholes.

This results in a circumferential loading of 16% around the borehole, with 12% of the stress at the borehole stopping overbreak from occurring and 4% of the stress causing a fracture to form between boreholes. This circumferential loading helps to explain why the presplit fracture aligns between boreholes and minimizes the overbreak past the intended presplit line. This loading is further discussed in Appendix D.

Assuming both boreholes are loaded with explosives the maximum split distance is defined as halfway between the boreholes, which produces a distance constant (A) of 0.5. Holding the borehole diameter and the explosive load as constants, the hoop stress field can be analyzed based on the borehole spacing. Figure 5.2 shows this relationship, of the hoop stress as a function of spacing. The hoop stress field is a function of the square of the distances, which is the same result that was found from empirical work.

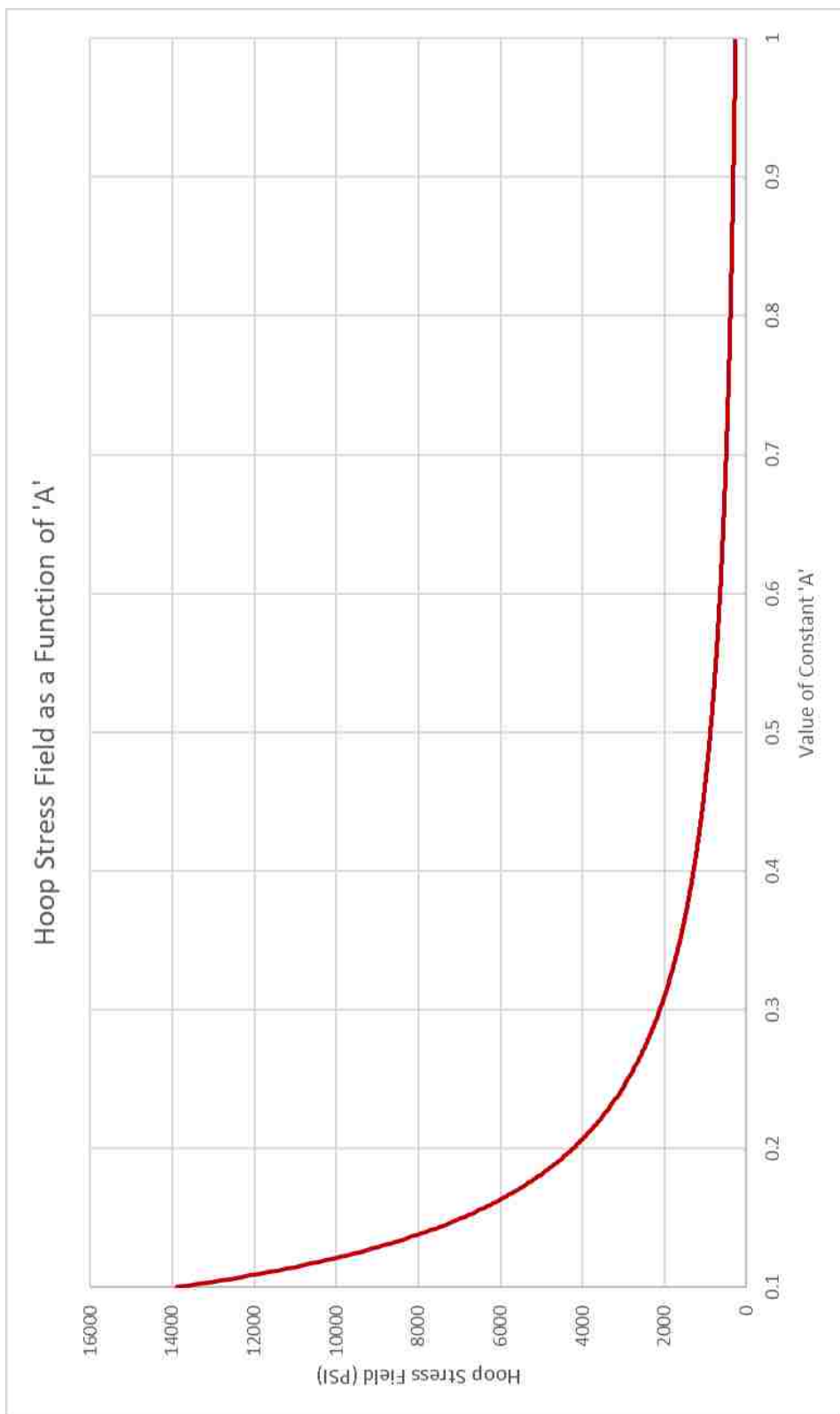
The effect of the borehole diameter can also be analyzed from the Hoop Stress Equation. The borehole diameter influences both the magnitude of the Hoop Stress field and the borehole pressure. The borehole pressure can be modeled from Equation 63 to determine the effects of borehole diameter and this borehole pressure can then be applied in Equation 72. The maximum split distance will again be assumed to be halfway between boreholes to observe a distance constant (A) of 0.5. The explosive load and spacing are then kept constant and the series of equations will only be a function of the borehole diameter.

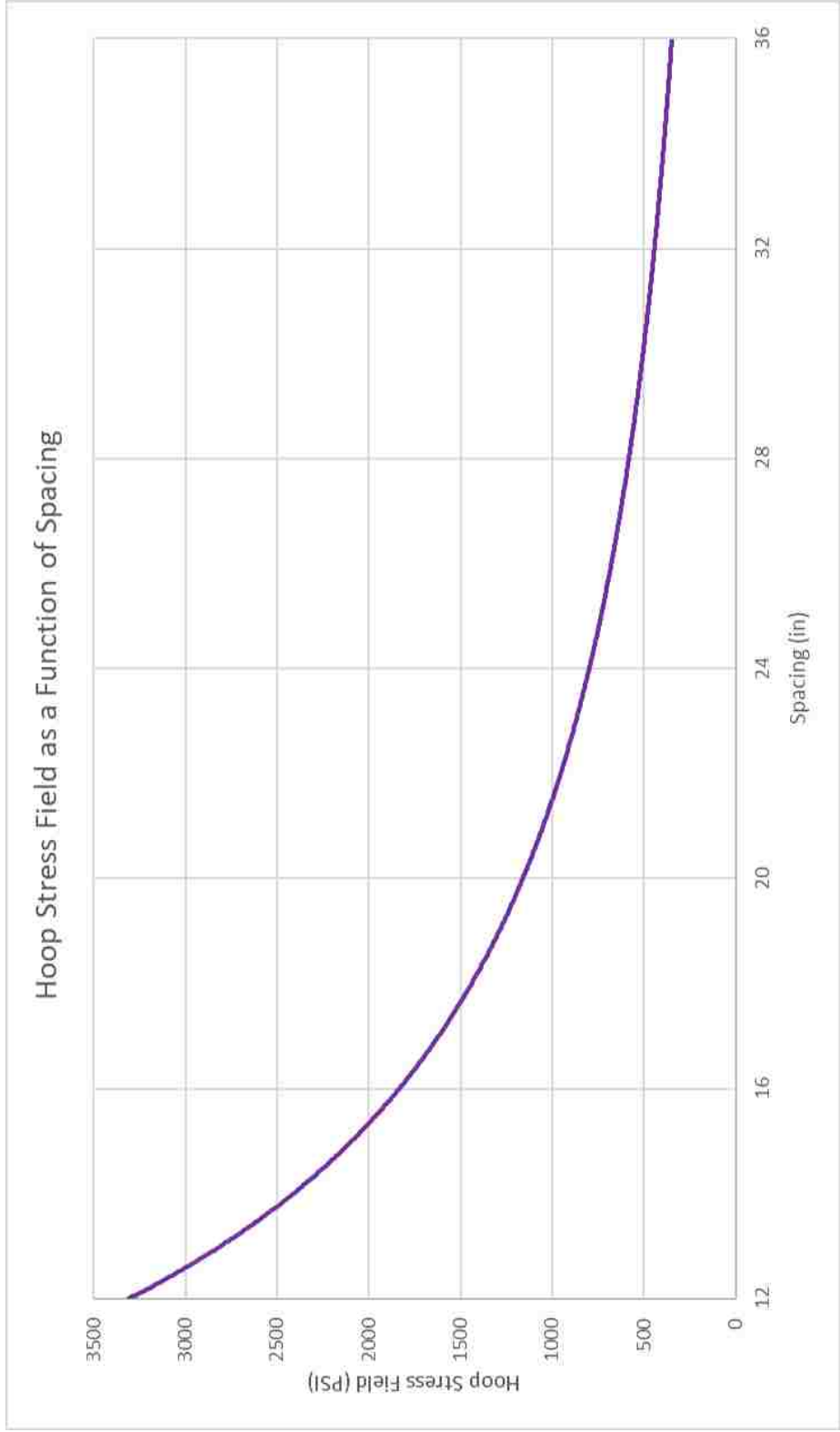
This analysis proves a phenomenon which has been discussed in the blasting industry. Experts in the blasting industry often state that the diameter of the borehole did not matter, if the explosive load is properly matched to the spacing of the boreholes (Konya & Walter, 1990). This confused many in the industry as it was believed that this changed the internal borehole pressure. This is often used by proponents of the shockwave breakage mechanisms as a proof against the gas pressure in the borehole causing the presplit. It is claimed that if the borehole pressure is reduced and no effect on the presplit occurs then it must be the shockwave, which does not change based on the borehole diameter, which causes the presplit to form.

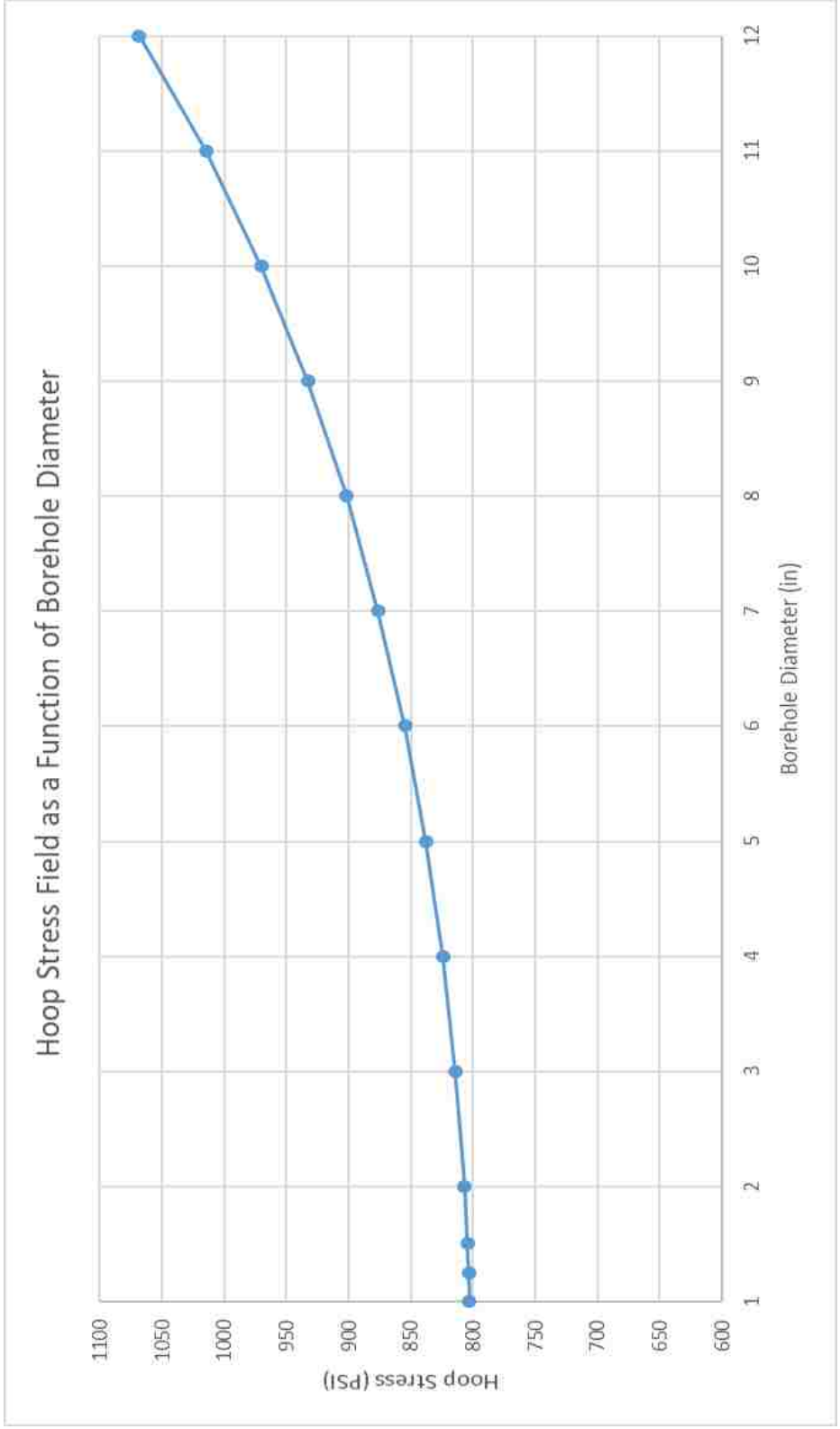
However, as the borehole diameter is increased, with spacing remaining constant, the web of rock between the boreholes decreases. The decrease in the total web of rock from an increasing borehole diameter has a larger impact on the hoop stress field than the decrease in the reduction of the borehole pressure from the increased diameter. This results in a minimal change in the rock stress when the borehole diameter is less than 25% of the spacing, and an increase in the stress field when the borehole diameter is larger than 25% of the spacing. This has been shown in Figure 5.3, which shows the magnitude of the hoop stress field halfway between the boreholes for variations in the borehole diameter.

This state then when the spacing is held constant and the borehole diameter is increased, the explosive load can remain the same to still cause the presplit to form. This has been found in the field for project which utilize Precision Presplitting. For example, if the spacing is held constant at 24 inches between boreholes, it does not matter if the borehole is 3" or 3.5" in diameter, the explosive load would be the same to generate the presplit. This is due to the decreased distance the explosive must split between boreholes.

However, in a majority of situations when the borehole diameter is increased, such as in the mining industry which can use up to 10-inch diameter boreholes for presplitting, the spacing is also increased. In this situation, where both the spacing and borehole diameter are increased, changes are visible to the Hoop Stress Field. This situation would not follow this relationship as the web of rock between holes increases.







5.2. SIMPLIFICATION OF HOOP STRESS MODEL

The combination of Equations 63, 64, and 72 results in Equation 73 which can be used to determine the Hoop Stress Field from a Precision Presplit Blast from the equivalent explosive load in grains per foot.

$$\sigma_c = \frac{(0.00684 * EL_e^2 + 85.5 * EL_e)(A^2 + 1)}{A^2(S^2 - d_h^2)} \quad (73)$$

where σ_c is the magnitude of the hoop stress field in psi, EL_e is the equivalent explosive load in grains per foot, A is the distance constant, S is the spacing in inches, and d_h is the borehole diameter in inches.

Equation 73 can be further simplified to develop a general equation for the typical case of a Precision Presplit. In this case the spacing is 24 inches and the borehole diameter is three inches. Furthermore, the maximum split distance is assumed to be halfway between the boreholes. This implies that each borehole will require enough explosive load to cause the presplit formation to halfway between boreholes. This would set a distance constant (A) value of 0.5. These assumptions for Equation 73 result in Equation 74, which is a simplified equation for the determination of the Hoop Stress from the explosive load in a Precision Presplit.

$$\sigma_c = 0.00006 * EL_e^2 + 0.76EL_e \quad (74)$$

where σ_c is the circumferential hoop stress in psi and EL_e is the equivalent explosive load in grains per foot.

The equivalent explosive load must generate enough stress to exceed the tensile strength of the rock mass in order to develop the presplit. The Brazilian Tensile Strength will be considered the tensile strength of the rock and denoted as σ_B . The circumferential hoop stress in Equation 74 is then equal to the tensile strength for the explosive load,

which will cause a presplit to form. Equation 74 can then be solved through the quadratic formula and simplified to Equation 75, which can be used to determine the equivalent explosive load necessary to cause a presplit to form based on the rock's tensile strength.

$$EL_e = -6300 + 130\sqrt{2,400 + \sigma_B} \quad (75)$$

where EL_e is the equivalent explosive load in grains per foot and σ_B is the Brazilian Tensile Strength of the rock in psi. This gives engineers a new tool to determine the explosive load for a Precision Presplit blast which has a 24" spacing between boreholes.

5.3. HOOP STRESS OF A PRECISION PRESPLIT BLAST

Previously published data has shown what average values for the explosive load are based on the rock type, which are provided in Table 5.1. These explosive loads are commonly used field loads for a 10-foot to 15-foot bench with a one-pound bottom load. The previous models can then be used in accordance with what is applied daily in the field to determine if the calculated magnitude of the hoop stress matches the application of this technology in the real world. This can be viewed as validation of this methodology.

Equations 66 and 67 can be used to find the equivalent explosive load for these situations assuming a 10-foot bench, which is commonly used in the final excavation of many large construction projects. The bottom explosive load for all these situations would then be equal to 700 grains per foot (EL_B).

The equivalent explosive load (EL_e) is then shown for these rock types in Table 5.2 which includes both the equivalent distributed bottom charge and the column charge.

Table 5.1 – Typical explosive loads for various rock types

<i>Rock Type</i>	<i>Explosive Load through Borehole (EL_c)</i>
Granite	700 grains per foot
Limestone	500 grains per foot
Shale	300 grains per foot
Sandstone	250 grains per foot
Siltstone	100 grains per foot

Table 5.2 – Equivalent explosive loads for various rock types

<i>Rock Type</i>	<i>Equivalent Explosive Load (EL_e)</i>
Granite	1400 grains per foot
Limestone	1200 grains per foot
Shale	1000 grains per foot
Sandstone	950 grains per foot
Siltstone	800 grains per foot

The values in Table 5.2 are derived from the typical form of Precision Presplitting which is applied in Equation 74. To determine the stress at the assumed maximum split distance of halfway between the boreholes, Equation 74 can be applied to each of these situations. These can then be compared to published Brazilian Tensile Strength Data for the rock types, which is shown in Table 5.3. Rock Strength are stated as a range, as the

strength widely varies based on weathering and structure and are compiled from various sources for what may be commonly observed in the field (Li & Wong, 2012; University of Texas, 2019; Hoek, Marinos, & Marinos).

Table 5.3 – Comparison of hoop stress at maximum split distance to rock tensile strength

<i>Rock Type</i>	<i>Hoop Stress at Maximum Split Distance</i>	<i>Tensile Strength</i>
Granite	1182 psi	1000 psi to 2500 psi
Limestone	998 psi	725 psi to 1500 psi
Shale	820 psi	300 psi to 1000 psi
Sandstone	776 psi	575 psi to 2500 psi
Siltstone	646 psi	400 psi

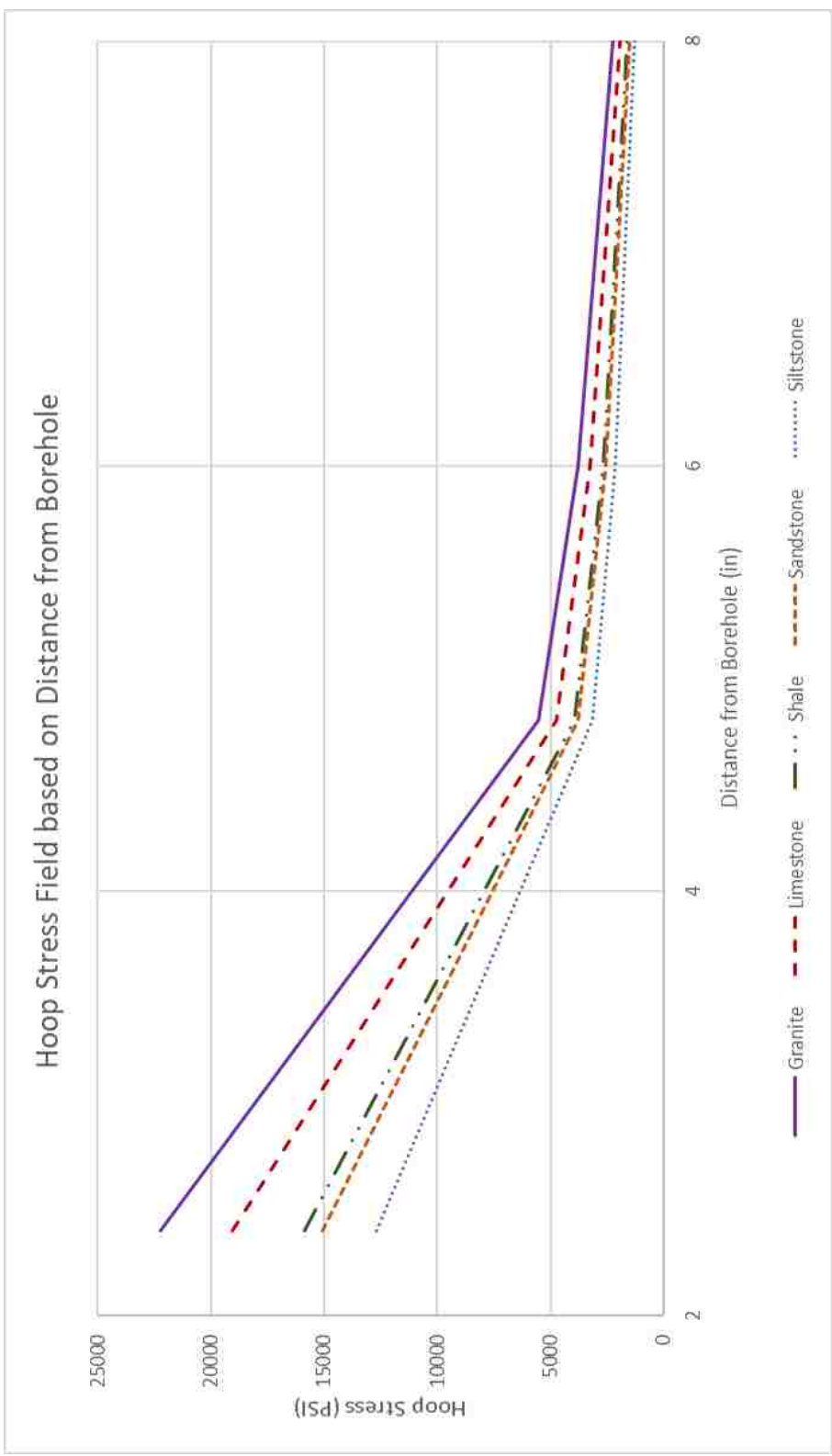
Table 5.3 clearly shows that in all situations the Hoop Stress Field at the assumed maximum split distance, which is halfway between the boreholes, is greater than the lower ranges of the measured Brazilian Tensile Strength for various rocks. It is important to note that the presplit fracture will form at the borehole wall and then this fracture will travel away from the borehole towards the second borehole. In order for the presplit to fully form, the fracture must extend to at least halfway between the boreholes.

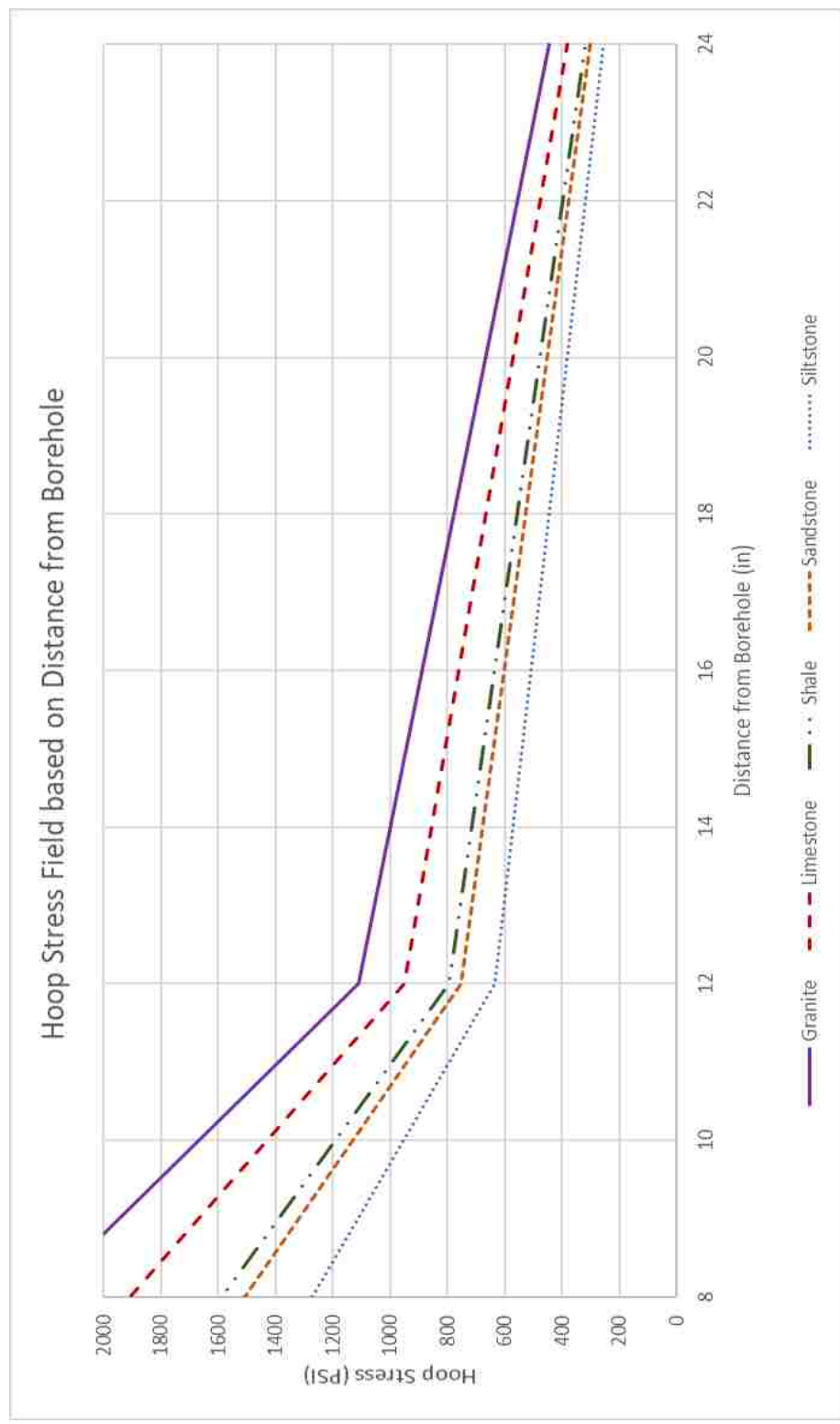
Furthermore, the tensile strength which is reported here is oftentimes much greater than what is actually observed in the field. It is well known in the field of rock mechanics that due to limitations of testing, based on sample screening and selection, the ‘best’ samples are chosen meaning those with the highest strength. The strength of the

rock mass is then typically weaker than the mass of the matrix due to structure. It has been documented that this does have large effects on the ability to presplit the material (Worsey P. , 1981). Additionally, rock which is typically being blasted is near the surface and exhibits large amounts of weathering, which leads to a large decrease in strength. For these reasons it is likely that the rock which is being presplit will typically fall into the lower end of the tensile strength ranges shown in Table 5.3.

The hoop stress field is not only applied at the maximum split distance but can be analyzed throughout the entire region of the spacing. The fracture will start at the wall of the borehole and move towards the maximum split distance. Figure 5.4 shows the hoop stress near the borehole from field loading conditions. Near the borehole the stress field is very large and is typically over 10,000 psi. As the distance from the borehole increases the magnitude of the hoop stress drops rapidly. Figure 5.5 shows the hoop stress field for the various rock types presented, from field loading conditions, as the distance is increased, and the stress drops below 2,000 psi. The presplit will form until the magnitude of the hoop stress field is less than the rock's tensile strength.

At this point, the formation of the presplit may still continue, as the fracture network will be filled with the explosive gases and the crack may be driven under gas-driven fracture growth. Under this mechanism the gas pressure would continue driving the fractures if the pressure is great enough after accounting for the increased volume. If the pressure is not great enough then the gas will vent to the surface. These details are beyond the purview of this dissertation and any effects of gas driven cracks are considered minimal.





6. MAGNITUDE OF THE SHOCKWAVE FROM PRESPLITTING

6.1. SHOCKWAVE MECHANICS

A full analysis of shockwave mechanics is beyond the purview of this dissertation and many texts treat the fundamental principles of shockwave motion and attenuation (Cooper, 1996). However, for the purposes of a full analysis of the mechanics of a presplit, the shockwave from precision presplitting will be calculated using impedance mismatch. This will answer the question of what the rock may receive in terms of shockwave pressures at the borehole wall.

To complete this analysis the starting conditions must be fully documented, which include critical assumptions. It is important to understand the concept of failure of structures in a dynamic situation, for this situation the rock will be assumed to break in tension and since it is from a blast it will break dynamically. When a rock is loaded dynamically, meaning that the time of loading is short, it has a much higher strength than a slower loading, as it cannot respond to the stress and strain to the correct degree for breakage to occur. The faster the loading the higher the strength and today there is no data that can show the strength of rock under loading mechanics such as that from a shockwave. The closest tensile strength which may be considered comes from Brazilian disk tests which are shown in Table 5.3. The minimum Brazilian tensile strength for granites is 1000 psi and will be the tensile strength used for this analysis.

Additionally, it will be assumed that for both situations the explosive is decoupled and not in contact with the rock wall. The Precision Presplit will utilize 700 grains per foot (150 grams per meter) of detonating cord as the explosive charge which has a

velocity of detonation (VOD) of 21,500 ft/s (6,500 m/s) and a density of 1.5 g/cc (approximated from detonation rate, likely an overestimate leading to higher shock pressures than actually observed in the field). The spacing for these boreholes in a Precision Presplit will be considered to be 2 feet. This will not account for non-ideal detonation of these explosives or attenuation of the shockwave through the rock mass.

It is important to note that the pressure of the shockwave from the explosive does not change based on the explosive weight. The shockwave magnitude is solely a function of the velocity of detonation and the density (Cooper, 1996; Lusk & Silva, 2018). Therefore, if a larger charge is used in a borehole, such as the bottom charge in a Precision Presplit, the magnitude of the shockwave would still be the same and mass difference do not need to be considered.

6.2. SHOCKWAVE MAGNITUDE FOR A PRECISION PRESPLIT

For the case of Precision Presplitting, the detonation pressure will need to be determined through a simplified CJ pressure equation, which is presented in Equation 6. When utilizing this for detonation cord, assuming the density of the PETN is 1.5 g/cc and the VOD is 6.5 km/s, the detonation pressure would be 2,297,000 psi.

$$P_{CJ} = \frac{1.5 \frac{g}{cc} * 6.5 \frac{km}{s}}{4} = 15.84 \text{ GPa} = 2,297,000 \text{ psi}$$

The impedance of the detonating cord is 9,750,000. The transmission of the shockwave from the detonating cord to the air is then 0.00016, or 0.016% of the shockwave will be transmitted from the explosive into the air. The transmission of the shockwave from the air to the rock is then 0.00009, or 0.009% of the shockwave is

transmitted from the air into the rock. The total transmission from the explosive to the rock would then be 0.000000014 or 0.0000014%.

With 2,291,000 psi of shockwave pressure developed from the explosive, the total pressure to reach the borehole wall would be 0.033 psi, which is well below the required minimum to break a granite under tensile loading of 1000 psi. From this simple analysis the shockwave cannot cause tensile breakage at the borehole wall, yet alone when reduced to account for the shockwaves decay (attenuation) through the rock mass.

The total shockwave pressures at the borehole walls from both of these methods are extremely small compared to the rock's tensile strength when only considering basic impedance mismatch concepts. If the analysis was completed using more advanced methods with the incorporation of additional field values the result would conclude smaller shockwave pressure values than what is calculated here. Furthermore, the shockwave is a unique wave which must be of a very large pressure to where it travels faster than the speed of sound in the material. The magnitude of the shockwave by the time it reaches the borehole wall is so low that it is unlikely a shockwave would be readily formed in the rock mass, in direct comparison to a borehole which is bulk loaded with explosives and has direct contact between the explosive and the rock. For the case of Precision Presplitting, the pressure of the shockwave is extremely low and likely unobservable in the rock mass, and as such would be considered to have no effect in the development of the presplit.

The magnitude of the shockwave is too low to cause any presplit fracture to form. This alone completely refutes any effects of the shockwave on the formation of the presplit. Further proof of the inapplicability of the shockwave to be used in presplit

fundamentals would be the application of propellant based explosives causing presplit formation, the actual time of the formation of the presplit compared to the time of arrival of the shockwave, and the inability to accurately time the blastholes to fire to cause shockwave collisions.

7. RESULTS AND DISCUSSION

The detonation of an explosive which is confined in a borehole results in two separate events which influence the breakage of the surrounding rock mass. The first of these events is the generation of the shockwave, which is a rapidly moving high pressure wave. The second event is the pressurization of the borehole as the high-temperature gases expand and put stress on the walls of the borehole.

A Precision Presplit is a specialty method of blasting which uses extremely light loads that are decoupled resulting in them not being in contact with the walls. This leads to large losses in the pressure of the shockwave, as it must move through the explosive and into the air then through the air and into the rock. Furthermore, the shockwave quickly attenuates, or decreases in pressure, as it moves through the rock. The shockwave is modelled through a simplified impedance mismatch approach to determine its stress at various points in the rock.

The gas pressure from the Precision Presplit quickly expands to fill the borehole and results in the generation of a hoop stress field in the rock. The borehole pressure has been modelled from three separate approaches which all show excellent accuracy to experimentation. A model is presented in this dissertation to determine the magnitude of the hoop stress field from the borehole pressure. This allows for the generation of the magnitude of both the shockwave stress and hoop stress at a distance of one borehole diameter away from the borehole wall, and this is shown in Table 7.1.

Table 7.1 clearly shows that the hoop stress field is extremely large near the borehole and exceeds the Brazilian Tensile Strength of the rock in all situations. The

shockwave stress does not exceed the tensile strength of the rock near the borehole in any situation. This clearly shows that in close vicinity to the borehole the shockwave can have no effect and the hoop stress easily results in presplit fracture formation. This is based on the real field loading conditions that have been applied on projects all over the world for various rock types.

Table 7.1 – Stresses from Precision Presplitting at one borehole diameter from charge

ROCK TYPE	SHOCK STRESS (PSI)	HOOP STRESS (PSI)	TENSILE STRENGTH OF ROCK (PSI)
GRANITE	0.033	22,222	1000 - 2500
LIMESTONE	0.033	19,048	725 - 1500
SHALE	0.033	15,873	300 - 1000
SANDSTONE	0.033	15,079	575 - 2500
SILTSTONE	0.033	12,698	400

The maximum split distance has been defined as the maximum distance that the borehole causes the generation of a presplit fracture. It has been assumed that the maximum presplit distance must, at minimum, be half the distance of the spacing. This would result in each borehole causing the presplit to form halfway between holes. Table 7.2 has been generated which shows the magnitude of the shockwave stress and the hoop stress at a maximum split distance which is equal to half the spacing. The shockwave stress is well below the Brazilian Tensile strength of the rock, which would result in no presplit fracture formation. The Hoop stress exceeds the Brazilian Tensile Strength in all situations, which would result in presplit fracture formation. This work clearly shows that

the shockwave has no effect on the presplit fracture formation, while the hoop stress field has the proper magnitude to be the major mechanism in the presplit fracture formation.

Table 7.2 – Stresses from Precision Presplitting at maximum split distance

ROCK TYPE	SHOCK STRESS (PSI)	HOOP STRESS (PSI)	TENSILE STRENGTH OF ROCK (PSI)
GRANITE	0.002	1182	1000 - 2500
LIMESTONE	0.002	998	725 - 1500
SHALE	0.002	820	300 - 1000
SANDSTONE	0.002	776	575 - 2500
SILTSTONE	0.002	646	400

The development of Tables 7.1 and 7.2 is based on the use of actual field data for the typical explosive loads which are used, in general, with various rock types. The fact that the hoop stress field exceeds the tensile strength of the rock at a distance of half the spacing is a remarkable finding. A theory is not applicable unless it provides the background and the reason why something occurs in the field. The shockwave theory has never been shown to be applicable to the field conditions which are used in the real world. The hoop stress theory has proven to show the reason behind the field conditions.

This theory would also hold with other common methods of presplitting. The hoop stress field is the only stress which is exerted in a propellant presplit blast. A traditional presplit blast also has large shockwave pressure losses due to impedance mismatches and would have larger hoop stresses than reported here. An airdeck presplit, which has only the bottom of the hole filled with explosive, would also have minimal shockwaves near the top of the hole but would have large hoop stress fields between

holes after the borehole has been pressurized fully. This hoop stress theory does not only hold for the case of Precision Presplitting, but can accurately define the stress fields around all the different types of commonly used presplit methods. This research then shows that the shockwave has no effect in any presplit blast and the hoop stress is the dominant breakage mechanic when a decoupled charge is used.

8. CONCLUSIONS

This work has shown that modelling a Precision Presplit blast as a function of hoop stresses, similar to that of thick-walled pressure vessel, is an accurate method to determine the stresses generated in a presplit blast. This work clearly shows that the shock wave has no effect on the formation of a presplit when using Precision Presplitting and the hoop stress field generated as a result of borehole gas pressurization is the major mechanism which leads to the formation of the presplit. The application of the hoop stress theory shows that the magnitude of the stress is available to cause the presplit to form from typical field conditions.

This work has taken empirical and field data and provided the basis for how a Precision Presplit actually works in the field and has theoretically proven many aspects of presplitting, which have been discussed in the field for decades. These include showing proof for why changing the borehole diameter does not require changes to the explosive load, the disproof of split factor design of presplits and shows why split factor does not work for design, and the proof of why delays can be used between presplit holes without degradation of the presplit.

This work has shown that the presplit parameters can be correlated and designed based on the Young's Modulus of the rock and the Brazilian Tensile Strength. This research has also shown that Precision Presplitting uses small borehole pressures to generate large hoop stresses, based on the close spacing. This explains why geologic structure affects a Precision Presplit less than a traditional presplit or other method of overbreak.

APPENDIX A.

CALCULATIONS OF BOREHOLE PRESSURE FOR PETN

Appendix A contains various runs of the Thermodynamic Borehole Pressure Model, for the charge loads which were used in experimentation completed by Otuonye. The work completed is in the same manner as the work shown in Section 4.3 of this dissertation to validate the Thermodynamic Model from field tested data and determine the total error of the Thermodynamic Model.

The starting variables for each charge size are shown, as well as calculations for the reduced temperature, which do not change as the explosive used is always PETN. These models were then completed with two to three iterations of the reduced pressure and application of the compressibility curves to arrive at a final calculated borehole pressure.

Temp of PETN 4900 K								
R =	0.08206 liter atm / mole K			Product	mole fraction	Crit Te	Tr	Tr Frac
T =	4900 K			H2O	0.363	647	7.573	2.749
V =	0.257 L			N2	0.182	126	38.889	7.078
n _g =	0.0348 mol/gm			CO2	0.273	304	16.118	4.400
weight =	10 grams			CO	0.182	133	36.842	6.705
n =	0.348 mol					Critical Temp	Tr =	20.933
P = (ZnRT)/V								
P =	544.47 Z (atm)							
P =	8004 Z (psi)							
Assume P =	8000 PSI							
Product	mole fraction	Press (Pc)	Prod (Pr)	Pr (Frac)				
H2O	0.363	3205	2.496	0.906				
N2	0.182	493	16.227	2.953				
CO2	0.273	1072	7.463	2.037				
CO	0.182	507	15.779	2.872				
		Critical Pressure	Pr =	8.769				
Compressibility Curve								
Tr	21							
Pr	8.77							
Z =	1.04							
P =	8323.85272							
Assume P =	8325 PSI							
Product	mole fraction	Press (Pc)	Prod (Pr)	Pr (Frac)				
H2O	0.363	3205	2.598	0.943				
N2	0.182	493	16.886	3.073				
CO2	0.273	1072	7.766	2.120				
CO	0.182	507	16.420	2.988				
			Pr =	9.125				
Compressibility Curve								
Tr	21							
Pr	9.12							
Z =	1.05							
P =	8403.889765							
Assume P =	8400 PSI							
Product	mole fraction	Press (Pc)	Prod (Pr)	Pr (Frac)				
H2O	0.363	3205	2.621	0.951				
N2	0.182	493	17.039	3.101				
CO2	0.273	1072	7.836	2.139				
CO	0.182	507	16.568	3.015				
			Pr =	9.207				
Compressibility Curve								
Tr	21							
Pr	9.21							
Z =	1.05							
P =	8403.889765							
Pressure =	8400 PSI							

Temp of PETN 4140 K								
R =	0.08206 liter atm / mole K			Product	mole fract	Crit Te	Tr	Tr Frac
T =	4140 K			H2O	0.363	647	6.399	2.323
V =	0.257 L			N2	0.182	126	32.857	5.980
n _g =	0.0348 mol/gm			CO2	0.273	304	13.618	3.718
weight =	10 grams			CO	0.182	133	31.128	5.665
n =	0.348 mol			Critical Temp			Tr =	17.686
P = (ZnRT)/V								
P =	460.02 Z (atm)							
P =	6762 Z (psi)							
Assume P =	6760 PSI							
Product	mole fracti	Press (Pc)	Prod (Pr)	Pr (Frac)				
H2O	0.363	3205	2.109	0.766				
N2	0.182	493	13.712	2.496				
CO2	0.273	1072	6.306	1.722				
CO	0.182	507	13.333	2.427				
Critical Pressure			Pr =	7.409				
Compressibility Curve								
Tr	18							
Pr	7.41							
Z =	1.04							
P =	7032.8062							
Assume P =	7030 PSI							
Product	mole fracti	Press (Pc)	Prod (Pr)	Pr (Frac)				
H2O	0.363	3205	2.193	0.796				
N2	0.182	493	14.260	2.595				
CO2	0.273	1072	6.558	1.790				
CO	0.182	507	13.866	2.524				
			Pr =	7.705				
Compressibility Curve								
Tr	18							
Pr	7.71							
Z =	1.05							
P =	7100.4293							
Assume P =	7100 PSI							
Product	mole fracti	Press (Pc)	Prod (Pr)	Pr (Frac)				
H2O	0.363	3205	2.215	0.804				
N2	0.182	493	14.402	2.621				
CO2	0.273	1072	6.623	1.808				
CO	0.182	507	14.004	2.549				
			Pr =	7.782				
Compressibility Curve								
Tr	18							
Pr	7.78							
Z =	1.05							
P =	7100.4293							
Pressure =	7100 PSI							

R =	0.08206	liter atm / mole K			Product	mole fract	Crit Te	Tr	Tr Frac
T =	4140	K			H2O	0.363	647	6.399	2.323
V =	0.257	L			N2	0.182	126	32.857	5.980
$n_g =$	0.0348	mol/gm			CO2	0.273	304	13.618	3.718
weight =	20	grams			CO	0.182	133	31.128	5.665
n =	0.696	mol			Critical Temp			Tr =	17.686
P = (ZnRT)/V									
P =	920.04	Z (atm)							
P =	13525	Z (psi)							
Assume P =	15000	PSI							
Product	mole fract	Press (Pc)	Prod (Pr)	Pr (Frac)					
H2O	0.363	3205	4.680	1.699					
N2	0.182	493	30.426	5.538					
CO2	0.273	1072	13.993	3.820					
CO	0.182	507	29.586	5.385					
Critical Pressure			Pr =	16.441					
Compressibility Curve									
Tr	18								
Pr	16.44								
Z =	1.11								
P =	15012.336								
Assume P =	15000	PSI							
Product	mole fract	Press (Pc)	Prod (Pr)	Pr (Frac)					
H2O	0.363	3205	4.680	1.699					
N2	0.182	493	30.426	5.538					
CO2	0.273	1072	13.993	3.820					
CO	0.182	507	29.586	5.385					
			Pr =	16.441					
Compressibility Curve									
Tr	18								
Pr	16.44								
Z =	1.11								
P =	15012.336								
Assume P =	15000	PSI							
Product	mole fract	Press (Pc)	Prod (Pr)	Pr (Frac)					
H2O	0.363	3205	4.680	1.699					
N2	0.182	493	30.426	5.538					
CO2	0.273	1072	13.993	3.820					
CO	0.182	507	29.586	5.385					
			Pr =	16.441					
Compressibility Curve									
Tr	18								
Pr	16.44								
Z =	1.11								
P =	15012.336								
Pressure =	15000	PSI							

R =	0.08206	liter atm / mole K		Product	mole fract	Crit Te	Tr	Tr Frac
T =	4140	K		H2O	0.363	647	6.399	2.323
V =	0.257	L		N2	0.182	126	32.857	5.980
$n_g =$	0.0348	mol/gm		CO2	0.273	304	13.618	3.718
weight =	30	grams		CO	0.182	133	31.128	5.665
n =	1.044	mol		Critical Temp			Tr =	17.686
P = (ZnRT)/V								
P =	1380.06	Z (atm)						
P =	20287	Z (psi)						
Assume P =	25000	PSI						
Product	mole fract	Press (Pc)	Prod (Pr)	Pr (Frac)				
H2O	0.363	3205	7.800	2.832				
N2	0.182	493	50.710	9.229				
CO2	0.273	1072	23.321	6.367				
CO	0.182	507	49.310	8.974				
Critical Pressure			Pr =	27.402				
Compressibility Curve								
Tr	18							
Pr	27.40							
Z =	1.18							
P =	23938.59							
Assume P =	24000	PSI						
Product	mole fract	Press (Pc)	Prod (Pr)	Pr (Frac)				
H2O	0.363	3205	7.488	2.718				
N2	0.182	493	48.682	8.860				
CO2	0.273	1072	22.388	6.112				
CO	0.182	507	47.337	8.615				
			Pr =	26.306				
Compressibility Curve								
Tr	18							
Pr	26.31							
Z =	1.17							
P =	23735.721							
Assume P =	23750	PSI						
Product	mole fract	Press (Pc)	Prod (Pr)	Pr (Frac)				
H2O	0.363	3205	7.410	2.690				
N2	0.182	493	48.174	8.768				
CO2	0.273	1072	22.155	6.048				
CO	0.182	507	46.844	8.526				
			Pr =	26.032				
Compressibility Curve								
Tr	18							
Pr	26.03							
Z =	1.17							
P =	23735.721							
Pressure =	23750	PSI						

R =	0.08206	liter atm / mole K			Product	mole fract	Crit Te	Tr	Tr Frac
T =	4140	K			H2O	0.363	647	6.399	2.323
V =	0.257	L			N2	0.182	126	32.857	5.980
$n_g =$	0.0348	mol/gm			CO2	0.273	304	13.618	3.718
weight =	40	grams			CO	0.182	133	31.128	5.665
n =	1.392	mol			Critical Temp			Tr =	17.686
P = (ZnRT)/V									
P =	1840.09	Z (atm)							
P =	27049	Z (psi)							
Assume P = 33000 PSI									
Product	mole fract	Press (Pc)	Prod (Pr)	Pr (Frac)					
H2O	0.363	3205	10.296	3.738					
N2	0.182	493	66.937	12.183					
CO2	0.273	1072	30.784	8.404					
CO	0.182	507	65.089	11.846					
Critical Pressure			Pr =	36.170					
Compressibility Curve									
Tr	18								
Pr	36.17								
Z =	1.24								
P = 33541.076									
Assume P = 33550 PSI									
Product	mole fract	Press (Pc)	Prod (Pr)	Pr (Frac)					
H2O	0.363	3205	10.468	3.800					
N2	0.182	493	68.053	12.386					
CO2	0.273	1072	31.297	8.544					
CO	0.182	507	66.174	12.044					
			Pr =	36.773					
Compressibility Curve									
Tr	18								
Pr	36.77								
Z =	1.25								
P = 33811.568									
Assume P = 33800 PSI									
Product	mole fract	Press (Pc)	Prod (Pr)	Pr (Frac)					
H2O	0.363	3205	10.546	3.828					
N2	0.182	493	68.560	12.478					
CO2	0.273	1072	31.530	8.608					
CO	0.182	507	66.667	12.133					
			Pr =	37.047					
Compressibility Curve									
Tr	18								
Pr	37.05								
Z =	1.25								
P = 33811.568									
Pressure =	33800	PSI							

APPENDIX B.

PRECISION PRESPLIT BOREHOLE PRESSURE

Appendix B contains the calculations of Borehole Pressure for specific Precision Presplitting applications and loads based on the Thermodynamic Borehole Pressure Model shown in Section 4.3 of this dissertation. This work was completed to determine the actual borehole pressures found in Precision Presplitting and verify that the simplified Thermodynamic equations, such as Equation 65, is accurate for predicting the pressure from a Precision Presplit. This work does not include the bottom load calculations and is solely for the column load.

The calculations for reduced pressure are not shown here, as they are the same for previous sections as the explosive used is PETN. The starting variables are shown at the top of each spreadsheet and the reduced pressure calculations are shown for various iterations until a steady-state pressure is achieved.

Precision Presplitting Borehole Pressure 100gr/ft - Equ 33				
EL =	100	gr/ft		
EL =	21.3	g/m		
dh =	3	inches		
dh =	76.2	mm		
P =	65.30	Z (atm)		
P =	959.86	Z (psi)		
Tr =	21			
Assume P =	1500	PSI		
Product	mole fraction	Press (Pc)	Prod (Pr)	Pr (Frac)
H2O	0.363	3205	0.468	0.170
N2	0.182	493	3.043	0.554
CO2	0.273	1072	1.399	0.382
CO	0.182	507	2.959	0.538
Critical Pressure			Pr =	1.644
Tr =	21			
Pr =	1.644			
Z =	1.01			
P =	969.4565999			
Assume P =	1000	PSI		
Product	mole fraction	Press (Pc)	Prod (Pr)	Pr (Frac)
H2O	0.363	3205	0.312	0.113
N2	0.182	493	2.028	0.369
CO2	0.273	1072	0.933	0.255
CO	0.182	507	1.972	0.359
Critical Pressure			Pr =	1.096
Tr =	21			
Pr =	1.096			
Z =	1.01			
P =	969.4565999			

Precision Presplitting Borehole Pressure 200gr/ft - Equ 33				
EL =	200	gr/ft		
EL =	42.6	g/m		
dh =	3	inches		
dh =	76.2	mm		
P =	130.59	Z (atm)		
P =	1919.72	Z (psi)		
Tr =	21			
Assume P =	2250	PSI		
Product	mole fraction	Press (Pc)	Prod (Pr)	Pr (Frac)
H2O	0.363	3205	0.702	0.255
N2	0.182	493	4.564	0.831
CO2	0.273	1072	2.099	0.573
CO	0.182	507	4.438	0.808
Critical Pressure			Pr =	2.466
Tr =	21			
Pr =	2.466			
Z =	1.02			
P =	1958.11036			
Assume P =	2000	PSI		
Product	mole fraction	Press (Pc)	Prod (Pr)	Pr (Frac)
H2O	0.363	3205	0.624	0.227
N2	0.182	493	4.057	0.738
CO2	0.273	1072	1.866	0.509
CO	0.182	507	3.945	0.718
Critical Pressure			Pr =	2.192
Tr =	21			
Pr =	2.192			
Z =	1.02			
P =	1958.11036			

Precision Presplitting Borehole Pressure 300gr/ft - Equ 33				
EL =	300	gr/ft		
EL =	63.9	g/m		
dh =	3	inches		
dh =	76.2	mm		
P =	195.89	Z (atm)		
P =	2879.57	Z (psi)		
Tr =	21			
Assume P =	3000	PSI		
Product	mole fraction	Press (Pc)	Prod (Pr)	Pr (Frac)
H2O	0.363	3205	0.936	0.340
N2	0.182	493	6.085	1.108
CO2	0.273	1072	2.799	0.764
CO	0.182	507	5.917	1.077
Critical Pressure			Pr =	3.288
Tr =	21			
Pr =	3.288			
Z =	1.03			
P =	2965.961281			
Assume P =	3000	PSI		
Product	mole fraction	Press (Pc)	Prod (Pr)	Pr (Frac)
H2O	0.363	3205	0.936	0.340
N2	0.182	493	6.085	1.108
CO2	0.273	1072	2.799	0.764
CO	0.182	507	5.917	1.077
Critical Pressure			Pr =	3.288
Tr =	21			
Pr =	3.288			
Z =	1.03			
P =	2965.961281			

Precision Presplitting Borehole Pressure 500gr/ft - Equ 33				
EL =	500	gr/ft		
EL =	106.5	g/m		
dh =	3	inches		
dh =	76.2	mm		
P =	326.48	Z (atm)		
P =	4799.29	Z (psi)		
Tr =	21			
Assume P =	5000	PSI		
Product	mole fraction	Press (Pc)	Prod (Pr)	Pr (Frac)
H2O	0.363	3205	1.560	0.566
N2	0.182	493	10.142	1.846
CO2	0.273	1072	4.664	1.273
CO	0.182	507	9.862	1.795
Critical Pressure			Pr =	5.480
Tr =	21			
Pr =	5.480			
Z =	1.04			
P =	4991.261703			
Assume P =	5000	PSI		
Product	mole fraction	Press (Pc)	Prod (Pr)	Pr (Frac)
H2O	0.363	3205	1.560	0.566
N2	0.182	493	10.142	1.846
CO2	0.273	1072	4.664	1.273
CO	0.182	507	9.862	1.795
Critical Pressure			Pr =	5.480
Tr =	21			
Pr =	5.480			
Z =	1.04			
P =	4991.261703			

Precision Presplitting Borehole Pressure 700gr/ft - Equ 33				
EL =	700	gr/ft		
EL =	149.1	g/m		
dh =	3	inches		
dh =	76.2	mm		
P =	457.08	Z (atm)		
P =	6719.01	Z (psi)		
Tr =	21			
Assume P =	7000	PSI		
Product	mole fraction	Press (Pc)	Prod (Pr)	Pr (Frac)
H2O	0.363	3205	2.184	0.793
N2	0.182	493	14.199	2.584
CO2	0.273	1072	6.530	1.783
CO	0.182	507	13.807	2.513
Critical Pressure			Pr =	7.672
Tr =	21			
Pr =	7.672			
Z =	1.05			
P =	7054.956445			
Assume P =	7000	PSI		
Product	mole fraction	Press (Pc)	Prod (Pr)	Pr (Frac)
H2O	0.363	3205	2.184	0.793
N2	0.182	493	14.199	2.584
CO2	0.273	1072	6.530	1.783
CO	0.182	507	13.807	2.513
Critical Pressure			Pr =	7.672
Tr =	21			
Pr =	7.672			
Z =	1.05			
P =	7054.956445			

Precision Presplitting Borehole Pressure 100gr/ft - Equ 33				
EL =	100	gr/ft		
EL =	21.3	g/m		
dh =	2	inches		
dh =	50.8	mm		
P =	146.92	Z (atm)		
P =	2159.68	Z (psi)		
Tr =	21			
Assume P =	2250	PSI		
Product	mole fraction	Press (Pc)	Prod (Pr)	Pr (Frac)
H2O	0.363	3205	0.702	0.255
N2	0.182	493	4.564	0.831
CO2	0.273	1072	2.099	0.573
CO	0.182	507	4.438	0.808
Critical Pressure			Pr =	2.466
Tr =	21			
Pr =	2.466			
Z =	1.02			
P =	2202.874155			
Assume P =	2200	PSI		
Product	mole fraction	Press (Pc)	Prod (Pr)	Pr (Frac)
H2O	0.363	3205	0.686	0.249
N2	0.182	493	4.462	0.812
CO2	0.273	1072	2.052	0.560
CO	0.182	507	4.339	0.790
Critical Pressure			Pr =	2.411
Tr =	21			
Pr =	2.411			
Z =	1.02			
P =	2202.874155			

Precision Presplitting Borehole Pressure 200gr/ft - Equ 33				
EL =	200	gr/ft		
EL =	42.6	g/m		
dh =	2	inches		
dh =	50.8	mm		
P =	293.83	Z (atm)		
P =	4319.36	Z (psi)		
Tr =	21			
Assume P =	4500	PSI		
Product	mole fraction	Press (Pc)	Prod (Pr)	Pr (Frac)
H2O	0.363	3205	1.404	0.510
N2	0.182	493	9.128	1.661
CO2	0.273	1072	4.198	1.146
CO	0.182	507	8.876	1.615
Critical Pressure			Pr =	4.932
Tr =	21			
Pr =	4.932			
Z =	1.04			
P =	4492.135532			
Assume P =	4500	PSI		
Product	mole fraction	Press (Pc)	Prod (Pr)	Pr (Frac)
H2O	0.363	3205	1.404	0.510
N2	0.182	493	9.128	1.661
CO2	0.273	1072	4.198	1.146
CO	0.182	507	8.876	1.615
Critical Pressure			Pr =	4.932
Tr =	21			
Pr =	4.932			
Z =	1.04			
P =	4492.135532			

Precision Presplitting Borehole Pressure 300gr/ft - Equ 33				
EL =	300	gr/ft		
EL =	63.9	g/m		
dh =	2	inches		
dh =	50.8	mm		
P =	440.75	Z (atm)		
P =	6479.04	Z (psi)		
Tr =	21			
Assume P =	6500	PSI		
Product	mole fraction	Press (Pc)	Prod (Pr)	Pr (Frac)
H2O	0.363	3205	2.028	0.736
N2	0.182	493	13.185	2.400
CO2	0.273	1072	6.063	1.655
CO	0.182	507	12.821	2.333
Critical Pressure			Pr =	7.124
Tr =	21			
Pr =	7.124			
Z =	1.05			
P =	6802.993715			
Assume P =	6800	PSI		
Product	mole fraction	Press (Pc)	Prod (Pr)	Pr (Frac)
H2O	0.363	3205	2.122	0.770
N2	0.182	493	13.793	2.510
CO2	0.273	1072	6.343	1.732
CO	0.182	507	13.412	2.441
Critical Pressure			Pr =	7.453
Tr =	21			
Pr =	7.453			
Z =	1.05			
P =	6802.993715			

Precision Presplitting Borehole Pressure 500gr/ft - Equ 33				
EL =	500	gr/ft		
EL =	106.5	g/m		
dh =	2	inches		
dh =	50.8	mm		
P =	734.59	Z (atm)		
P =	10798.40	Z (psi)		
Tr =	21			
Assume P =	11000	PSI		
Product	mole fraction	Press (Pc)	Prod (Pr)	Pr (Frac)
H2O	0.363	3205	3.432	1.246
N2	0.182	493	22.312	4.061
CO2	0.273	1072	10.261	2.801
CO	0.182	507	21.696	3.949
Critical Pressure			Pr =	12.057
Tr =	21			
Pr =	12.057			
Z =	1.06			
P =	11446.30689			
Assume P =	11500	PSI		
Product	mole fraction	Press (Pc)	Prod (Pr)	Pr (Frac)
H2O	0.363	3205	3.588	1.302
N2	0.182	493	23.327	4.245
CO2	0.273	1072	10.728	2.929
CO	0.182	507	22.682	4.128
Critical Pressure			Pr =	12.605
Tr =	21			
Pr =	12.605			
Z =	1.07			
P =	11554.29091			

Precision Presplitting Borehole Pressure 700gr/ft - Equ 33				
EL =	700	gr/ft		
EL =	149.1	g/m		
dh =	2	inches		
dh =	50.8	mm		
P =	1028.42	Z (atm)		
P =	15117.76	Z (psi)		
Tr =	21			
Assume P =	16750	PSI		
Product	mole fraction	Press (Pc)	Prod (Pr)	Pr (Frac)
H2O	0.363	3205	5.226	1.897
N2	0.182	493	33.976	6.184
CO2	0.273	1072	15.625	4.266
CO	0.182	507	33.037	6.013
Critical Pressure			Pr =	18.359
Tr =	21			
Pr =	18.359			
Z =	1.1			
P =	16629.54019			
Assume P =	16630	PSI		
Product	mole fraction	Press (Pc)	Prod (Pr)	Pr (Frac)
H2O	0.363	3205	5.189	1.884
N2	0.182	493	33.732	6.139
CO2	0.273	1072	15.513	4.235
CO	0.182	507	32.801	5.970
Critical Pressure			Pr =	18.228
Tr =	21			
Pr =	18.228			
Z =	1.1			
P =	16629.54019			

Precision Presplitting Borehole Pressure 100gr/ft - Equ 33				
EL =	100	gr/ft		
EL =	21.3	g/m		
dh =	4	inches		
dh =	101.6	mm		
P =	36.73	Z (atm)		
P =	539.92	Z (psi)		
Tr =	21			
Assume P =	550	PSI		
Product	mole fraction	Press (Pc)	Prod (Pr)	Pr (Frac)
H2O	0.363	3205	0.172	0.062
N2	0.182	493	1.116	0.203
CO2	0.273	1072	0.513	0.140
CO	0.182	507	1.085	0.197
Critical Pressure			Pr =	0.603
Tr =	21			
Pr =	0.603			
Z =	1.01			
P =	545.3193375			
Assume P =	550	PSI		
Product	mole fraction	Press (Pc)	Prod (Pr)	Pr (Frac)
H2O	0.363	3205	0.172	0.062
N2	0.182	493	1.116	0.203
CO2	0.273	1072	0.513	0.140
CO	0.182	507	1.085	0.197
Critical Pressure			Pr =	0.603
Tr =	21			
Pr =	0.603			
Z =	1.01			
P =	545.3193375			

Precision Presplitting Borehole Pressure 200gr/ft - Equ 33				
EL =	200	gr/ft		
EL =	42.6	g/m		
dh =	4	inches		
dh =	101.6	mm		
P =	73.46	Z (atm)		
P =	1079.84	Z (psi)		
Tr =	21			
Assume P =	1100	PSI		
Product	mole fraction	Press (Pc)	Prod (Pr)	Pr (Frac)
H2O	0.363	3205	0.343	0.125
N2	0.182	493	2.231	0.406
CO2	0.273	1072	1.026	0.280
CO	0.182	507	2.170	0.395
Critical Pressure			Pr =	1.206
Tr =	21			
Pr =	1.206			
Z =	1.01			
P =	1090.638675			
Assume P =	1100	PSI		
Product	mole fraction	Press (Pc)	Prod (Pr)	Pr (Frac)
H2O	0.363	3205	0.343	0.125
N2	0.182	493	2.231	0.406
CO2	0.273	1072	1.026	0.280
CO	0.182	507	2.170	0.395
Critical Pressure			Pr =	1.206
Tr =	21			
Pr =	1.206			
Z =	1.02			
P =	1101.437078			

Precision Presplitting Borehole Pressure 300gr/ft - Equ 33				
EL =	300	gr/ft		
EL =	63.9	g/m		
dh =	4	inches		
dh =	101.6	mm		
P =	110.19	Z (atm)		
P =	1619.76	Z (psi)		
Tr =	21			
Assume P =	1700	PSI		
Product	mole fraction	Press (Pc)	Prod (Pr)	Pr (Frac)
H2O	0.363	3205	0.530	0.193
N2	0.182	493	3.448	0.628
CO2	0.273	1072	1.586	0.433
CO	0.182	507	3.353	0.610
Critical Pressure			Pr =	1.863
Tr =	21			
Pr =	1.863			
Z =	1.01			
P =	1635.958012			
Assume P =	1650	PSI		
Product	mole fraction	Press (Pc)	Prod (Pr)	Pr (Frac)
H2O	0.363	3205	0.515	0.187
N2	0.182	493	3.347	0.609
CO2	0.273	1072	1.539	0.420
CO	0.182	507	3.254	0.592
Critical Pressure			Pr =	1.809
Tr =	21			
Pr =	1.809			
Z =	1.01			
P =	1635.958012			

Precision Presplitting Borehole Pressure 500gr/ft - Equ 33				
EL =	500	gr/ft		
EL =	106.5	g/m		
dh =	4	inches		
dh =	101.6	mm		
P =	183.65	Z (atm)		
P =	2699.60	Z (psi)		
Tr =	21			
Assume P =	2750	PSI		
Product	mole fraction	Press (Pc)	Prod (Pr)	Pr (Frac)
H2O	0.363	3205	0.858	0.311
N2	0.182	493	5.578	1.015
CO2	0.273	1072	2.565	0.700
CO	0.182	507	5.424	0.987
Critical Pressure			Pr =	3.014
Tr =	21			
Pr =	3.014			
Z =	1.02			
P =	2753.592694			
Assume P =	2750	PSI		
Product	mole fraction	Press (Pc)	Prod (Pr)	Pr (Frac)
H2O	0.363	3205	0.858	0.311
N2	0.182	493	5.578	1.015
CO2	0.273	1072	2.565	0.700
CO	0.182	507	5.424	0.987
Critical Pressure			Pr =	3.014
Tr =	21			
Pr =	3.014			
Z =	1.02			
P =	2753.592694			

Precision Presplitting Borehole Pressure 700gr/ft - Equ 33				
EL =	700	gr/ft		
EL =	149.1	g/m		
dh =	4	inches		
dh =	101.6	mm		
P =	257.10	Z (atm)		
P =	3779.44	Z (psi)		
Tr =	21			
Assume P =	4000	PSI		
Product	mole fraction	Press (Pc)	Prod (Pr)	Pr (Frac)
H2O	0.363	3205	1.248	0.453
N2	0.182	493	8.114	1.477
CO2	0.273	1072	3.731	1.019
CO	0.182	507	7.890	1.436
Critical Pressure			Pr =	4.384
Tr =	21			
Pr =	4.384			
Z =	1.03			
P =	3892.824181			
Assume P =	3900	PSI		
Product	mole fraction	Press (Pc)	Prod (Pr)	Pr (Frac)
H2O	0.363	3205	1.217	0.442
N2	0.182	493	7.911	1.440
CO2	0.273	1072	3.638	0.993
CO	0.182	507	7.692	1.400
Critical Pressure			Pr =	4.275
Tr =	21			
Pr =	4.275			
Z =	1.03			

Precision Presplitting Borehole Pressure 100gr/ft - Equ 33				
EL =	100	gr/ft		
EL =	21.3	g/m		
dh =	1.5	inches		
dh =	38.1	mm		
P =	261.19	Z (atm)		
P =	3839.43	Z (psi)		
Tr =	21			
Assume P =	4000	PSI		
Product	mole fraction	Press (Pc)	Prod (Pr)	Pr (Frac)
H2O	0.363	3205	1.248	0.453
N2	0.182	493	8.114	1.477
CO2	0.273	1072	3.731	1.019
CO	0.182	507	7.890	1.436
Critical Pressure			Pr =	4.384
Tr =	21			
Pr =	4.384			
Z =	1.03			
P =	3954.615041			
Assume P =	4000	PSI		
Product	mole fraction	Press (Pc)	Prod (Pr)	Pr (Frac)
H2O	0.363	3205	1.248	0.453
N2	0.182	493	8.114	1.477
CO2	0.273	1072	3.731	1.019
CO	0.182	507	7.890	1.436
Critical Pressure			Pr =	4.384
Tr =	21			
Pr =	4.384			
Z =	1.03			
P =	3954.615041			

Precision Presplitting Borehole Pressure 200gr/ft - Equ 33				
EL =	200	gr/ft		
EL =	42.6	g/m		
dh =	1.5	inches		
dh =	38.1	mm		
P =	522.37	Z (atm)		
P =	7678.86	Z (psi)		
Tr =	21			
Assume P =	8000	PSI		
Product	mole fraction	Press (Pc)	Prod (Pr)	Pr (Frac)
H2O	0.363	3205	2.496	0.906
N2	0.182	493	16.227	2.953
CO2	0.273	1072	7.463	2.037
CO	0.182	507	15.779	2.872
Critical Pressure			Pr =	8.769
Tr =	21			
Pr =	8.769			
Z =	1.05			
P =	8062.807366			
Assume P =	8050	PSI		
Product	mole fraction	Press (Pc)	Prod (Pr)	Pr (Frac)
H2O	0.363	3205	2.512	0.912
N2	0.182	493	16.329	2.972
CO2	0.273	1072	7.509	2.050
CO	0.182	507	15.878	2.890
Critical Pressure			Pr =	8.823
Tr =	21			
Pr =	8.823			
Z =	1.05			
P =	8062.807366			

Precision Presplitting Borehole Pressure 300gr/ft - Equ 33				
EL =	300	gr/ft		
EL =	63.9	g/m		
dh =	1.5	inches		
dh =	38.1	mm		
P =	783.56	Z (atm)		
P =	11518.30	Z (psi)		
Tr =	21			
Assume P =	12500	PSI		
Product	mole fraction	Press (Pc)	Prod (Pr)	Pr (Frac)
H2O	0.363	3205	3.900	1.416
N2	0.182	493	25.355	4.615
CO2	0.273	1072	11.660	3.183
CO	0.182	507	24.655	4.487
Critical Pressure			Pr =	13.701
Tr =	21			
Pr =	13.701			
Z =	1.07			
P =	12324.57697			
Assume P =	12350	PSI		
Product	mole fraction	Press (Pc)	Prod (Pr)	Pr (Frac)
H2O	0.363	3205	3.853	1.399
N2	0.182	493	25.051	4.559
CO2	0.273	1072	11.521	3.145
CO	0.182	507	24.359	4.433
Critical Pressure			Pr =	13.536
Tr =	21			
Pr =	13.536			
Z =	1.07			
P =	12324.57697			

Precision Presplitting Borehole Pressure 500gr/ft - Equ 33				
EL =	500	gr/ft		
EL =	106.5	g/m		
dh =	1.5	inches		
dh =	38.1	mm		
P =	1305.93	Z (atm)		
P =	19197.16	Z (psi)		
Tr =	21			
Assume P =	21000	PSI		
Product	mole fraction	Press (Pc)	Prod (Pr)	Pr (Frac)
H2O	0.363	3205	6.552	2.378
N2	0.182	493	42.596	7.753
CO2	0.273	1072	19.590	5.348
CO	0.182	507	41.420	7.538
Critical Pressure			Pr =	23.017
Tr =	21			
Pr =	23.017			
Z =	1.13			
P =	21692.79125			
Assume P =	21700	PSI		
Product	mole fraction	Press (Pc)	Prod (Pr)	Pr (Frac)
H2O	0.363	3205	6.771	2.458
N2	0.182	493	44.016	8.011
CO2	0.273	1072	20.243	5.526
CO	0.182	507	42.801	7.790
Critical Pressure			Pr =	23.785
Tr =	21			
Pr =	23.785			
Z =	1.13			
P =	21692.79125			

Precision Presplitting Borehole Pressure 700gr/ft - Equ 33				
EL =	700	gr/ft		
EL =	149.1	g/m		
dh =	1.5	inches		
dh =	38.1	mm		
P =	1828.30	Z (atm)		
P =	26876.02	Z (psi)		
Tr =	21			
Assume P =	30000	PSI		
Product	mole fraction	Press (Pc)	Prod (Pr)	Pr (Frac)
H2O	0.363	3205	9.360	3.398
N2	0.182	493	60.852	11.075
CO2	0.273	1072	27.985	7.640
CO	0.182	507	59.172	10.769
Critical Pressure			Pr =	32.882
Tr =	21			
Pr =	32.882			
Z =	1.18			
P =	31713.70897			
Assume P =	32000	PSI		
Product	mole fraction	Press (Pc)	Prod (Pr)	Pr (Frac)
H2O	0.363	3205	9.984	3.624
N2	0.182	493	64.909	11.813
CO2	0.273	1072	29.851	8.149
CO	0.182	507	63.116	11.487
Critical Pressure			Pr =	35.074
Tr =	21			
Pr =	35.074			
Z =	1.19			
P =	31982.46922			

APPENDIX C.

VALIDATION OF ISOTHERMAL ASSUMPTION

Appendix C will focus on defining the characteristics which show that the expansion of gases in a borehole can be modeled as an isothermal process without introducing significant error in the approximations of the magnitude of the pressure.

An isothermal system is a system that has no change in temperature while changes in pressure and volume occur. This is often associated with slow phenomena in which the outside environment contributes (or removes) heat as the system takes place. If the isothermal reaction was true for decoupled charges, the explosive gases would expand without any changes to temperature. However, this is not the case in the detonation of explosives, which is a very rapid environment. The magnitude of the temperature changes are relatively small, and the final calculations do not significantly change based on changes to temperature in the magnitudes that appear which allow for the treatment of the system as an isothermal system. The calculation of temperatures changes is extremely complex and current enough data is not available to determine and validate these changes.

An adiabatic reaction is one which does not have heat transfer to the outside surroundings. This can occur for multiple reasons, including a reaction occurring so fast that the time is not sufficient for the heat transfer to occur. This is an assumption which is often made in explosive processes and has been made since the 1800s when it was found that explosives detonated in wood did not burn the wood. An adiabatic reaction and an isothermal reaction cannot theoretically occur together, because for an isothermal reaction to occur the process has to take in heat from the environment. However, the detonation of a decoupled explosive charge can be assumed to follow the principles held

in both; this allows for the disregard of heat transfer from the high temperature gas to the rock mass and the use of Boyle's law to determine pressure at changes in volume.

It is important to address the actual gas dynamics which occur in the borehole from a decoupled charge. When the explosive detonates the solid chemicals are converted to a plasma which have a diameter smaller than that of the original explosive charge (Cook M. A., 1974). At this point, the gases are considered to be at the temperature of the explosion, T_e , which is calculated in section 4.1 of this dissertation. As the gases expand, the temperature decreases. When the gases impact the borehole wall, the temperature is raised due to a stagnation effect if the gases are traveling at a supersonic speed. It is currently unknown at what distance away from the charge this ceases to exist. If the gas is not traveling at a supersonic speed, then the heat sources are (Baird, 2019):

- The combined heat from the detonation
- The compressive heating caused by the passage of the air shock created by the detonation front

The air shock or the stagnation effect would both cause increases to the temperature which would likely be equivalent to losses from expansion.

The changes in temperature can also be modelled from a simplified approach which is used on rarefield gases which are released into a vacuum (Molmud, 1960; Zel'dovich & Raizer, 2002). This is completed using Equation C.1.

$$\Delta T = t^{-3(\gamma-1)} \quad (C.1)$$

where ΔT is the change in temperature in ° K, t is time in seconds, γ is the specific heat ratio which for these gases has been determined to be 1.2. At maximum γ can be 1.66, which takes place at complete freezing of internal degrees of freedom.

The importance of the temperature change occurs when the maximum pressure is calculated. This corresponds to a time of 0.1ms to 0.3ms (Otuonye, 1981). Using Equation A3-1, this results in a change in temperature of 50° K to 250° K; with a typical change in temperature of between 100° K to 150° K. This is considered minimal when considering a temperature of explosion for PETN of 4900° K.

A sensitivity analysis can be completed to view how a change in 100° K would affect the borehole pressure. This can be completed using Equation C.2

$$\frac{P_1 V_1}{T_1} = \frac{P_2 V_2}{T_2} \quad (C.2)$$

where P_1 is the original pressure in psi, V_1 is the original volume in L, T_1 is the original temperature in °K, P_2 is the final pressure in psi, V_2 is the final volume in L, and T_2 is the final temperature in ° K. Assuming that P_1 is 10,000 psi, V_1 is 0.067 L, T_1 is 4900° K, V_2 is 0.257L, and T_2 is 4800°K, the final pressure can be computed.

$$\frac{10000 * 0.067}{4900} = \frac{P_2 * 0.257}{4800}$$

P_2 is then equal to 2554 psi.

The process can be completed with the assumption of isothermal conditions and using Boyle's Law, which is presented again as Equation C.3

$$P_1 V_1 = P_2 V_2 \quad (C.3)$$

Using the same pressure and volumes as before, the final pressure can be calculated, as shown below.

$$10,000 * 0.067 = P_2 * 0.257$$

P_2 is then equal to 2,607 psi.

The difference in pressure between taking into account the temperature difference associated with the gas expansion result in an error in the calculation of the borehole pressure of 2%. This can be considered minimal and insignificant compared to other potential sources of error.

Furthermore, other authors have treated the detonation and expansion of the gases as an isothermal process and found good agreement with the measured data for borehole pressures (Otuonye, Skidmore, & Konya, 1983). This confirms that the assumption of the isothermal process results in minimal error. This has also been validated in this dissertation by the use of the explosion temperature in the Thermodynamic Model for borehole pressure calculations. The temperature used in this equation is the explosion temperature and this shows excellent fit of data with the measured results. If treatment of the process as isothermal introduced significant error, then this would cause incorrect prediction of the borehole pressure. Instead, the temperature of the gases after expansion volume expansion would be required. This goes to prove that while the process is not perfectly isothermal, it can be modeled as isothermal without introducing major error.

APPENDIX D.

CIRCUMFERENTIAL STRESSES AROUND A BOREHOLE

In addition to the general hoop stress field that is applied to the rock mass from the boreholes detonating, another stress field occurs due to the position of boreholes near the one detonating. The detonation of one borehole will cause a hoop stress on the adjacent borehole, this can be calculated by setting the 'A' value as $S - \frac{d_h}{2}$. This stress field on the adjacent borehole puts the adjacent borehole into circumferential loading as would be exhibited from an underground opening with overburden stresses. This can be seen in Figure D.1 which shows the detonation of Borehole 1, the generation of the hoop stress field, and the circumferential stresses on borehole two.

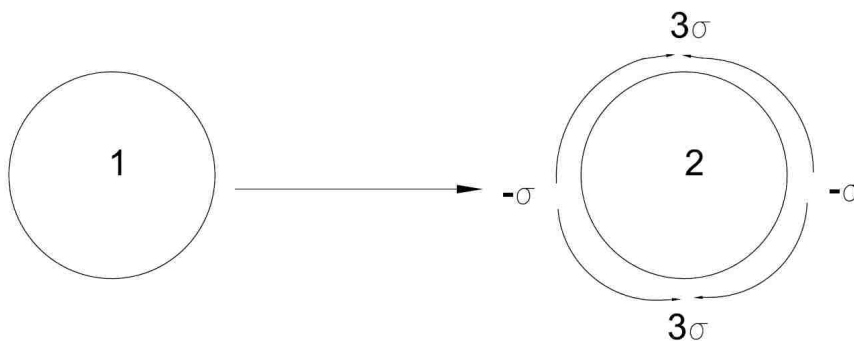


Figure D.1 – Circumferential stresses generated on borehole 2 from the detonation of borehole 1

Figure D.1 is the stresses which are generated from a single borehole, but the hoop stress field remains in the rock until well after all the adjacent boreholes have detonated (many milliseconds). This causes circumferential loading on the borehole from both adjacent boreholes. This is shown in Figure D.2 where both boreholes labeled as '1' are detonated with the resulting circumferential stress field which is generated on the borehole labeled as 2. It can be seen that this has doubled the stress compared to that of a

single hole firing. This leads to the borehole having a tensile stress between boreholes (in the direction the presplit should occur) and compression above and below the borehole, preventing overbreak from occurring.

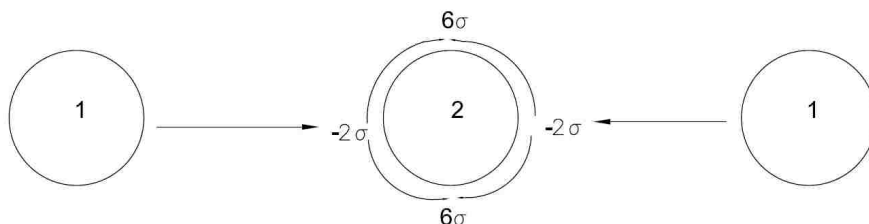


Figure D.2 – Two boreholes (#1) firing causing circumferential stresses around borehole #2

This circumferential loading creates a 16% difference in loading around adjacent boreholes, which would lead to proper alignment and help in the formation of the presplit fracture. For a typical Precision Presplit, it has been shown that approximately 2% of the hoop stress field remains at the adjacent borehole wall (that of borehole #2 from borehole #1) this would lead to 12% of the hoop stress generated at borehole(s) 1 being utilized in compression to stop overbreak and 4% to help align and extend the presplit fracture. This is an important consideration in the stress loading, which has not been analyzed in the general hoop stress formation.

BIBLIOGRAPHY

- Akhavan, J. (2011). *The Chemistry of Explosives*. Cambridge: RSC Publishing.
- Andre, G. G. (1878). *Rock Blasting. A Practical Treatise on the Means Employed in Blasting Rocks for Industrial Purposes*. London: E. & F.N. Spon.
- Ash, R. (1963a, August). Mechanics of Rock Breakage - Part 1. *Pit and Quarry*, 98-112.
- Ash, R. (1963b, September). Mechanics of Rock Breakage - Part 2. *Pit and Quarry*, 118-123.
- Ash, R. (1973). *The Influence of Geological Discontinuities on Rock Blasting - Doctoral Thesis*. University of Minnesota.
- Ash, R. (1974). Considerations for Proper Blasting Design. *Second Annual Blasting Conference of the Kentucky Dept of Mines and Minerals*, 45-59.
- Bacon, R. (1733). *Fratris Rogeri Bacon, ordinis Minorum, opus majus ad Clementem IV, pontificem Romanum*. (R. Burke, Trans.) London.
- Baird, J. (2019, October). Personal Communication.
- Bauer, A., Harris, G., Lang, L., Preziosi, P., & Selleck, D. (1965, September). How IOC Puts Crater Research to Work. *Engineering and Mining Journal*, 166(9), 117-121.
- Becher, J. (1667). *Physica Subterranea*.
- Becker, R. (1922a). Physikalisches uber feste und gasformige Sprengstoffe. *Z. Techn. Phys.*, 4, 152.
- Becker, R. (1922b). Stosswlle and Detonation. *Zs. Phys.*, 8, 321.
- Becker, R. (1929). *Impact, Waves and Detonation*.
- Ben-Dor, G., & Takayama, K. (1992). The Phenomena of Shock Wave Reflection - a Review of Unsolved problems and Future Research Needs. *Shock Waves*.
- Berthelot, P. (1881). Sur la vitesse de propagation des phenomenes explosifs dans les gaz. *C. R. Acad. Sci*, 18-22.
- Berthelot, P. (1892). *Explosives and Their Power*. London: John Murray.
- Berthollet, C. (1786). Observations sur quelques combinaisons de l'acide marin dephlogistique ou de l'acide muriatique oxygene. *Acad. Roy Sci.*, 385-396.

- Biot, J. (1802). Theorie mathematique de la propagation du son. *J. Phys. Theor. Appl.*, 173-182.
- Boufadi, F., Bidai, K., Ameri, M., Bentouaf, A., Bensaid, D., Azzaz, Y., & Ameri, I. (2016). First Principles Study of Mechanical Stability and Thermodynamic Properties of K₂S under Pressure and Temperature Effect. *Acta Physica Series*, 315-322.
- Brinkley, S. R., & Kirkwood, J. G. (1947a). Theory of the Propagation of Shock Waves. *Physical Review*, 71(9), 606-611.
- Brinkley, S. R., & Kirkwood, J. G. (1947b). Theory of the Propagation of Shock Waves from Infinite Cylinders of Explosives. *Physical Review*, 72(11), 1109-1113.
- Brinkley, S., & Wilson Jr., E. (1942). *Revised Method of Predicting the Detonation Velocities of Solid Explosives*.
- Brode, H. (1947). *A Calculation of the Blast Wave from a Spherical Charge of TNT: Rand Corporation Research Memorandum (RM-1965)*. Santa Monica.
- Brown, E. M. (1673). *Brief Account of some Travels in Hungaria as also some observations on Gold, Silver, Copper, Quick-silver Mines, Baths, and Mineral Waters*. London: T.R.
- Brown, M., & Rugunanan, R. (1989). A Temperature-Profile Study of the Combustion of Black Powder and its Constituent Binary Mixtures. *Propellants, Explosives, Pyrotechnics*, 69-75.
- Burgoyne, J. (1874). *A Treatise on the Blasting and Quarrying of stone for Building and Other Purposes*. London: Crosby Lockwood and Co.
- Cevizci, H., & Ozkahraman, H. (2012). The effect of Blast Hole Stemming Length to Rockpile Fragmentation at Limestone Quarries. *International Journal of Rock Mechanics and Mining Science*.
- Christoffel, E. (1877a). Fortpflanzung von Stoben durch elastische feste Korper. *Ann. di Mat. Pura Appl.*, 193-243.
- Christoffel, E. (1877b). Untersuchungen uber die mit dem Forbestehen linearer partieller Differentialgleichungen vertraglichen Unstetigkeiten. *Ann. di Met. Pura Appl.*, 81-112.
- Cole, R. (1948). *Underwater Explosions*. Princeton: Princeton University Press.
- Cook, M. (1947). An Equation of State for Gases at Extremely High Pressure and Temperature for the Hydrodynamic Theory of Detonation. *J. Chem. Phys.*, 518.
- Cook, M. (1958). *The Science of High Explosives*. New York: Reinhold Publishing Corp.

- Cook, M. A. (1974). *The Science of Industrial Explosives*. Salt Lake City: IRECO Chemicals.
- Cooper, P. (1996). *Explosive Engineering*. New York, New York: VCH Publishers Inc.
- Cosgrove, J. (1913). *Rock Excavating and Blasting*. Pittsburgh: J.J. Cosgrove.
- Count of Rumford, B. (1797). Experiments to Determine the Force of Fired Gunpowder. *Phil. Trans. Roy Soc*, 222-294.
- Cranz, C. (1926). *Lehrbuch der Ballistik: II Innere Ballistik*. Berlin: Springer.
- Croll, O. (1609). *Osvaldi Crollii Basilica chymica*. Geneva.
- Crosby, W., & Bauer, A. (1982). Wall Control Blasting in Open Pits. *Mining Engineering*, 34(2), 155-158.
- Crussard, L. (1907). Ondes de choc et onde explosive. *Bull. Soc. Industrie Minerale*, 257-364.
- Daehnke, A., Rossmanith, H., & Kouzniak, N. (1996, June). Dynamic Fracture Propagation due to Blast-Induced High Pressure Gas Loading. *2nd North American Rock Mechanics Symposium*.
- Daw, A., & Daw, Z. (1898). *The Blasting of Rocks in Mines, Quarries, Tunnels, Etc.* London: E. & F.N.
- Day, P. (1982). Controlled Blasting to Minimize Overbrak with Big Boreholes Underground. *Proceedings of the Eighth Conference on Explosives and Blasting Technique*, 264-274.
- De Lagrange, J. (1781). Memoire sur la theorie du mouvement des fluides. *Acad. Roy. Sci. & Belles Lettres*, 151-198.
- Dodge, B. (1944). *Chemical Engineering Thermodynamics*. New York: McGraw-Hill.
- Duhem, P. M. (1909). Sur la propagation des ondes de choc au sein des fluides. *Z. Physik. Chem*, 169-186.
- DuPont. (1975). *DuPont Blasters Handbook*. DuPont.
- Duvall, W. (1953). Strain-Wave Shapes in Rock Near Explosions. *Geophysics*, 18, 310-323.
- Duvall, W., & Atchison, T. (1957). *Rock Breakage by Explosives*. U.S. Bureau of Mines.
- Duvall, W., & Petkof, B. (1959). *Spherical Propagation of Explosion Generated Strain Pulses in Rock*. U.S. Bureau of Mines.

- Einstein, A. (1906). Theorie der Strahlung und die Theorie der Spezifischen Wärme. *Annalen der Physik*, 180-190.
- Euler, L. (1759). *Euler's two letters to Lagrange*. (C. I. Truesdell, Trans.)
- Fenning, R., & Whiffin, A. (1939). The Specific Heat of Gases at High Temperatures. *Phil. Trans. Roy. Soc.*, 149-228.
- Goodman, R. (2014). *Introduction to Rock Mechanics - 2nd Edition*. John Wiley & Sons Inc.
- Grant, C. (1964, November). Simplified Explanation of Crater Method. *Engineering and Mining Journal*, 165(11), 84-89.
- Guttman, O. (1892). *Blasting: A Handbook for the Use of Engineering and Others Engaged in Mining, Tunnelling, Quarrying, etc.* London: Charles Griffin and Company.
- Harari, Y. N. (2011). *Sapiens: A Brief History of Humankind*. Isreal.
- Hino, K. (1959). *Theory and Practice of Blasting*. Japan: Nippon Kayaku Co.
- Hire, D. L. (1702). Unknown Title.
- Hoek, E., Marinos, P., & Marinos, V. (n.d.). Characterization and engineering properties of tectonically undisturbed but lithologically varied sedimentary rock masses. *International Journal of Rock Mechanics and Mining Science*.
- Hugoniot, P. (1887). Memoire sur la propagation du mouvement dans les corps et plus specialement dans les gaz parfaits. *Partie. J. Ecole Polytech*, 3-97.
- Hutton, C. (1778). The Force of Fired Gunpowder. *Phil. Trans. Roy. Soc.*, 50-85.
- International Society of Explosive Engineers. (2016). *Blasters Handbook 18th Edition*. International Society of Explosive Engineers.
- Jaffe, B. (1930). *Crucibles: The Story of Chemistry*. New York: Simon and Schuster.
- Jeremic, J. (1994). *Rock Mechanics in Salt Mining*. Netherlands: Rotterdam.
- Johansson, C., & Persson, P. (1970). *Detonics of High Explosives*. New York: Academic Press.
- Johnson, G., & Steele, W. (1981). The standard enthalpy of formation of potassium sulfide by flourine bomb calorimetry. *The Journal of Chmical Thermodyanmics*, 985-990.

- Johnson, N. (1974). Explosives. In Macropaedia, *Encyclopedia Britannica* (Vol. 7, p. 85). Chicago: Benton & Hemingway.
- Johnson, S. (1971). *NCG Technical Report No. 21*. Livermore, California: U.S. Army Engineer Nuclear Cratering Group.
- Johnsson, G., & Hofmeister, W. (1961, February). The Influence of Stemming on the Efficiency of Blasting. (G. Clark, Ed.) *Proceedings of the International Symposium on Mining Research*, 91-102.
- Jouget, E. (1906). Sur la propagation des reactions chimiques dans les gaz. *J. Math Pures Appl.*, 347-425.
- Jouget, E. (1917). *Mechanics of Explosives*. Paris: O. Dion & Fils.
- Jouguet, E. (1904). Sur l'onde explosive. *C.R. Acad. Sci*, 121-124.
- Kapoor, S. (1970). Berthollet, Claude-Louis. In C. Gillespie, *Dictionary of Scientific Biography* (pp. 73-82). New York: Scribner's Sons.
- Kirk, R., & Othmer, D. (1947). *Encyclopedia of Chemical Technology*. New York: The Interscience Encyclopedia Inc.
- Kistiakowsky, G., & Wilson Jr., E. (1941a). *Report on the Prediction of Detonation Velocities of Solid Explosives*.
- Kistiakowsky, G., & Wilson Jr., E. (1941b). *The Hydrodynamic Theory of Detonation and Shock Waves*.
- Klapotke, T. (2012). *Chemistry of High-Energy Materials*. Berlin: Walter de Gruyter.
- Kojovic, T. (2005). Investigation of Aggregate Stemming in Blasting on SAG Mill Performance. *Minerals Engineering*, 1398-1404.
- Konya, A. J., & Konya, C. J. (2017a). Precision Presplitting. *Proceedings of the Society for Mining, Metallurgy, and Exploration*.
- Konya, A., & Konya, C. (2017b). Precision Presplitting - Explosive Variations with Spacing. *Proceedings of the 43rd International Conference on Explosive and Blasting Technique*.
- Konya, A., & Konya, C. J. (2016). Precision Presplitting Optimization. *Proceedings of the Forty-Second Annual Conference on Explosives and Blasting Technique* (pp. 65-74). Las Vegas: International Society of Explosive Engineers.
- Konya, C. (1973). High Speed Photographic Analysis of the Mechanics of Presplit Blasting. *Proceedings of Sprengtechnik International*.

- Konya, C. (1980). Pre-split Blasting: Theory and Practice. *Preprint AIME*, 80-97.
- Konya, C. (1982). Seminar on Blasting to the Ohio Laborers Union. Mont Vernon, Ohio.
- Konya, C. (2015). *Rock Blasting and Overbreak Control*. Montville: Academy of Blasting and Explosive Technology.
- Konya, C., & Konya, A. (2015, November). Precision Presplitting Optimization. *8th Drilling-Blasting Symposium*, (pp. 1-10). Istanbul, Turkey.
- Konya, C., & Konya, A. (2018). Effect of Hole Stemming Practices on Energy Efficiency of Comminution. In K. Awuah-Offei, *Energy Efficiency in the Minerals Industry* (pp. 31-54). Springer.
- Konya, C., Barret, D., & Smith, J. E. (1986). Presplitting Granite Using Pyrodex, A Propellant. *Proceedings of the Twelfth Conference on Explosive and Blasting Technique*, 159-166.
- Konya, C., Britton, R., & Gozon, J. (1985). Explosive Selection - A New Approach. *International Society of Explosive Engineers*, 340.
- Konya, C., Britton, R., & Lukovic, S. (1987). Charge Decoupling and Its Effect on Energy Release and Transmission for One Dynamite and Water Gel Explosive. *Proceedings of the Thirteenth Conference on Explosives and Blasting Technique*.
- Konya, C., Otounye, F., & Skidmore, D. (1982). Airblast Reduction from Effective Blasting Stemming. *Proc. of the Eighth Conference on Explosives and Blasting Technique*, 145-156.
- Konya, D. C., & Walter, E. (1990). *Surface Blast Design*. Englewood Cliffs, New Jersey: Prentice-Hall Inc.
- Krehl, P. (2009). *History of Shock Waves, Explosions, and Impacts*. Berlin: Springer.
- Lang, L., & Favreau, R. (1974, June). A Modern Approach to Open-Pit Blast Design and Analysis. *CIM Bulletin*, 37-44.
- Langefors, U., & Kihlstrom, B. (1973). *The Modern Technique of Rock Blasting*. Uppsala: Almqvist & Wiksell Informationsindustri AB.
- Le Rond D'Alembert, J. (1747). Recherche sur la courbe que forme une onde tendue mise en vibration. *Hist. Acad. Roy. Sci. & Belles Lettres*, 214-249.
- Leet, L. D. (1960). *Vibrations from Blasting Rock*. Cambridge, Massachusetts: Harvard University Press.
- Li, D., & Wong, L. (2012). The Brazilian Disc Test for Rock Mechanics Applications. *Rock Mechanics and Rock Engineers*.

- Livingston, C. (1950). An Introduction to the design of underground openings for defense. *Quarterly of the Colorado School of Mines*, 46(1), 61.
- Livingston, C. (1956). Fundamentals of Rock Failure. *Quarterly of the Colorado School of Mines*, 51(3), 1-14.
- Livingston, C. (1961). *Cratering from High Explosive Charges - Analysis of Crater Data: Technical Report 2-547*. Vicksburg: U.S. Army Corp of Engineers.
- Lusk, B., & Silva, J. (2018). Energy Distribution in the Blast Fragmentation Process. In K. Awuah-Offei, *Energy Efficiency in the Minerals Industry* (pp. 11-30). Springer.
- Mach, E., & Somner, J. (1877). Uber die Fortpflanzungsgeschwindigkeit von Explosionsschallwellen. *Sitzungsber. Akad. Wiss Wien*, 101-130.
- Mader, C. (1963). *Detonation Properties of Condensed Explosives Computed using the BKW Equation of State*. Los Alamos Scientific Laboratory.
- Matheson, G., & Swindells, C. (1981). Seismic Detection and Measurement of Blast Disturbances. *Transport and Road Resarch Laboratoy*.
- Mikhel'son, V. (1893). On the normal ignition velocity of explosive gaseous mixtures. *Scientific Papers of the Moscow Imperial University on Mathematics & Physics*, 1-93.
- Molmud, P. (1960). Expansion of a rarefield gas cloud into a vacuum. *Phys. Fluids*.
- Munroe, C., & Hall, C. (1915). *Explosives in Metal Mining and Quarry Operations*. Washington D.C.: U.S. Bureau of Mines.
- Needham, C. (2018). *Blast Waves*. Springer.
- Nobel, A. (1867). *Britian Patent No. 102*.
- Nobel, S. A. (1892). Preliminary Note on the Pressure Developed by some New Explosives. *Proc. Roy. Soc.*
- Nobel, S. A., & Abel, S. F. (1875). Research on Explosives - Part 1. *Trans. Roy. Soc.*, 100-211.
- Noren, C. (1956). Blasting Experiments in Granite Rock. *Quarterly of the Colorado School of Mines*, 51(3).
- Obert, L., & Duvall, W. (1949). *Gage and Recording Equipment for Measuring Dynamic Strain in Rock*. U.S. Bureau of Mines.

- Obert, L., & Duvall, W. (1950). *Generation and Propagation of Strain Waves in Rock - Part I*. U.S. Bureau of Mines.
- Otuonye, F. (1981). Effective Blasthole Stemming. *PhD Thesis*. The Ohio State University.
- Otuonye, F., Skidmore, D., & Konya, C. (1983). Measurements and Predictions of Borehole Pressure Variations in Model Blasting Systems. *First International Symposium on Rock Fragmentation by Blasting*, 7-20.
- Paine, R., Holmes, D., & Clark, H. (1961, June). Presplit Blasting at the Niagara Power Project. *The Explosives Engineer*, 72-91.
- Paine, R., Holmes, D., & Clark, H. (1962). Controlling Overbreak by Presplitting. *Proceedings of a Symposium held at the University of Missouri*, 179-209.
- Person, P.-A., Holmberg, R., & Lee, J. (1994). *Rock Blasting and Explosive Engineering*. New York: CRC Press.
- Persson, P., Ladegaard-Pedersen, A., & Kihlstrom, B. (1969). The Influence of Borehole Diameter on the Rock Blasting Capacity of an Extended Explosive Charge. *Int. J. Rock Mech. Min. Sci.*, 6, 277-284.
- Persson, P., Lundborg, N., & Johansson, C. (1970). The Basic Mechanisms in Rock Blasting. *Proceedings of the Congress of the International Society of Rock Mechanics*, 19-33.
- Petit, A., & Dulong, P. (1819). Recherches sur quelques points importants de la Theorie de la Chaleur. *Annales de Chimie et de Physique*, 395-413. Retrieved from <http://web.lemoyne.edu/~giunta/PETIT.html>
- Poisson, S.-D. (1808). Memoire sur la theorie du son. *Journal Ecole Polytechnique*, 7, 319-392.
- Prandtl, L. (1906). Zur Theorie des Verdichtungsstobes. *Z. ges Turbinenwesens*, 241-245.
- Qian, Q., Qi, C., & Wang, M. (2009). Dynamic Strength of Rocks and Physical nature of Rock Strength. *Jounrla of Rock Mechanics and Geotechnical Engineering*, 1-10.
- Quinan, W. (1912). *High Explosives*. London: Sir Isaac Pitman and Sons LTD.
- Rayleigh, L. J. (1877). *The Theory of Sound* (Vol. 2).
- Rayleigh, L. J. (1910). Aerial Plane Waves of Finite Amplitude. *Proc. Roy. Soc. Lond.*, 247-284.

- Reaugh, J., Curtis, J., & Maheswaran, M.-A. (2017). Modelling of Deflagration to Detonation Transition in Porous PETN of Density 1.4 g/cc with HERMES. *APS Conference on Shock Compression of COndensed Matter*.
- Robbins, B. (1743). An Account of a Book entitled New Principles of Gunnery. *Proc. Roy. Soc*, 437-456.
- Roscoe, H. (1924, Oct). The Rock-Dust Cartridge Method of Stemming Shots. *Annual Western meeting*, 638-642.
- Saadati, M., Forquin, P., Weddfelt, K., & Larsson, P.-L. (2016). On the Tensile Strength of Granite at High Strain Rates considering the Influence from Preexisting Cracks. *Advances in Materials Science and Engineering*.
- Salmi, E., & Hosseinzadch, S. (2014). A Further Study on the Mechanisms of Pre-splitting in Mining Engineering. *App Mech Mater*, 553, 476-481.
- Sarran, E. (1884). Theoretical Researches on the Effects of Cunpowder and other explosives. (T. L. Ingersoll, Ed.) *Proc. U.S. Naval Ins*.
- Sharma, S., & Rai, P. (2015). Investigation of Crushed Aggregate as Stemming Material in Bench Blasting - A Case Study. *Geotech. Geo. Eng*, 1449-1463.
- Smith, J., Van Ness, H., & Abbot, M. (2005). *Introduction to Chemical Engineering Thermodynamics*.
- Snelling, W., & Hall, C. (1912). *The Effects of Stemming on the Efficiency of Explosives*. Washington D.C.: USBM.
- Sobrero, A. (1847). Sur plusieurs composes detonants produits avec l'acide nitrique et le sucre, la dextrimine, la lactine, la marnite, et la glycerine. *C.R. Acad. Sci.*, 247-248.
- Spagna, S., Konya, C., & Smith, E. (2005). Utilization of Detonation Cord to Pre-Split Pennsylvanian Aged Sandstone and Shale, Grundy, Virginia. *Proceedings of the International Conference on Explosives and Blasting Technique*.
- Spathis, A., & Wheatley, M. (2016, July). Dynamic Pressure Measured in a Water-filled Hole Adjacent to a Short Explosive Charge Detonated in Rock. *Blasting and Fragmentation Journal*, 10(1), 33-42.
- Starfield, A. (1966). Strain Wave Theory in Rock Blasting. *Proceedings of the 8th Symposium on Rock mechanics*, 538-548.
- Tariq, S., & Worsey, P. (1996). An Investigation into the effects of some aspects of jointing and single decoupled blast holes on pre-splitting and boulder blasting. *Rock Fragmentation by Blasting - Fragblast 5*, 438.

- Taylor, G. (1940a). Notes on the Dynamics of Shock-Waves From Bare Explosive Charges. *Civil Defence Research Committee, Ministry of Home Security*.
- Taylor, G. (1940b). Pressures on Solid Bodies Near an Explosion. *Civil Defence Research Committee, Ministry of Home Security*.
- Taylor, G. I. (1910). The Conditions Necessary for Discontinuous Motion in Gases. *Proc. Roy. Soc. Lond.*, 371-377.
- Taylor, G. I. (1939). The Propagation and Decay of Blast Waves. *Civil Defense Research Committee*.
- Taylor, G. I. (1950a). A Formation of a Blast Wave by a Very Intense Explosion - Theoretical Discussions. *Proc. Roy. Soc.*, 159-174.
- Taylor, G. I. (1950b). The Formation of a Blast Wave by a Very Intense Explosions - The Atomic Explosion of 1945. *Proc. Roy. Soc.*, 175-186.
- Taylor, J. (1945, November 10). The Resistance of Stemming - Dynamical investigations. *The Mining Institute of Scotland*, 51-74.
- Toepler, A. (1864). *Beobachtungen nach einer neuen optischen Methode*. Bonn: M. Cohen & Sohn.
- U.S. Army Corp of Engineers. (2018). *Blasting for Rock Excavations*. US Army Corps of Engineers.
- University of Berkley. (2019, September 10). *NASA Polynomials*. Retrieved from http://combustion.berkeley.edu/gri_mech/data/nasa_plnm.html
- University of Texas. (2019). Some Useful Numbers on the Engineering Properties of Materials. *GEOL 615*.
- Wark, K. J. (1988). *Thermodynamics*. McGraw-Hill Inc.
- Weber, E., & Weber, W. (1825). *Wellenlehre auf Experimente gegründet ober über die Wellen tropfbarer Flussigkeiten mit Anwendung auf die Schall*.
- Worsey, P. (1981). *Geotechnical Factors Affecting the Application of Pre-Split Blasting to Rock Slopes*. University of Newcastle Upon Tyne.
- Worsey, P. (1984). The Effect of Discontinuity Orientation on the Success of Pre-Split Blasting. *10th Annual Society of Explosive Engineers Conference on Explosives and Blasting Technique*, 197-217.
- Worsey, P. (2016). Environmental Aspects of Blasting. *Course Taught at Missouri S&T*. Rolla, Missouri, USA: Missouri S&T.

- Worsey, P., & Qu, S. (1987). Effect of Joint Separation and Filling on Pre-split Blasting. *13th Society of Explosive Engineers Conference on Explosives and Blasting Technique*.
- Worsey, P., Farmer, I., & Matheson, G. (1981). The Mechanics of Pre-splitting in Discontinuous Rocks. *22nd U.S. Symposium on Rock Mechanics*, 205-210.
- Yoo, C., Holmes, C., Souers, P., Wu, C., & Ree, F. (2000). Anisotropic shock sensitivity and detonation temperature of pentaerythritol tetranitrate single crystal. *Journal of Applied Physics*.
- Zel'dovich, Y., & Raizer, Y. (2002). *Physics of Shock Waves and High-Temperature Hydrodynamic Phenomena*. Mineola: Dover Publications.
- Zhang, Z.-X. (2016). *Rock Fracture and Blasting Theory and Applications*. Elsevier Inc.

VITA

Anthony J. Konya received a Bachelor of Science in Mining Engineering from the Missouri University of Science and Technology in December of 2016, a Graduate Certificate in Explosive Engineering from the Missouri University of Science and Technology in August of 2017, a Master of Science in Explosive Engineering from the Missouri University of Science and Technology in December of 2017, a Graduate Certificate in Financial Engineering from the Missouri University of Science and Technology in May of 2019, and a Doctorate of Philosophy in Explosive Engineering from the Missouri University of Science and Technology in December of 2019.

Anthony worked for Fairmont Santrol, Cargill Inc., Freeport McMoRan, RJH Consultants, Kesco Inc., and Intercontinental Development Inc. – Precision Blasting Services. Anthony also was the founder and owner of Konya Industries and AcademyBlasting.com.

Anthony wrote over 50 technical publications, taught over 18 seminars and courses, and gave over 25 technical presentations. Anthony was a certified MSHA Safety instructor for Surface and Underground Mining, he had Experience Miner (5000.23) certification, was a licensed blaster in the state of Missouri, was awarded the Diamond Crystal Achiever Award (Cargill), Outstanding Undergraduate Research Award (the Missouri University of Science and Technology), Graduate Educator Award for Explosive Engineering, Graduate Research Award for Explosive Engineering, and Dean's Graduate Educator Award all from the Missouri University of Science and Technology.